U.S. Department
of Transportation
Federal Railroad
Administration

Office of Research,
Development and Technology
Washington, DC 20590

Prototype Commuter Rail Seat in CEM Passenger Railcars

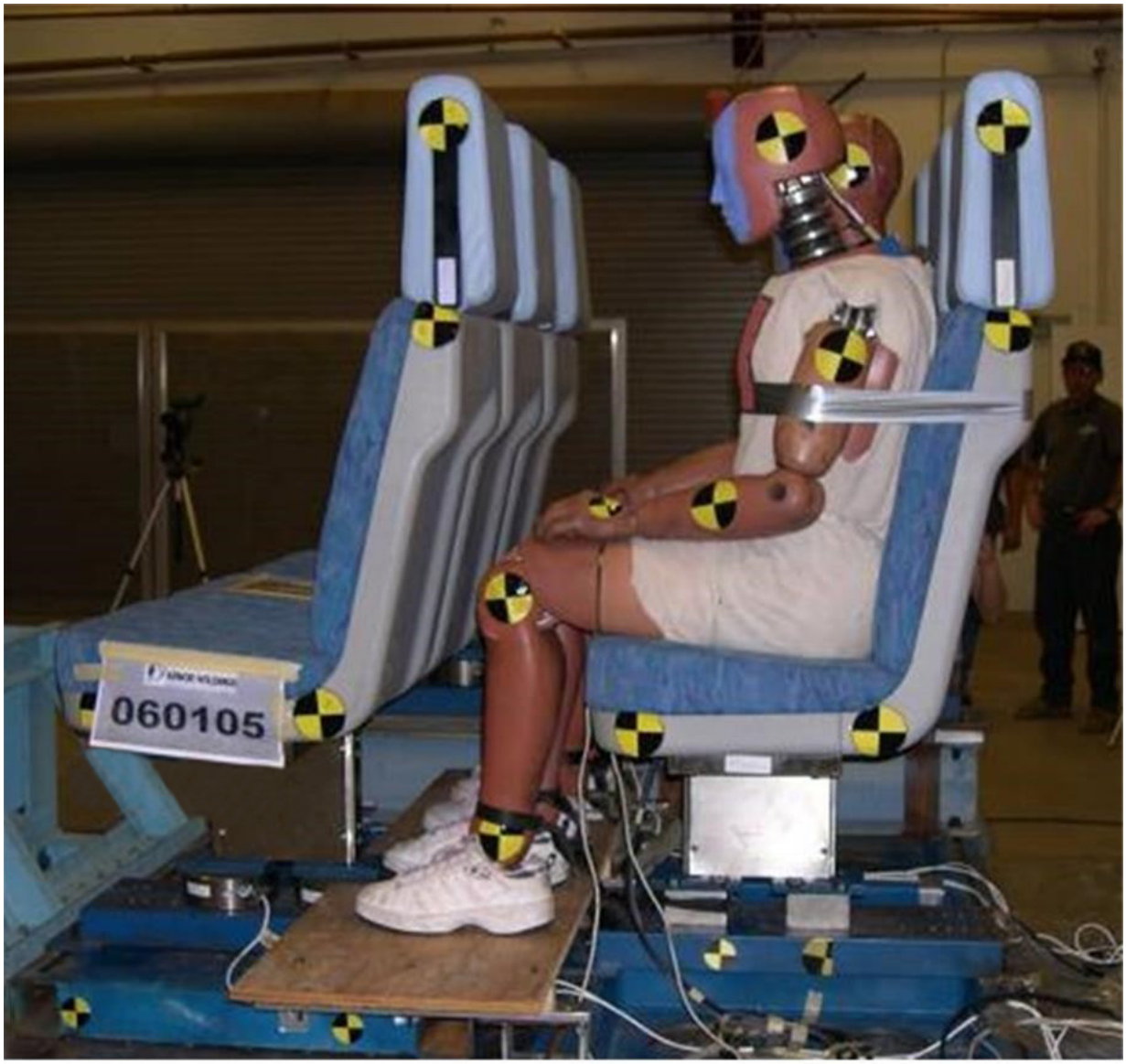

DOT/FRA/ORD-21/11

Final Report | March 2021

NOTICE

This document is disseminated under the sponsorship of the Department of Transportation in the interest of information exchange. The United States Government assumes no liability for its contents or use thereof. Any opinions, findings and conclusions, or recommendations expressed in this material do not necessarily reflect the views or policies of the United States Government, nor does mention of trade names, commercial products, or organizations imply endorsement by the United States Government. The United States Government assumes no liability for the content or use of the material contained in this document.

NOTICE

The United States Government does not endorse products or manufacturers. Trade or manufacturers' names appear herein solely because they are considered essential to the objective of this report.

REPORT DOCUMENTATION PAGE

Form Approved
OMB No. 0704-0188

1. REPORT DATE *(DD-MM-YYYY)*	2. REPORT TYPE	3. DATES COVERED *(From - To)*
03/08/2020	Technical Report	03/2005 - 04/2008

4. TITLE AND SUBTITLE
Development of Prototype Commuter Rail Passenger Seats for Use in CEM Passenger Rail Cars

5a. CONTRACT NUMBER
DTRS57-04-D-30008

5b. GRANT NUMBER

5c. PROGRAM ELEMENT NUMBER
T0005

6. AUTHOR(S)
Robert Rancatore, Richard Stringfellow

5d. PROJECT NUMBER
RR28

5e. TASK NUMBER
DB037

5f. WORK UNIT NUMBER

7. PERFORMING ORGANIZATION NAME(S) AND ADDRESS(ES)
TIAX LLC
15 Acorn Park
Cambridge, MA 02140

8. PERFORMING ORGANIZATION REPORT NUMBER

9. SPONSORING/MONITORING AGENCY NAME(S) AND ADDRESS(ES)
U.S. Department of Transportation
Federal Railroad Administration
Office of Research and Development
1200 New Jersey Avenue, SE
Washington, DC 20590

10. SPONSOR/MONITOR'S ACRONYM(S)

11. SPONSOR/MONITOR'S REPORT NUMBER(S)
DOT/FRA/ORD-21/11

12. DISTRIBUTION/AVAILABILITY STATEMENT
This document is available to the public through the FRA website.

13. SUPPLEMENTARY NOTES

14. ABSTRACT
In support of the Federal Railroad Administration's Equipment Safety Research Program, the Volpe Center has been conducting research to improve occupant protection during accidents for rail car passengers. This report describes a project conducted to develop and test a prototype design for a more crashworthy three-person seat that reduces passenger injury levels and compartmentalizes the occupants in a full-scale train-to-train impact test of equipment using crash energy management (CEM). The seat designed in this project will help to protect occupants whether they are seated in forward-facing or rear-facing seats.

15. SUBJECT TERMS
Crashworthiness, occupant protection, full-scale train-to-train test, crash energy management, crush zones, rail cars, occupant survivability, collision, injury, impacts

16. SECURITY CLASSIFICATION OF:			17. LIMITATION OF ABSTRACT	18. NUMBER OF PAGES	19a. NAME OF RESPONSIBLE PERSON
a. REPORT	b. ABSTRACT	c. THIS PAGE			Kristine Severson
Unclassified	Unclassified	Unclassified		122	19b. TELEPHONE NUMBER *(Include area code)* 952-270-0646

METRIC/ENGLISH CONVERSION FACTORS

ENGLISH TO METRIC	METRIC TO ENGLISH
LENGTH (APPROXIMATE)	**LENGTH (APPROXIMATE)**
1 inch (in) = 2.5 centimeters (cm)	1 millimeter (mm) = 0.04 inch (in)
1 foot (ft) = 30 centimeters (cm)	1 centimeter (cm) = 0.4 inch (in)
1 yard (yd) = 0.9 meter (m)	1 meter (m) = 3.3 feet (ft)
1 mile (mi) = 1.6 kilometers (km)	1 meter (m) = 1.1 yards (yd)
	1 kilometer (km) = 0.6 mile (mi)
AREA (APPROXIMATE)	**AREA (APPROXIMATE)**
1 square inch (sq in, in^2) = 6.5 square centimeters (cm^2)	1 square centimeter (cm^2) = 0.16 square inch (sq in, in^2)
1 square foot (sq ft, ft^2) = 0.09 square meter (m^2)	1 square meter (m^2) = 1.2 square yards (sq yd, yd^2)
1 square yard (sq yd, yd^2) = 0.8 square meter (m^2)	1 square kilometer (km^2) = 0.4 square mile (sq mi, mi^2)
1 square mile (sq mi, mi^2) = 2.6 square kilometers (km^2)	10,000 square meters (m^2) = 1 hectare (ha) = 2.5 acres
1 acre = 0.4 hectare (he) = 4,000 square meters (m^2)	
MASS - WEIGHT (APPROXIMATE)	**MASS - WEIGHT (APPROXIMATE)**
1 ounce (oz) = 28 grams (gm)	1 gram (gm) = 0.036 ounce (oz)
1 pound (lb) = 0.45 kilogram (kg)	1 kilogram (kg) = 2.2 pounds (lb)
1 short ton = 2,000 pounds (lb) = 0.9 tonne (t)	1 tonne (t) = 1,000 kilograms (kg) = 1.1 short tons
VOLUME (APPROXIMATE)	**VOLUME (APPROXIMATE)**
1 teaspoon (tsp) = 5 milliliters (ml)	1 milliliter (ml) = 0.03 fluid ounce (fl oz)
1 tablespoon (tbsp) = 15 milliliters (ml)	1 liter (l) = 2.1 pints (pt)
1 fluid ounce (fl oz) = 30 milliliters (ml)	1 liter (l) = 1.06 quarts (qt)
1 cup (c) = 0.24 liter (l)	1 liter (l) = 0.26 gallon (gal)
1 pint (pt) = 0.47 liter (l)	
1 quart (qt) = 0.96 liter (l)	
1 gallon (gal) = 3.8 liters (l)	
1 cubic foot (cu ft, ft^3) = 0.03 cubic meter (m^3)	1 cubic meter (m^3) = 36 cubic feet (cu ft, ft^3)
1 cubic yard (cu yd, yd^3) = 0.76 cubic meter (m^3)	1 cubic meter (m^3) = 1.3 cubic yards (cu yd, yd^3)
TEMPERATURE (EXACT)	**TEMPERATURE (EXACT)**
[(x-32)(5/9)] °F = y °C	[(9/5) y + 32] °C = x °F

QUICK INCH - CENTIMETER LENGTH CONVERSION

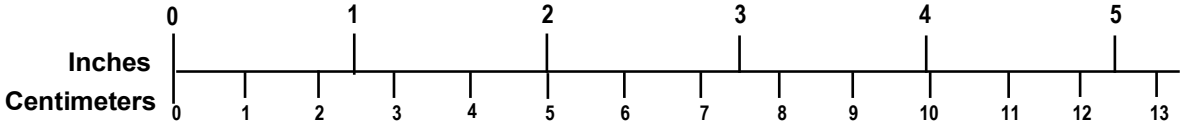

QUICK FAHRENHEIT - CELSIUS TEMPERATURE CONVERSIO

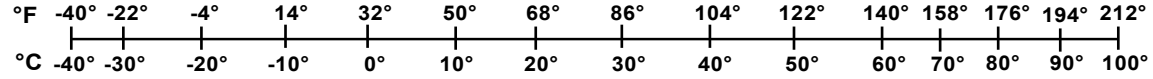

For more exact and or other conversion factors, see NIST Miscellaneous Publication 286, Units of Weights and Measures. Price $2.50 SD Catalog No. C13 10286

Updated 6/17/98

Acknowledgements

The work covered in this report was performed as part of the Equipment Safety Research Program within the Federal Railroad Administration (FRA) Office of Research, Development and Technology (RD&T). The authors would like to thank Eloy Martinez, FRA Program Manager (at the time the work was performed), and Claire Orth, Division Chief, Equipment and Operating Practices Research Division, FRA RD&T (at the time the work was performed), for their guidance and support.

The authors would also like to thank Kristine Severson, Senior Engineer, from the Structures and Dynamics Division, Volpe Center, for her guidance, support, and assistance throughout the program.

The project team included the Volpe Center, TIAX LLC, Technical Metal Specialties, Inc., CVID Consulting Services, LLC, Armor Holdings Aerospace and Defense Group (Armor Holdings), and Altair Engineering.

Contents

Illustrations

Tables

Executive Summary

In support of the Federal Railroad Administration's Equipment Safety Research Program, the Volpe Center has been conducting research to improve the structural crashworthiness of passenger railcars and to improve occupant protection for railcar passengers. As a part of this work, crash energy management (CEM) strategies, in the form of crush zones incorporated at the ends of passenger cars, have been developed and tested with the aim of preserving the occupant volume in passenger cars in collisions with closing speeds up to 35 mph. One potential consequence of the use of CEM in railcars is the increased level of accelerations experienced by the occupants, increasing the risk of severe injury from secondary impacts.

This report describes a project conducted to address this concern by providing a design for a more crashworthy three-person seat that reduces passenger injury levels and compartmentalizes the occupants. The seat designed in this project will help to protect occupants whether they are seated in FF or rear-facing seats.

A team of researchers, led by TIAX LLC, developed a set of requirements to guide the seat design. These project design requirements are above and beyond the requirements defined in the APTA safety standard for passenger seats. The design requirements included static and dynamic loading conditions; maximum injury levels for several body components, including the head, chest, neck, and femur; and the level of compartmentalization. Researchers imposed these conditions for a scenario in which three 50th percentile male ATDs are seated in either forward-facing (FF) or rear-facing (RF) configurations. The instrumented 50th percentile male ATD weighs about 170 lbm and is 5'9" tall. These occupants are subjected to an 8g, 250 ms triangular acceleration pulse for FF seats and a 12g, 250 ms triangular acceleration pulse for RF seats. The attachments of the seat to the car were required to withstand the loads imparted by all three occupants without failure.

The research team surveyed several rail industry contacts to generate information on current seat designs and to determine if the crashworthiness of these designs met the requirements and standards set forth in the APTA Standards or the Code of Federal Regulations, as well as the more stringent requirements defined for this project. None of the seats identified in the survey was found to meet all of these requirements.

The team generated concepts for several seat components, such as the seat back structure, the seat attachment, and the cushion attachment. The focus of concept generation activities was to reduce injury to passengers by absorbing enough of the impact energy through deformation of the seat structure when an occupant strikes the seat. The concepts generated included ideas to help provide compartmentalization of the occupant. Researchers placed one constraint on the seat design – it must be effective regardless of whether the seat was in a FF or RF configuration.

Researchers combined the various concepts, as appropriate, to create several alternative seating systems, ranked according to how well they met the requirements. Based on the rankings, they selected one concept for the detailed design, a modular seating arrangement. This means that each seat interacts with and must absorb the impact energy of a single occupant, making the seat performance independent of the number and location of the occupants in the seat, for up to three seated occupants.

The selected design was similar to an existing two-person seat design fabricated by Technical Metal Specialties, Inc. Using the existing design as a starting point, modifications were made so that the seating system met the design requirements. The baseline seat design was modified so it was appropriate for three occupants.

To improve compartmentalization and reduce the possibility of neck injuries for RF occupants, the height of the headrest was increased by 2.5 inches. The higher headrest better supports the back of the head and reduces the possibility of the head becoming unsupported during a collision.

Foam padding that was about 20 percent stiffer than that used in the headrests of the baseline two-person seats was selected to help reduce injury levels when the head of a person in a FF seat impacts the rear of the headrest during a collision. Occupant response analyses suggested that a foam pad that was stiffer than that typically used would help reduce the head injury level.

To meet the requirements of both the 8g FF pulse and the 12g RF pulse, the yield strength of the round tubing that constitutes the seat frame was increased from 50 ksi to 70 ksi. Researchers explored several variations of shape, tube diameter, and wall thickness. The 0.083-inch thick, 1.5-inch diameter tubing was chosen because it has a reasonable thickness-to-diameter ratio to promote buckling deformation but not allow the tube to collapse for the defined loading conditions.

Researchers performed finite element analyses to guide the detailed design and verify that the seating system could withstand the operating loads without permanent deformation. They also performed quasi-static analyses to develop the moment versus rotation response of the seat under dynamic load. The quasi-static seat response was used as input to occupant response models that were performed to predict occupant injury levels.

The team conducted three quasi-static tests to measure the force versus displacement behavior of the seat back, and to verify that the seats remained attached to the test fixture under these loading conditions. These test results were compared to the quasi-static analysis results. The model was adjusted accordingly.

The team conducted dynamic sled tests with instrumented ATDs in both FF and RF configurations. The test results indicated that the seats met all test requirements. The injury criteria for the head, chest, neck, and femur were within specified parameters. The seats remained attached to the test sled. All ATDs were compartmentalized between rows of seats.

1. Introduction

The Volpe Center supports the Federal Railroad Administration (FRA) by conducting research and development studies to improve rail equipment crashworthiness. This research includes the addition of crash energy management (CEM) systems, comprising crush zones at the ends of rail vehicles, as a means of providing increased occupant survivability during a collision. Studies have shown that one of the consequences of using CEM strategies is a potential increase in the risk of injury to occupants due to secondary impacts during a collision. These injuries could be caused by impacts between occupants and the back of the seat in front of them, or by a failure to compartmentalize occupants due to the collapse of the seat structure or propelling them into an adjacent row.

1.1 Background

Seats designed for rail equipment must meet the requirements of the Code of Federal Regulations (CFR), Title 49, Part 238, Section 233 and the APTA SS-C&S-016-99, Standard for Row-to-Row Seating in Commuter Rail Cars [1] (APTA seat standard). Among other requirements, these regulations and standards state the magnitudes and characteristics of static and dynamic loadings the seating system must meet. They also state the allowable levels of "injury" that can be sustained by instrumented anthropomorphic test devices (ATD) during dynamic sled tests. Historically, the acceleration pulse used for dynamic testing has been an 8g, 250 ms triangular pulse, which represents the longitudinal acceleration environment of a railcar in an inline collision [4]. This acceleration pulse has been specified in the APTA seat standard since its initial authorization in 1999, for both forward-facing (FF) and rear-facing (RF) seat configurations.

Research and testing has shown, however, that for a cab car-led, CEM-based passenger train in an inline collision, the acceleration environment for the lead car can be more severe than for conventional equipment [2]. This higher acceleration environment has led to the strategy of using RF seats in the cab car of CEM-based trains as a means of better protecting cab car occupants during a collision. Analyses and full-scale train-to-train impact test results indicated that the longitudinal acceleration pulse experienced by the occupants in this car can be approximated by a 12g, 250 ms triangular acceleration pulse [3]. The seats designed in this program were therefore tested with this 12g pulse in the RF seat configuration, as well as with the typical 8g, 250 ms triangular pulse in the FF seat configuration.

1.2 Objectives

The objective of this research was to design, manufacture, and test a three-passenger commuter seat that complies with the performance requirements identified in the APTA seat standard (APTA SS-C&S-016-99) using a 12g crash pulse in the RF configuration, and an 8g crash pulse in the FF configuration.

1.3 Overall Approach

This project utilized several steps in a product development process that included design, analysis, and fabrication. The first of these steps began with a definition of the requirements of the seating system. Refinements were made to these requirements as the program progressed.

A review of existing seat designs was then made to identify any current designs that attempted to improve the crashworthiness performance of seats beyond the standards and regulations.

With this information in hand, a number of concepts for a more crashworthy seat were developed. These concepts were ranked in order to produce a single concept on which to focus the design effort. Detailed analyses were performed to guide the design and help predict the level of injuries to the occupant. As needed, the design was modified so that it was better able to meet requirements.

1.4 Scope

A total of eight rows of seats were fabricated by Technical Metal Specialties, Inc. (TMS) per the design drawings. Four rows of seats were delivered to Transportation Technology Center, Inc. (TTCI) in Pueblo, Colorado, to be included in the CEM train-to-train test performed in March, 2006 [5]. The remaining four rows of seats were delivered to Armor Holdings in Phoenix, Arizona for quasi-static testing and dynamic sled testing. The rest of this report describes the results of these tests.

1.5 Organization of the Report

The report describes the seat design process, including the design requirements, a review of existing designs, component testing, and MADYMO analyses. The seat fabrication is described in detail, followed by a description of the test setup, test results, and comparison with computer analyses.

2. Design Requirements

The design requirements for an improved commuter rail passenger seat that provides occupant compartmentalization during an inline collision of CEM equipment while simultaneously limiting the occupant injury criteria are described in this section. The commuter seat developed for this project was installed in passenger rail equipment, as described in 49 CFR Part 238. The design requirements listed here for the purpose of this project were derived from Federal regulations and industry standards and are included in Appendix A. Some of the relevant definitions are listed in Appendix A, Section A.1. The applicable regulations and standards are listed in Appendix A, Section A.2. A few of the important design requirements are summarized in Table 1 below and are divided into five categories:

- Collision requirements
- Seat attachment requirements
- Seat contact requirements
- Performance requirements
- Fabrication requirements

Note that some of the requirements in the APTA seat standard related to seat components, such as arm rests and grab handles, included in Appendix A for completeness, are met by the baseline design chosen for this program and are not directly included in the delivered seat design nor explicitly demonstrated in the project. The focus of the design effort was primarily on improving compartmentalization and minimizing injury levels for passengers seated in FF and RF seats. Listed in Table 1 are the requirements that directly impact the design of the seat. As noted, a complete set of requirements can be found in Appendix A.

Table 1. Seat requirements

1.	Collision Requirements
Dynamic Tests	• The FF three-position seat will be subjected to a triangular crash pulse, or acceleration time history, with three seated 50th percentile male ATDs. The pulse peak shall be 8gs and the duration shall be 0.25 seconds, as shown in Figure 1. • The RF three-position seat will be subjected to a triangular crash pulse, or acceleration time history, with three seated 50th percentile male ATDs. The pulse peak shall be 12gs and the duration shall be 0.25 seconds, as shown in Figure 1.
Moment vs. Rotation Characteristics	• As a guideline, the moment vs. rotation characteristic of the seat back may fall within the range highlighted in Figure 2. • Seat designs whose performance falls outside the highlighted range in Figure 2 are acceptable as long as they meet all the other performance requirements set forth in this project.
Cushion Retention	• The seat and back cushions must not become loose during a simulated collision. • No tools are needed/necessary to fasten the cushions in place or replace them.
2.	**Seat Attachment Requirements**
Attachment Points	• The seat must be attached to an existing passenger car by way of seat rails/tracks on the floor and/or wall of the carbody
Mounting Hardware	• The mounting hardware should not require modification of the seat rails. • The mounting hardware should conform to 49 CFR Part 238, Section 233, Article (d): "To the extent possible, all interior fittings in a passenger car, except seats, shall be recessed or flush-mounted."
Seat Attachment Strength	• Seat attachments to the floor and/or wall should not experience significant permanent deformation under a static horizontal load of 500 lbf (2,225 N) applied in a longitudinal direction at any point along the seat base/seat pan in the fore and aft directions.
3.	**Seat Contact Requirements**
Geometry	• Longitudinal distance measured from the forward most point of the seat to the rearward most point should not exceed 26 inches. • There are no limitations on the seat height. • The width of a three occupant seat should be maintained at approximately 59 inches.
Service Loads	• Seat frames and components should be designed to meet the individually applied static load requirements given in APTA SS-C&S-16-99, Rev. 1 (Rev. 1 was the current revision at the time this work was performed), with no permanent yielding of structural materials, loss of function or change in appearance of the seat or component, including:

	– Seat Back Strength – Apply a 300 lbf static load, per occupant, perpendicular to the seat back at the upper back of the seat frame at the midpoint of each seat frame, and at a distance of 3 inches below the top of the seat back (Figure 3). The load is to be distributed across the seat back. This load should be applied separately in both directions. – Vertical Seat Strength – Apply a 450 lbf load per occupant on the seat frame near the front edge of each occupant placement in a vertical downward direction at the midpoint of each occupant position (Figure 4). – The contact area of the applied load should not exceed 4 square inches.
4.	**Performance Requirements**
Seat Performance	• The seat must remain attached to the railcar at all attachment points for all defined static and dynamic loads. • The deformation of the seat back should not result in any sharp edges with which the occupant is at risk of coming into contact. • The seat back must not rotate more than 30° in either direction.
Occupant Response	• For the applied dynamic acceleration pulse, all of the ATDs must be compartmentalized. Successful compartmentalization requires that the resting position of the ATD after the impact be between the initial seating position and the adjacent seat. • The injury estimates (derived from measurements taken from all of the ATDs during the applied dynamic pulse) must meet the following criteria, defined in 49 CFR Part 571, Standard No. 208: Occupant Crash Protection: a) HIC15 must not exceed 700. b) Nij must not exceed 1.0. c) Neck tension must not exceed 937 lbf (4,170 N). d) Neck compression must not exceed 899 lbf (4,000 N). e) Chest deceleration must not exceed 60g over a 3 ms clip. f) Axial femur loads must not exceed 2,250 lbf (10,000 N).
5.	**Fabrication Requirements**
Materials and Workmanship	• The design should utilize materials and fabrication methods suitable to the railroad environment. • The materials should meet the flammability and smoke requirements given in 49 CFR Part 238, Appendix B. • The seat design should minimize the use of protrusions, sharp edges or corners that could cause injury, catch, or damage the clothing of passengers or crew members. The use of exposed fasteners should be minimized. • All parts of the seat should be interchangeable with parts of like seats.
Safety Requirements	• The materials used for seat construction should meet the requirements of 49 CFR Part 238, Appendix B.

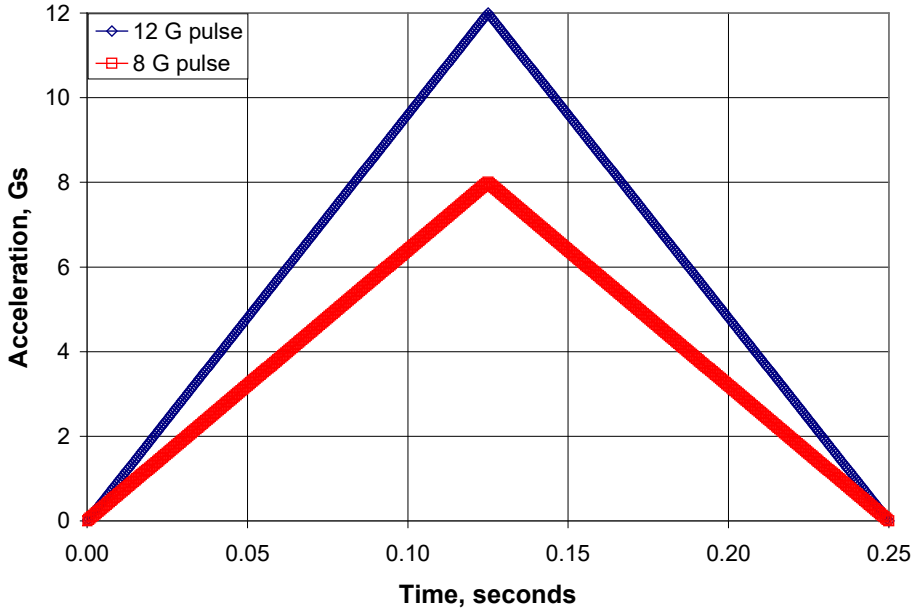

Figure 1. Crash pulses

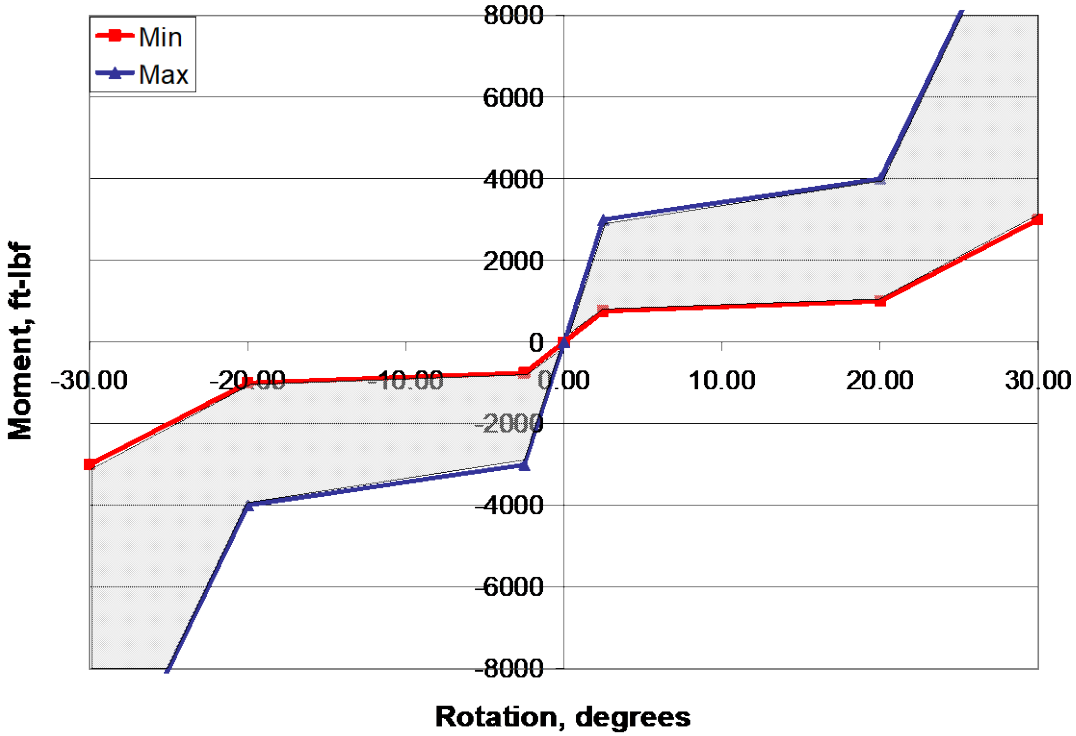

Figure 2. Limits for allowed moment vs. rotation characteristics of seat back

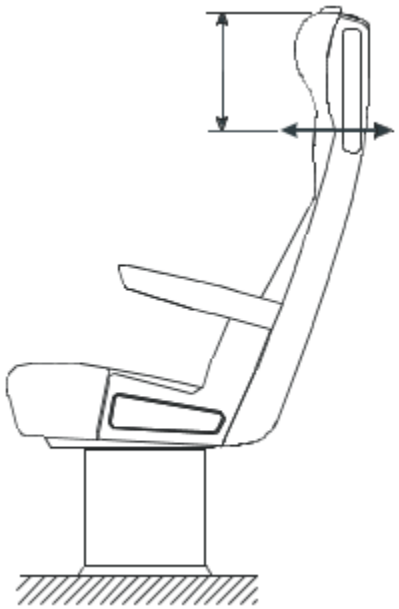

Figure 3. Loading conditions for backrest strength test

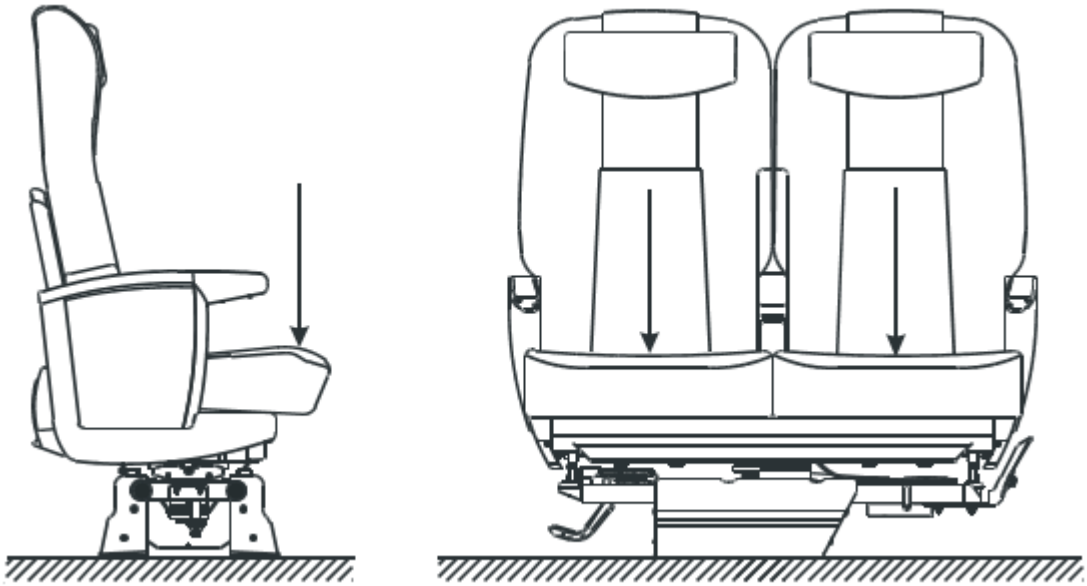

Figure 4. Loading conditions for vertical seat strength test

3. Review of Existing Seat Designs

A review of existing commuter rail passenger seats was conducted to document their geometry, construction, and methods of attachment to railcar bodies. The objective of this review was to use this and related information to assist in the design of a commuter rail seat that enhances occupant collision safety by compartmentalizing occupants without inducing severe injury loads.

The following approach was used to conduct this review:

- Develop a list of rail industry contacts in North America and in Europe.
- Develop a list of key seating system attributes (including energy absorption strategy, geometry, construction, manufacturing methods, attachment methods, and crashworthiness features), construct a questionnaire, and collect responses from the rail industry contacts.

The information collected suggests that there were some seating systems that met the requirements of APTA SS-C&S-016-99, Standard for Row-to-Row Seating in Commuter Rail Cars. Such seating systems had been tested to meet either the original version of this standard or the revised version (Rev. 1). The original version required two dynamic sled tests for forward facing seats: one measures seat structural integrity and required three un-instrumented 95th percentile ATDs; the other measured human injury tolerances and required three 50th percentile ATDs, only one of which is instrumented. Rev. 1 of the standard combines these two tests into one FF seat test requirement to evaluate seat structural response and occupant injury levels, using three fully-instrumented 50th percentile ATDs. Additionally, Rev. 1 requires a dynamic sled test for a RF seat. All newly designed commuter seats must meet the APTA Rev. 1 standard, whereas replacement seats in existing cars do not need to meet this standard.

Seats designed to comply with the APTA standard typically have a tubular steel frame and a deformable seat back panel. The seat back height is raised to support the head during impact. No seats were identified as being manufactured with discrete energy-absorbing devices, such as the extrusion tubes incorporated into two intercity seats used in prior full-scale crash testing [6]. Only seating systems manufactured by US Railcar appear to incorporate a passive stop to resist forward collapse of the seat under impact from behind.

In the U.K., seats have been designed and tested to meet the Association of Train Operating Companies (ATOC) Vehicles Standard, AV/ST9001. AEA Technology (AEAT) provided video of dynamic tests and some corresponding test data. It appears that these seats provide occupant compartmentalization and limit head and neck loads, but axial femur loads tend to be higher than desired. While the test data suggest that they meet the APTA femur loading requirements (max 2,250 lbf, or 10 kN), the measured femur loads do not meet the more stringent ATOC requirements (max. 899 lbf, or 4 kN). According to Peter Matthews from AEAT, this injury criterion was established to correspond to elderly, mainly female, passengers who may have osteoporosis. Results from cadaveric work indicate that a 6.8 kN (1,528 lbf) axial load is acceptable. With this revised criterion, the seats pass.

Some specific information was obtained for seat components during the discussions with industry contacts. Table 2 below summarizes some of the specific seat features that were identified in the survey.

Table 2. Summary of seat descriptions

Feature	Description
Seat Frame	Mostly steel frame, some tubular in shape, some aluminum
Back Panel	Fiberglass, polycarbonate, or aluminum
Seat Back Height and Headrest	Mostly high seat backs/headrests to protect the head: 42 inches to 50 inches above the floor
Cushions	Mostly foam covered in either vinyl or fabric
Discrete Energy Absorbing (EA) Device	Some with no EA device; those that did relied on frame bending/deforming, or stiffened joint and floor attachments, or an inertial locking mechanism.

4. Seat Design Concepts

With seating system requirements and the results from the survey of existing seat designs in hand, concepts for a more crashworthy seating system were generated based on the known issues and the identified requirements. A concept generation session was held to discuss the issues and gather ideas from a multi-disciplinary group of engineers, scientists, and designers. Three general categories of seating system concepts were identified:

- Energy-absorbing seat structure
- Energy-absorbing attachment mechanism
- Energy-absorbing seat pan

More detailed ideas were generated within each one of these three system categories. The concepts generated were screened against an initial set of criteria. Those that passed the initial screening were refined to produce a set of concepts that could be evaluated against a detailed set of criteria based on the requirements. The concepts were ranked and compared against each other until the top three concepts were identified.

The top three concepts were refined further. Simplified analyses were performed to determine if a given concept could meet a specific requirement, such as the expected amount of energy to be absorbed in an incident. Several component-level ideas were recommended as part of the final system concept. They included:

- The use of a modular design
- The use of bucket seats
- An increase in the height of the seat back
- An increase in the padding on the seat back
- The use of a knee bolster attached to the seat back

Based on the ranking of the various system concepts, methods and mechanisms for implementing the concepts were analyzed and evaluated. The best-performing concept was chosen as the basis for the seat design. This section of the report summarizes this selection process and reports on the results of this work.

4.1 Concept Generation

A structured concept generation session, led by a moderator, was held at TIAX. At the beginning of this session, the objective of the program was described. Some of the problems/issues associated with design of a more crashworthy seat were described, the performance of existing seat designs in sled tests was reviewed, and some guiding parameters were defined. A document containing pertinent rail industry seat requirements and existing commuter seating systems was generated for review by the participants in preparation for the session. In addition, a few of the participants, including industry, Volpe, and some TIAX personnel, who were familiar with important operational and manufacturing issues, helped to guide some of the idea generation. As they were generated, the ideas were sketched and documented. As has been observed in other concept generation sessions, ideas were built upon, with one idea typically sparking another idea. As a result of the process, three general categories of seat system concepts were identified: energy absorbing seat structure, energy absorbing seat pan, and energy absorbing attachment

mechanism. Several other ideas were presented that pertained to specific seat components, such as seat cushion design, head rest design, and seat-to-car connections. These and other component-level concepts, such as mechanisms to absorb energy, were recognized as concepts that could be used in many of the system-level concepts. Table 3 lists the concepts that were generated within each category.

Table 3. Railcar seat concepts identified for improving crashworthiness response

Energy-Absorbing Seat Back	Energy-Absorbing Seat Pan	Energy-Absorbing Mechanism	Cushion Retention Concepts	Head Rest Concepts	General Concepts
Continuous variable stiffness frame	Deformation between seat pan and pedestal/wall	Swage outer tube with a piston	Kevlar webbing	Bi-directional tuned torsion spring	Energy absorber at floor and wall
Multiple stiffness frame sections	Crushable seat pan	Straighten a bent tube	Metal plate backing	Taller headrest	Increase seat height
Deformable frame	Sliding seat pan to improve impact	Inversion tube	Slide in cushions	Additional padding	
Crushable seat	Seat pan buckles	Sliding EA	Zipper/button/snap		
Pivoting seat spring	Crushable pedestal	Crushing EA			
Pivoting seat crush					
Additional seatback cushions					

4.2 Concept Selection

Individual concepts identified in Section 4.1 were evaluated in an initial screening by the project team to determine if they should be included in the next level of evaluation. This initial screening used several criteria, including: likelihood of meeting requirements, probability of success, feasibility of manufacturing, and cost. Given the desire to test the seats in an upcoming CEM full-scale test, components, processes, and materials that required a long lead-time for fabrication were screened out at this stage.

Next, the concepts were ranked using a set of criteria weighted in accordance with importance. The criteria were generated based on seating system requirements, including the following:

- The seat mounts shall not permanently deform for vertical and longitudinal operating loads.
- The seats and attachments can permanently deform, but must remain attached to the floor and/or wall.
- The seats can deform but shall not impinge upon the space needed for egress after an accident.
- The seats shall compartmentalize the occupants.
- The seats shall meet all of the requirements whether or not all seating positions are occupied.

These requirements led to the set of criteria and associated weighting values listed in Table 4. Weighting values of 1, 3, and 5 were used, where 5 means the criterion is highest in importance.

Table 4. Evaluation criteria and weights

Weight	Criteria	Comment
5	Energy Absorbed	Can the concept meet the amount of energy to be absorbed as well as the desired force/crush curve shape?
5	Reduces Injury	Both FF and RF seat configurations were evaluated for each concept.
5	Compartmentalization	Can the concept help to keep occupants in their row/seat area?
5	Operational Load Requirements	Can the concept meet the required loads?
5	Affect Ingress or Egress	Can the concept minimize ingress and egress concerns?
5	Weight Concerns	Will the concept adversely increase the weight of the seats?
5	Maintenance	Does the seat concept increase maintenance time or car cleaning time?
3	Simplicity of Design	Does the concept include complex mechanisms; are there many variables to control?
3	Knee Space/Comfort	Is the comfort of the passenger affected by the concept?
1	Materials Costs	Are materials costs comparable to other concepts?
1	Manufacturing Ease	How easily can the seats be manufactured?

Evaluations of the concepts against the criteria were made based on experience, and in some cases, simplified analyses. Team members applied a score to each concept for each criterion.

Table 5 shows the results of the evaluation for each concept. The values listed are the average of the study team's scores. The average scores were then multiplied by the weighted rating and summed across all the criteria. The three highest scoring concepts within each of the energy-absorbing categories, highlighted in Table 5, were the concepts chosen to be evaluated in more detail. The selected concepts were energy absorbed through frame deformation, energy absorbed through cushioning/sliding for better impact control, and energy absorbed through the use of a mechanism. Several of the other concepts generated were also incorporated into the final design.

Table 5. Weighted concept evaluation results

	Energy Absorbed (efficiency)	Reduces Injury FF	Reduces Injury RF	Compartmentalization	Operational Load Requirement	Weight	Effects Ingress or Egress	Simplicity of design	Material cost	mfg ease	Independent of # occupants	Little seat maint. Req.	Little car maint. Req	Knee Space - Comfort	SUM
RATING	5	5	5	5	5	5	5	3	1	1	5	5	5	3	
Energy Absorbing Seat Structure															
Frame Design with Variable stiffness	4.00	4.00	3.67	3.33	3.67	4.00	3.67	1.17	2.67	3.00	3.00	3.33	2.67	4.20	198.43
Frame Design with Multiple stiffness Sections	4.00	4.00	3.67	3.33	3.67	4.00	3.67	1.50	3.00	3.33	3.33	3.33	2.67	4.20	201.77
Frame Design with Deformation	4.00	4.00	4.00	4.00	4.50	4.00	4.50	0.83	4.00	3.50	4.00	4.00	0.83	3.60	209.97
Crushable	3.67	3.33	3.33	3.33	3.33	3.00	3.67	1.17	4.00	2.67	3.00	3.67	2.33	3.40	183.70
Pivoting - spring	3.00	3.00	2.33	3.00	2.17	3.33	3.67	1.17	2.00	2.67	3.00	3.33	2.33	3.40	164.20
Pivoting - crush	4.00	4.00	2.33	3.33	2.83	3.50	3.67	0.83	2.00	2.33	3.33	3.33	2.33	3.80	181.57
Cushioned back	3.00	4.00	2.00	4.00	2.83	3.33	3.00	2.17	4.00	3.67	4.33	4.00	1.67	3.80	186.40
Cushions on back TOP only	2.00	3.33	1.67	3.33	2.50	3.67	3.33	2.17	4.00	4.00	4.33	4.33	2.00	4.60	180.80
Energy Absorbing Seat Pan															
Placed between bench and pedestal	3.00	3.00	2.67	3.67	3.33	3.00	4.00	1.83	3.33	2.67	2.33	3.33	2.00	3.40	173.37
Crushable pan	3.33	3.00	2.00	4.00	3.00	4.00	4.33	1.17	2.67	2.33	3.33	4.00	2.33	3.40	185.37
Crushing/sliding for better head and chest impact	4.00	4.67	3.00	4.00	2.67	3.00	3.00	1.17	2.67	3.00	3.33	4.00	2.00	3.00	186.50
Buckling pan frame	2.67	2.67	1.67	3.67	2.67	4.67	3.00	1.50	3.33	3.33	2.67	4.00	2.67	3.40	173.03
Crushable pedestal - moment induced	3.00	3.33	3.00	3.00	3.33	3.67	3.33	1.17	3.00	3.00	2.33	2.67	2.67	3.40	171.37
Energy Absorbing Mechanism															
Swage outer tube with piston	2.67	2.33	2.67	3.00	2.67	2.67	4.00	0.83	2.67	1.67	2.00	3.00	2.00	2.60	149.63
Straighten bent tube	3.00	3.00	3.00	3.00	2.67	2.67	4.00	1.17	2.33	1.67	2.67	3.33	2.00	3.00	163.17
Inversion tube	2.67	2.67	2.33	2.67	3.00	3.33	4.00	1.17	2.00	2.67	2.67	3.33	2.00	2.60	159.30
Mechanism	3.17	2.83	2.17	2.83	3.17	3.50	3.83	2.33	2.50	2.50	3.17	3.17	3.17	3.20	176.60
Headrest Modifications															
Torsion Spring - bi-directional	2.67	3.33	2.67	3.00	3.00	3.33	4.33	1.50	2.67	2.67	3.33	3.67	2.00	3.40	176.70
U-shaped	1.67	1.67	1.67	3.00	3.67	4.00	4.00	2.17	4.00	3.33	3.33	4.00	2.67	3.40	172.37
Mechanism to oppose seat direction	1.33	2.33	1.67	3.67	3.67	2.33	3.67	0.83	1.67	1.33	2.67	3.33	1.67	2.20	143.77
Cushion Solution															
Kevlar Webbing	3.00	3.00	2.67	2.67	3.67	4.67	4.67	1.17	2.67	1.33	3.00	2.67	1.67	3.80	177.23
Bucket seats	1.67	2.00	2.33	3.67	3.33	3.67	4.67	2.17	4.33	3.33	3.67	3.33	2.33	4.20	180.10
Metal plate backing	2.67	2.00	1.33	2.67	2.67	2.33	4.00	1.83	4.00	3.33	4.33	2.67	2.33	4.20	160.43
Slide in cushions	1.00	1.33	1.00	2.00	2.33	3.67	4.33	1.83	3.33	4.00	3.67	3.33	2.00	3.00	145.17
Zipper/button/'snap	1.00	1.33	1.00	2.00	2.33	4.00	4.33	2.17	3.67	3.67	4.00	3.33	1.67	3.00	147.83
System Solutions															
Superficial outer cover for modular seats concept	1.00	1.33	1.00	2.33	2.67	3.67	4.00	1.17	2.00	2.00	3.33	2.67	2.00	3.00	136.50
EA floor and wall mounts	3.67	3.00	2.67	2.67	2.67	2.67	4.33	0.83	2.33	2.00	3.00	2.67	2.33	3.40	165.37
Stiff mounting structure for individual seats	2.00	2.00	3.00	4.00	3.67	2.67	4.00	1.50	3.00	3.00	3.67	4.33	2.67	4.20	183.10
Pedestal at the aisle	1.67	2.00	2.67	4.00	3.67	3.67	3.33	1.50	3.67	4.00	3.33	3.33	2.67	4.20	176.43
Total height increased	3.00	4.00	4.67	5.00	2.33	3.00	3.00	2.50	4.00	4.00	4.33	4.33	2.67	4.20	209.77

In addition, based on the screening of the concepts, several component-level ideas were selected for implementation. They include:

Modular design – In order that a seat design works effectively for one to three occupants, the seat positions should be modular. The bench seat has advantages in cost and cleaning, but safety is paramount in the design.

Bucketing cushions – Utilizing bucket seats can influence lateral motion of the occupant. They can be effectively implemented no matter which energy absorbing method is used and are generally preferable for comfort and maintenance.

Add seatback height – Adding height to the seatback can safely support 95th percentile male occupants in RF configurations and will assist in compartmentalization for both FF and RF configurations.

Additional padding on the head rest – Thicker, firmer padding can better protect the occupant.

Include a knee bolster – A deformable structure helps to minimize the forces on the legs, which tend to be the first objects to strike the seat back in a FF seat configuration.

Each of these component-level ideas was ultimately used in the final design of the seats.

4.2.1 Concept 1: Energy-Absorbing Seat Structure

The primary method of energy absorption with this concept is through permanent deformation of the seat frame when the occupant strikes the seatback. A balance is required to allow some deformation in the form of seatback rotation, either forward or backward, without allowing so much rotation that the occupant is not compartmentalized, i.e., the ATD is thrown into the next row of seats. Simplified analyses were performed to determine how much energy could be absorbed through bending of a tube. Variations in tube diameter, wall thicknesses, and impact height were analyzed. Square tubes were also analyzed. Results from these simplified analyses showed that for a 170-lb. object striking the seat structure at 25 mph, two 1.5-inch diameter tubes or larger, with the appropriate thickness, could absorb the required amount of energy. Two 1.5-inch square tubes could also absorb the required energy in a more efficient manner. The tubes are made of steel with 50 ksi yield strength. Figure 5 shows plots of the energy absorbed versus travel for various tube diameters, thicknesses, and shapes.

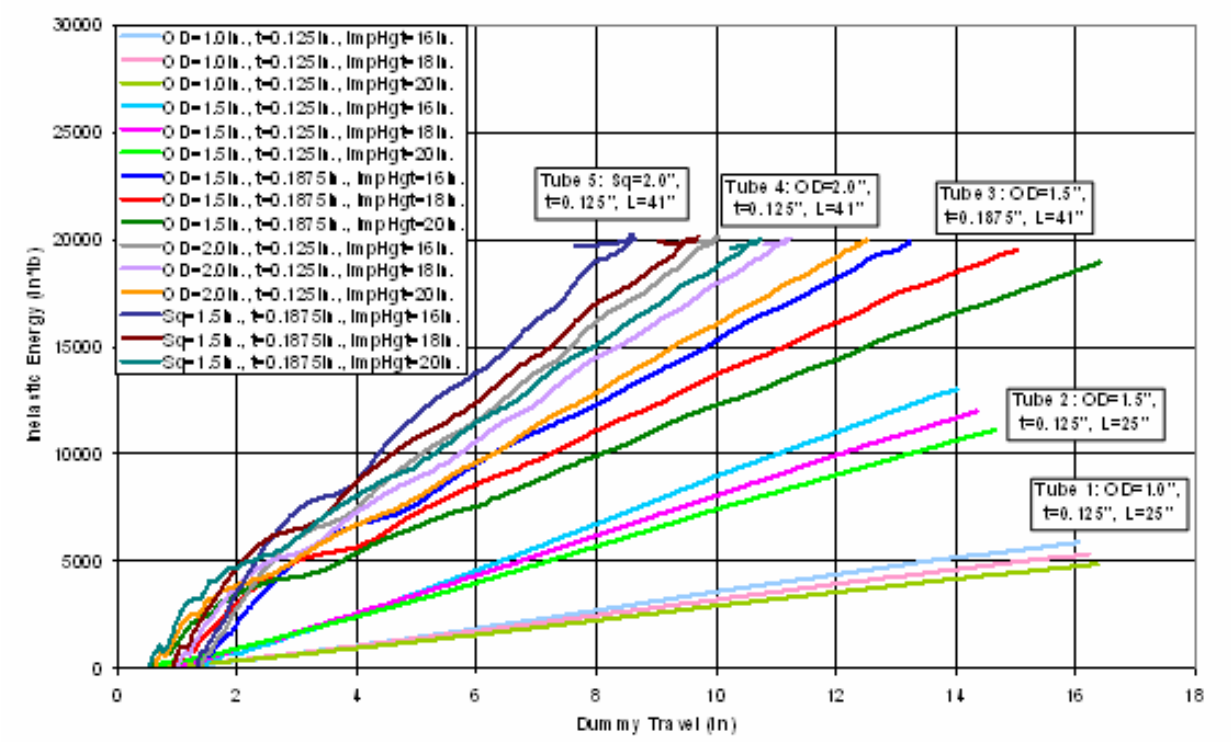

Figure 5. Energy absorbed vs. distance traveled for tube bending under a 170-lb. object striking two tubes at 25 mph

This straightforward concept allows for modification in tube wall thickness and materials to optimize the performance (energy absorbed). Note that deformation must be tightly controlled to absorb enough energy and also ensure the passenger is compartmentalized. In addition, the strength of the tubes will need to be controlled within a reasonable range to be certain the fabricated seat performs as planned.

4.2.2 Concept 2: Energy-Absorbing Mechanism

In this concept, a mechanism is added beneath the seat frame that is intended to absorb the required amount of energy as the seat back pivots.

Figure 6 shows a simplified schematic of one example of this concept. It uses a simple link and slide mechanism that absorbs energy as the slide.

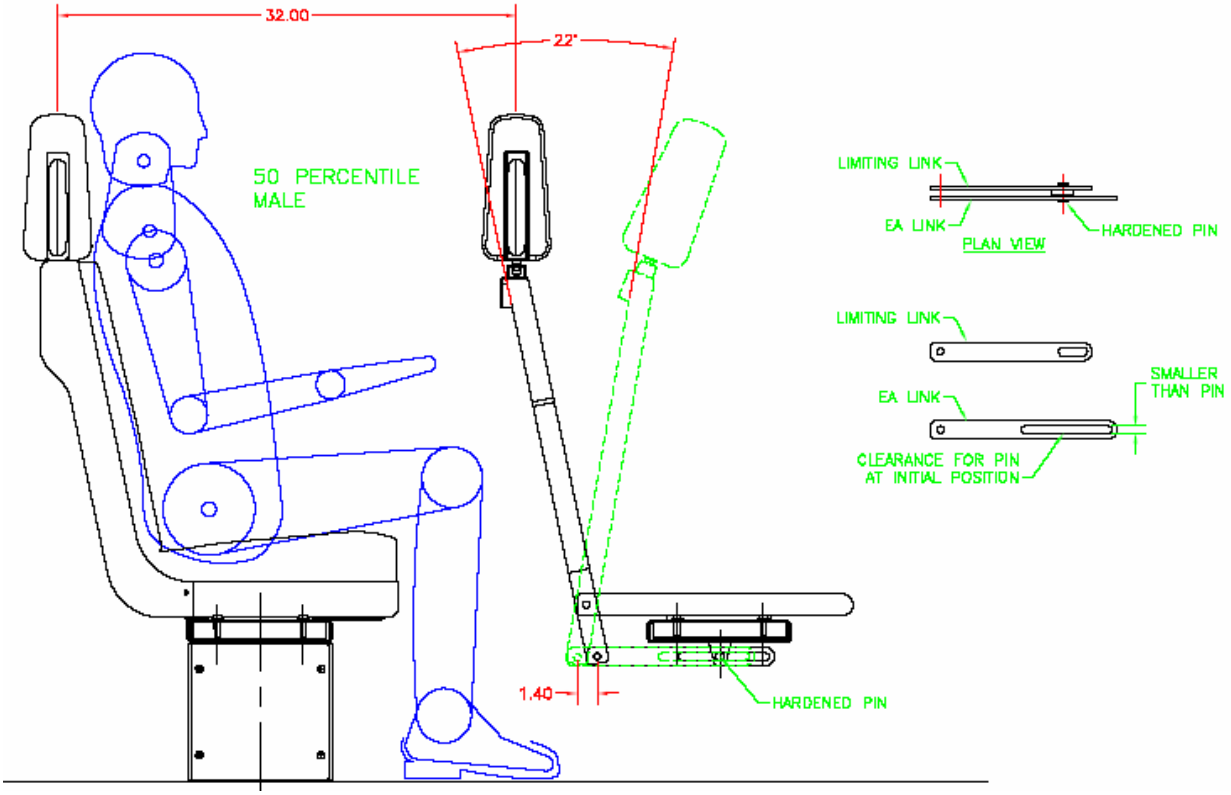

Figure 6. Example of an energy-absorbing mechanism placed below the seat pan

Analyses showed that a mechanism of this nature may not easily be designed to absorb the required amount of energy and operate in the forward and RF configurations. The energy absorption requirements could lead to a mechanism that may be larger than desired. An alternative to this mechanism could be to use a crushable material, such as aluminum honeycomb, which is crushed by a sliding mechanism. The required length of travel of the mechanism and the crush efficiency of the material (typically 60–70 percent) could also lead to a longer than desired crush stroke.

5. Design Summary

5.1 Design for Crashworthiness

The selected seating design is based on a TMS Model M844 modular seating system. This seat provides advantages for crashworthiness and safety and can be adapted for installation in a variety of car types as well as different locations within a car. The seats must protect the passengers in a variety of seating arrangements – one to three occupants seated in either a FF or RF direction.

5.1.1 Individual Seat Frames

It can be challenging to design seat frame components that can absorb the energy of one, two, or three passengers and ensure that the injury levels for all combinations of seated passengers are below the required limits. In this system, each passenger seat position is provided with its own "bucket" and seat frame. The three seat buckets are supported by a common support channel and a single pedestal designed to withstand the loads imposed by the impacts of the passengers during a collision. The individual seat frames allow the system to respond in a manner that is independent of the number of persons seated in the row or which of the seats is occupied.

5.1.2 Tubular Seat Frames

Each seat frame is made of a round, formed steel tube and is designed to absorb energy during a crash whether the seats are oriented in a FF or a RF direction. The frame is designed to deform plastically to absorb energy, but not to the extent that compartmentalization is lost and the occupant is thrown beyond the seat back into the next row.

5.1.3 Cushion Retention Devices

Previous tests have shown that the seat cushions can become projectiles during a collision if they are not securely fastened to the seat. Keeping seat cushions in place is made more difficult by the need to install and remove them periodically for cleaning/maintenance without the aid of a tool. This is an important consideration for some operators because their rules require that a car be put into a shop when tools are needed for any kind of repair. Thus, a back and/or bottom cushion that can be easily installed and removed but that can still remain attached to the seat during a collision is very desirable. For this seat design, the bottom cushion has a retention clip that engages with a retention feature that protrudes from the inside of the seat frame to ensure that the bottom cushion does not come loose during a crash (see Figure 7). Likewise, the back cushion is retained by the bottom cushion and a clip at the top of the seat frame. This arrangement allows easy installation without tools and has been shown to be effective in previous FF dynamic tests. An additional feature was needed to prevent the knees of a passenger seated behind from damaging and/or pushing out the back cushion upon impacting the seat back. For this reason, a thin plate welded to the vertical tubes of the seat frame is used as a knee brace (also shown in Figure 7).

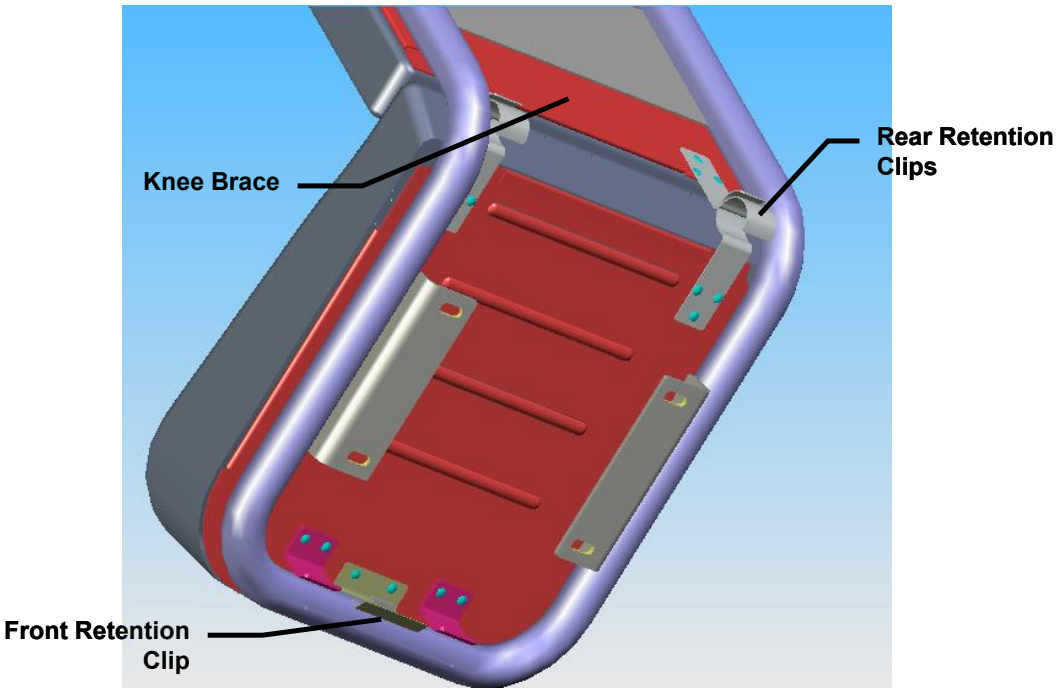

Figure 7. View of the seat pan cushion and frame from below the seat showing the retention clip engaged with the feature on the seat frame (the shroud has been removed)

5.1.4 Seat Back/Headrest Height and Padding

Another feature of the modified seat design is the taller seat back/headrest surface to help maintain occupant compartmentalization. Due to the time and cost of creating new tooling for plastic seat shrouds, the original seatback height was used in this design. The headrest was made taller to help prevent loss of compartmentalization and to keep the head of each passenger from rising above the headrest so as to avoid neck injuries. For RF passengers, the taller headrest better supports the back of the head in a collision. It has been observed in previous tests that a seat with only limited vertical head support can cause a serious neck injury to a passenger involved in a collision while seated in the RF orientation.

Another feature of the new seat design is the use of headrest padding with higher-density foam to minimize head injury levels when a FF passenger impacts the seat back during a collision.

5.2 Safety

The seats were designed to meet the performance requirements of APTA Specification SS-C&S-016-99 Rev. 1, and FRA Regulation 49 CFR 238.233. Sled testing performed for the baseline two-person seat in a two-occupant, FF configuration demonstrated that these seats meet the injury requirements of the APTA seat standard. All the materials used for seat construction were selected to meet the latest flame and smoke requirements.

5.3 Modular Design

The design of the seat is modular, making it adaptable to a variety of passenger railcars. The ability to easily exclude a module without having to re-design components of the seat was one of the reasons this design was selected. Table 6 lists the available modules and identifies those that

were used and/or modified in this program. For simplification, the armrests were not used or modified for this project, as they were not likely to influence the crashworthiness of the seats. Each seat component used from the original TMS design was modified in order to meet the design objectives of this project.

Table 6. Original two-person seat modules and components used and/or modified to make the three-person seat

Seat Module/Component	Used	Modified
Seat Bucket (including back and bottom cushion and frame)	•	•
Armrest		
Headrest – single	•	•
Seat Support Channel	•	•
Pedestal	•	•
Headrest Foam	•	•

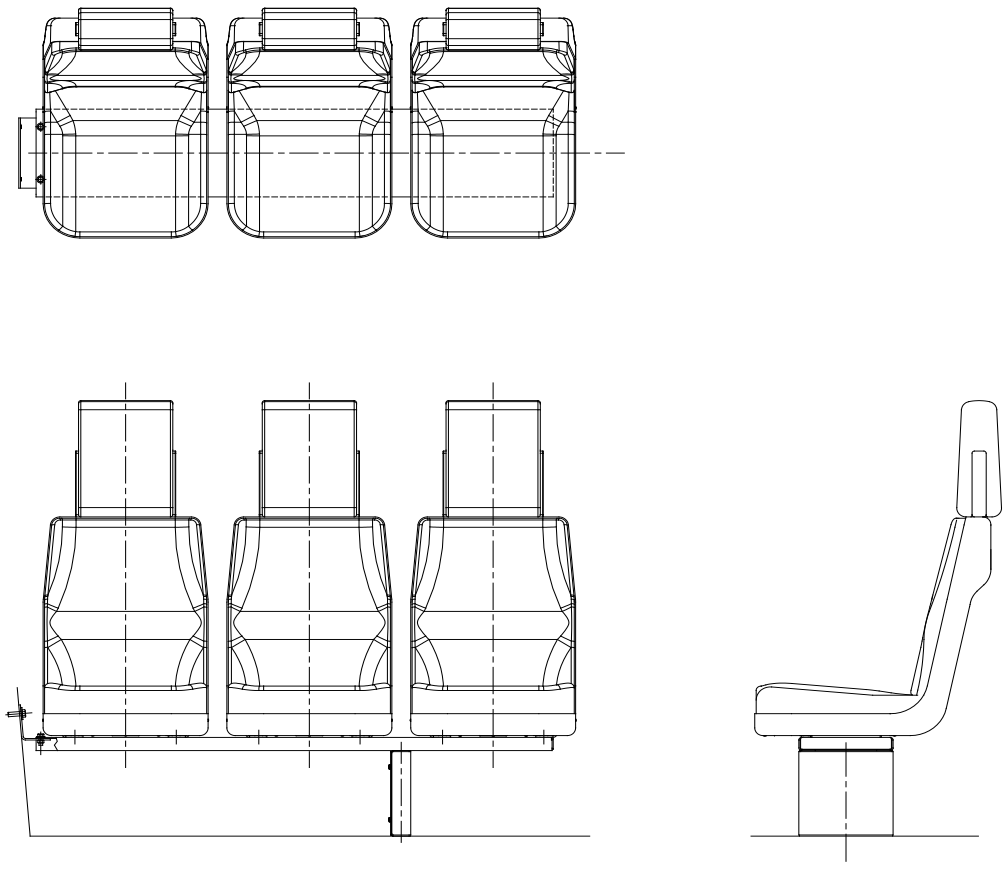

Figure 8. Front, side, and top views of the new three-person seat without handle holds or armrests

Figure 8 shows the seat as supplied for this project. Several modifications were made to the existing two-person seat configuration, including:

- Longer support channel to support 3 buckets
- Modified pedestal position
- Removal of grab handles
- Stronger material for seat frame tubes (nominally)
- Taller headrest to better support and protect the head of a passenger
- Stiffer headrest foam
- Increased length for pedestal weldment (requested, but inadvertently not implemented)

5.3.1 Modified Support Channel

The new seat design needed a longer seat support channel (Figure 9) to meet the requirement that the seating system be capable of seating three 50th percentile male ATDs. The baseline seating system had been designed for two seating positions per row. The length of the baseline seating system's support channel was increased from approximately 39 inches to almost 55 inches to accommodate the additional seat position. Analyses of the seating system (see Section 7) showed that the longer support channel could sustain the loads imposed by three 50th percentile male ATDs in collisions in FF and RF seating configurations.

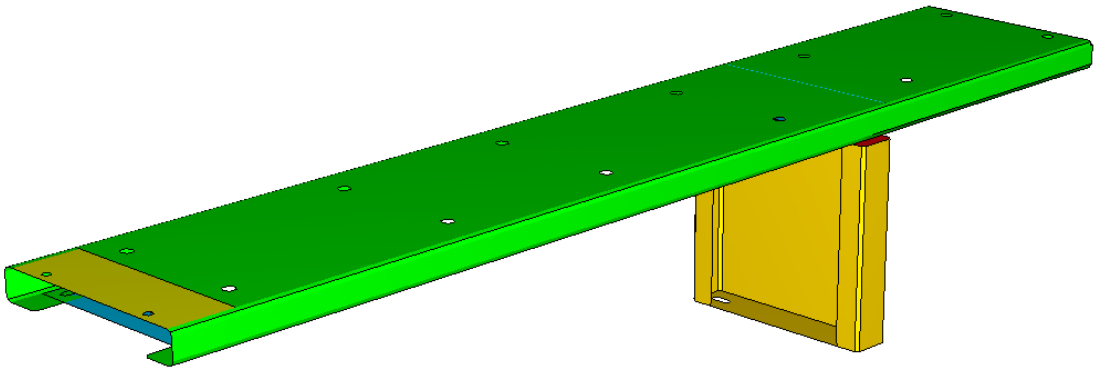

Figure 9. Modified seat support channel and pedestal location

5.3.2 Modified Pedestal Position

The longer seat design, when compared with the baseline design, requires that the location of the pedestal be modified. The pedestal in the three-person seat design was placed between the middle seat and the aisle seat. The attachment of the pedestal to the floor as well as to the support channel is accomplished with two 3/8-inch diameter bolts.

Figure 9 also shows the modified position of the pedestal. The position can be adjusted laterally to accommodate seat tracks in the passenger cars.

5.3.3 Modified Headrest

One of the issues identified in previous seat testing projects was the possibility of neck injuries due to the low height of the headrest, particularly when the seat is in the RF configuration. The concern for possible neck injury caused by the head not being completely supported as the seated occupant slides upward against the seat back suggests that either the length of the seat back or the headrest could be modified to reduce the chances of this type of injury occurring. Due to the long time and high cost associated with making new tooling for a new seatback shroud, it was decided that the headrest should be made taller to support the head and demonstrate this improvement without the need for a new seatback shroud.

The basic design of the headrest was the same as for the baseline seat. The headrest frame was elongated vertically by 2.5 inches to increase head support during a collision. The associated foam, upholstery, and inner headrest pan were also made larger to accommodate the revised frame.

One of the results of testing of the baseline design was that the head injury level, although below the requirement, was very close to the limit. In order to reduce the HIC level, firmer foam was used for the new design. The foam used in the headrest is Chestnut Ridge CR Safguard Extra Firm (65–85 IFD), the stiffest foam offered of this type by the manufacturer. This foam is significantly stiffer than the 45–65 IFD foam used in the baseline seat design. The firmer foam may decelerate the head more rapidly than the softer foam during compression, but it may prevent even higher head decelerations that occur after the soft foam bottoms out and the effective stiffness is then significantly higher.

5.3.4 Modified Pedestal

The original design of the pedestal called for intermittent welds between the pedestal frame and the pedestal bottom plate and between the pedestal and the floor channel. Preliminary analyses of the seating system highlighted that the pedestal bottom and top should be continuously welded to provide sufficient strength to keep the seat securely fastened to the floor.

Miscommunication of this need to the seat designer resulted in the pedestal being fabricated with intermittent welds, as originally designed in the baseline seating system. While such intermittent welds have been adequate in testing where two occupants were involved, the addition of a third occupant caused the pedestal to fail during the full-scale CEM train-to-train test [3]. Based upon a review of the failure and subsequent analysis, the pedestal was redesigned to include a bolted connection to the floor.

This modified design was sled-tested at Armor Holdings in October, 2006. The results of this test revealed that the vertical loads at the bolted connection to the floor exceeded the capacity of the bolts in the RF 12g test. Based upon a review of data from this test, the pedestal and channel designs were modified again to increase the size of the bolted connections.

5.4 Design Revision #1

The initial design of the crashworthy seating system described above was evaluated as one of several experiments performed as part of the CEM train-to-train collision test [3] that was conducted at TTC in Pueblo, Colorado in March, 2006. During the test, the welded connection between the RF seat pedestal and the floor failed at a vertical tensile load of about 6,800 lbf, causing the seat backs to rotate to a much larger extent than intended.

Based on the results of this test and subsequent analyses, the following revisions were made to the design of the seating system:

- The thickness of the material used to construct the pedestal was increased from 0.060 inch to 0.125 inch.
- The intermittent weld between the pedestal frame and bottom plate was replaced by a continuous weld.
- Bolted angle brackets were added at the four corners of the pedestal to provide redundant connections between the pedestal frame and bottom plate and between the pedestal and the channel.
- A seat channel cover plate was added to reduce twisting of the channel.
- A doubler plate was added to the seat channel where it is bolted at the car wall to prevent local deformation in this region.
- A rubber block was added to help retain the cushions during the RF test.

The revised pedestal is illustrated in Figure 10. The revised design includes a set of four angle brackets that provide bolted connections between the pedestal frame and the pedestal bottom plate and between the pedestal frame and the support channel. These connections provide redundancy to the welded connections.

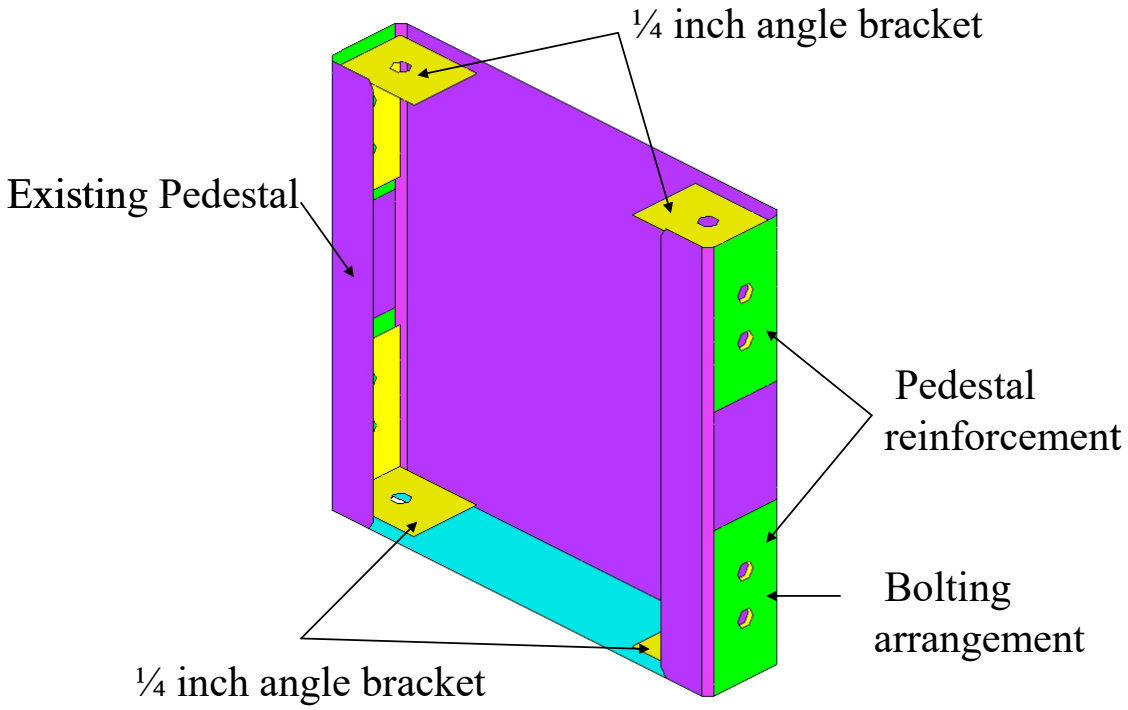

Figure 10. Revised pedestal design

Quasi-static finite element analyses (FEA) of the RF test showed excessive twisting of the seat channel. A cover plate was added to the bottom of the channel to make it more of a box-like section. Figure 11 shows the bottom view of a seat channel with the bottom plate welded to it. The cover plate is a 0.125-inch (3.2 mm) thick stainless steel plate that is welded at its sides to the channel.

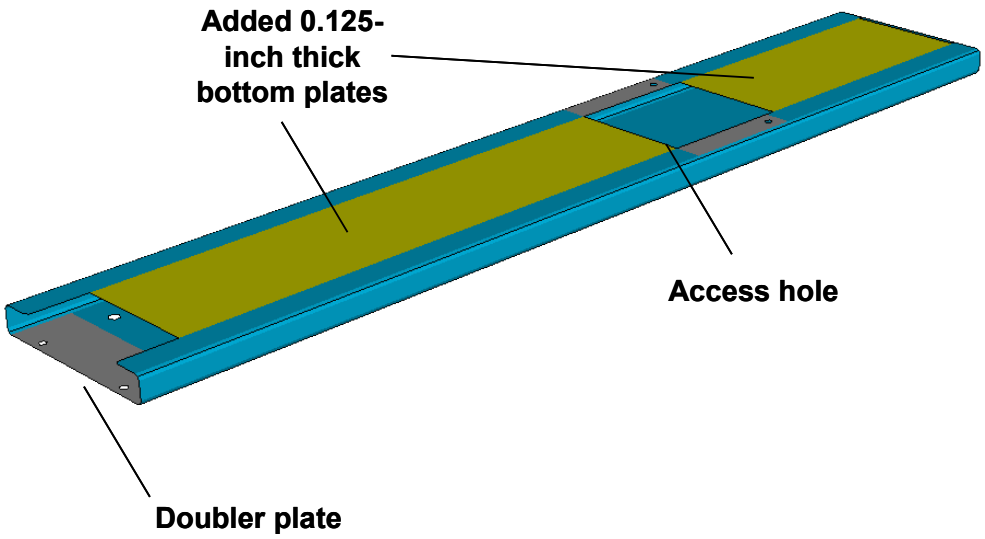

Figure 11. Modified seat support channel effectively closed off to form a box-type structure more resistant to twisting

Note that FEA were run that featured interrupted covers welded to the bottom of the channel, but the results of these calculations showed that there was still too much twisting compliance. A full-length cover plate, as shown in Figure 11, was determined to be the best solution, effectively making the open channel section into a closed box section for the majority of the seat channel. It is likely that lightening holes could be put in the cover plate to reduce weight and not greatly affect the compliance.

5.5 Design Revision #2

The revised design was dynamically tested at Armor Holdings in October, 2006. During the RF seat test, the pedestal connection to the floor again failed, despite the increase in strength of the connection. Load cell data indicate that the tensile load in the forward pedestal bolt reached 13,600 lbf prior to failure, nearly twice as great as the peak vertical force measured in the CEM train-to-train test. Because the connection to the floor again failed, a second revision of the design was made to improve seat attachment strength in the RF seat configuration. The following additional design modifications were incorporated:

Cushion-to-Seat Attachment

1. Additional seat cushion restraints were welded to the tubular seat frame to keep the cushions from popping out during impact.

Seat-to-Channel Attachment

2. An additional rivnut (i.e., a one-piece, internally threaded and counter-bored tubular rivet) was placed in the bracket that connects each seat module to the channel. Each additional rivnut was located so that there were two rivnuts on the forward side of the bracket, which was loaded in tension during the more stringent RF collision.

3. A slot was added to each frame mounting bracket to accommodate the additional rivnut.
4. Welds were added between the existing intermittent welds where the seat brackets are welded to the seat tubing, essentially making them continuous welds.

Channel-to-Pedestal Attachment

5. Larger (0.5-inch diameter) Grade 8 bolts were used for the pedestal-to-channel connection. These were installed upside-down to avoid interference with the doubler plate that was added to the top of the new pedestal.
6. The holes were opened up from 0.416 inch to 0.532 inch to accommodate the larger bolt size.

Pedestal-to-Floor Attachment

7. Larger (0.625-inch diameter) Grade 8 bolts were used for the pedestal-to-floor connection.
8. The widths of the slots cut into each end of the bottom plate of the new pedestal were increased from 0.532 inch to 0.656 inch to accommodate the increased bolt size.

Channel to Wall Attachment

9. Larger (0.5-inch diameter) Grade 8 bolts were used for the wall connection.
10. The bolt holes at this location were opened-up from 0.416 inch to 0.532 inch to accommodate the larger bolts.

The tensile strength (36,500 lbf) and shear strength (27,900 lbf) of the 0.625-inch diameter floor bolts provide sufficient safety margins relative to the expected 13,000–15,000 lbf tensile force and 2,500 lbf longitudinal force expected to arise at these locations during the RF dynamic sled test. The strength of the half-inch bolts provides even greater margins relative to expected loads.

6. Seat Component Testing

This section describes component tests performed in TIAX laboratories in support of the development of the seat design. Two types of tests were performed:

- Seat tube bending
- Headrest and seat foam compression

All the tests were quasi-static. A description of each of these tests is presented in the following sub-sections.

6.1 Seat Tube Bending Tests

Because of their importance to the overall crashworthiness of the seats and uncertainties regarding the exact strength properties of the material, the tubes forming the frame of the seats were tested in bending.

6.1.1 Specimen and Fixture Design

A total of three sets of tube bending specimens were made, all using 1.5-inch OD tube made from A572-50 steel. The first two sets of tubes were procured from TW Metals in Agawam, Massachusetts and formed by All Metal Fabricators in West Acton, Massachusetts. Based upon preliminary analysis results, these tubes were selected to have thicknesses of 0.095 inch and 0.109 inch. These thicknesses were greater than the 0.083-inch thick tubing used in the existing TMS seat. Later in the program, when it was learned that the steel tube material that TMS was using had a yield strength of over 70 ksi (despite the fact that A572-50 is rated to have a minimum yield strength of only 50 ksi), a third specimen with a thickness of 0.083 inch was cut directly from a seat provided by TMS and tested.

Figure 12 shows a sketch of the tube bending test specimen. To load the test specimens in a manner similar to how they are expected to be loaded in practice, they were designed to have a 102-degree bend. The specimen was designed so that the section of the tube that represented the seat bottom was long enough to be held along several inches of its length and still allow enough length of tube for the focused deformation at the bend. The part of the tube representing the seat back was made long enough to apply a load parallel to the seat base part of the tube with a moment arm of about 14 inches. This moment arm was chosen to keep the total load below the 1,000 lbf capacity of the Instron testing machine and still provide for the application of a bending moment that was consistent with the research team's expectations for the seat experiment.

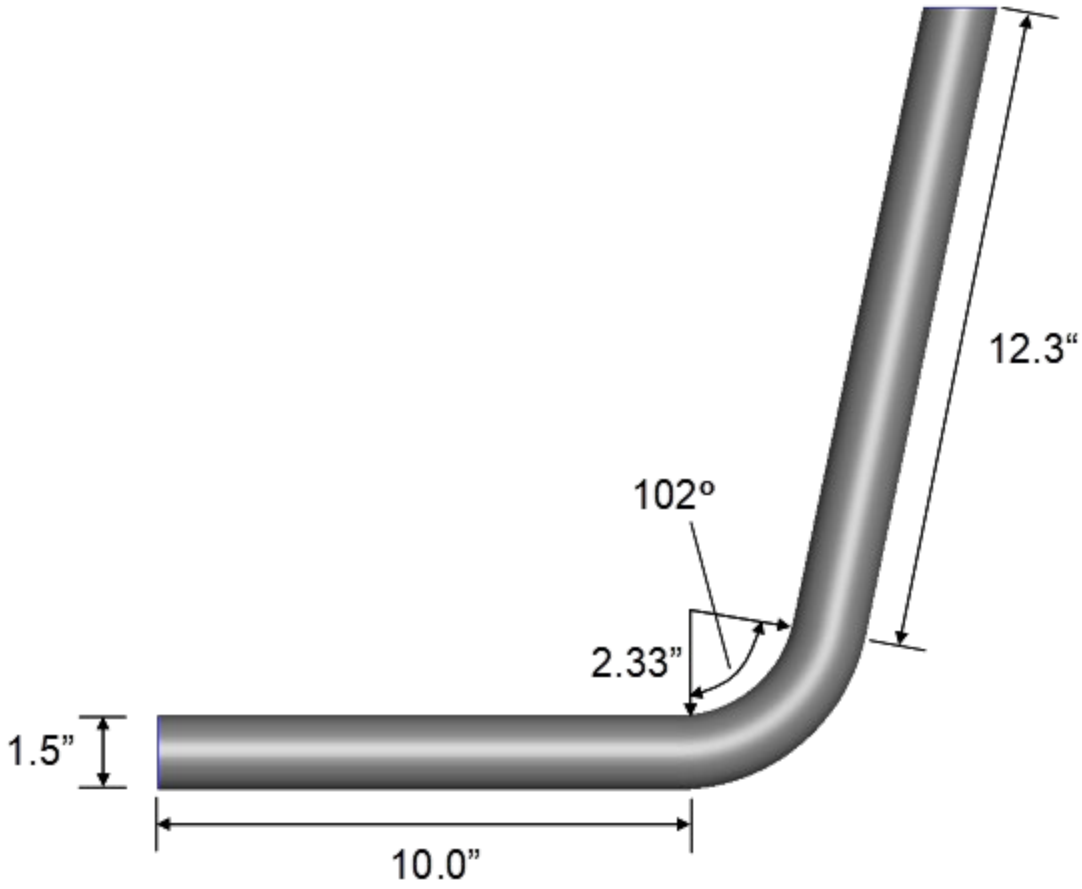

Figure 12. Tube bending specimen

To constrain the section of the tube that represents the seat base and support the load applied to the section of the tube that represents the seat back, a fixture was designed and constructed. The fixture, as shown in Figure 13, was constructed of steel. It consisted of the following pieces:

- A C-channel, approximately 22.5 inches long, 4 inches wide and 1.75 inches in height, with a thickness of 0.31 inches
- An 8-inch long pipe, welded at one end to the base of the channel, about 1.5 inches from one end; this pipe has a 2-inch outer diameter and a 1.56-inch inner diameter (a wall thickness of 0.22 inch).
- A 1.31 by 1.31-inch angle, approximately 7 inches long, welded to the base of the channel on one of its ends and to the pipe on its other end; the angle increases the bending resistance of the fixture significantly.

The C-channel had holes cut through it so that it could be bolted to the Instron table. Threaded holes were tapped into the pipe at approximately 1 inch and 6 inches below its top end so that set screws (with knobs mounted on them) could be used to manually fasten the seat tube to the pipe. With these screws tightened onto the seat tube, it behaved as a cantilevered beam.

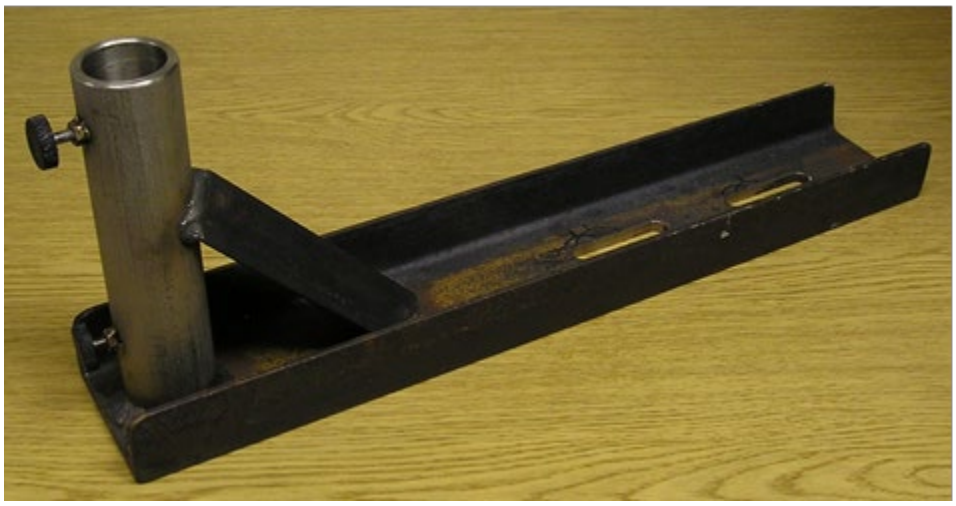

Figure 13. Fixture used to hold the tube bending test specimen

6.1.2 Test Setup and Procedure

Figure 14 shows a tube specimen inserted into the fixture and placed into the Instron testing machine. The base of the channel had two 3-inches long by 0.5-inch wide slots cut into it. These slots were positioned 12 inches and 17 inches away from the center of the pipe and were used to fasten the fixture to the Instron table during testing. The slots permitted adjustment of the applied moment.

The constrained end of the tube was held vertically in the fixture, approximately 14 inches from the center of the applied load. The initial test was performed using a grip with a cylindrical head with a diameter of approximately 2 inches, oriented with its flat end facing the specimen. This resulted in a moment-rotation curve that was not smooth, as the load application point (and moment arm) changed from one side of the head to the other during the test. For the remaining tests a grip with a semi-cylindrical head of diameter 0.5 inch, oriented with its axis perpendicular to the specimen so that its rounded outside surface faced the specimen, was used to transfer load to the tube. This change resulted in a smooth moment-rotation curve. Tests were conducted at a rate of 1.0 inch per minute. Data were collected and recorded electronically at displacement intervals of 0.00183 inch.

Figure 14. A pre-test photograph of A572-50 tube bending specimen inserted into the fixture and mounted on the Instron testing machine

6.1.3 Results

A total of five tests were run. The results of these tests are summarized in Figure 15. As noted, the first test conducted – for a tube thickness of 0.109 inch – used a round, flat-bottomed loading head (as shown in Figure 14). For this reason, the moment-rotation curve had an undulation in it. For the remaining tests, the smaller-diameter, rounded head was used and the associated curves were all smooth.

Note that the moment that develops for the 0.083-inch thickness tube was actually higher than the moment for the 0.095-inch tubes. This appeared to be due to the very high yield strength of this particular tube. Material certifications indicate that, despite the fact that this material is A572-50, a nominally 50 ksi yield material, its actual yield strength is over 70 ksi. So, even though the preliminary modeling suggested that a tube stronger than those used in the baseline TMS two-seat system would be required, in the end the tube thickness did not need to be increased, assuming that all of the 0.083-inch thick tubes have a similarly higher-than-specified yield strength.

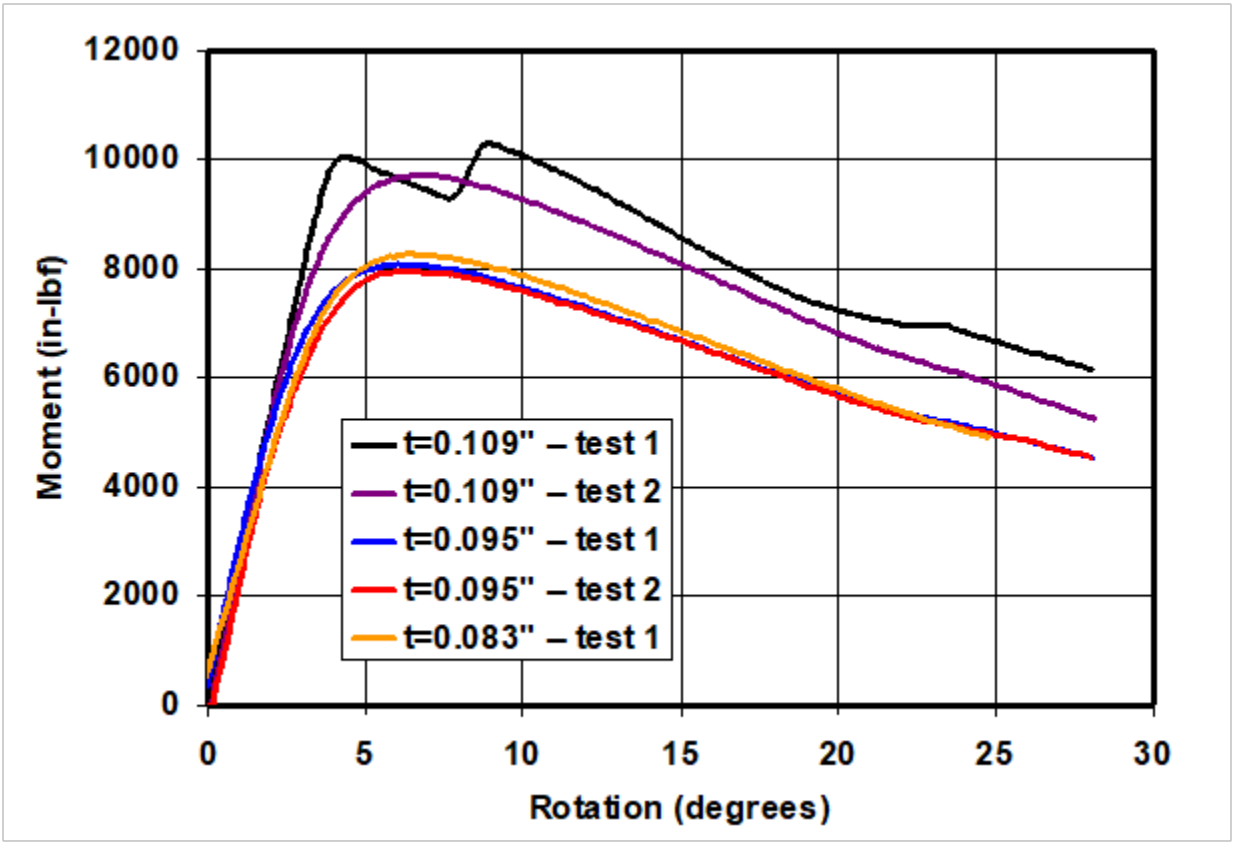

Figure 15. Moment-rotation results for seat tube bending tests

6.2 Foam Compression Tests

Due to concerns regarding the potential for impact of an occupant's face into the headrest in front of him or her during a FF collision, foam compression tests were performed to evaluate the performance of the foam used in the headrests. The baseline TMS seats use a grade of seat foam referred by the manufacturer as "Firm." The foam is also available in a stiffer version referred to as "Extra Firm."

To quantify the difference between these variations of foam and to determine parameters for the foam for use in the finite element modeling of seat performance, specimens of Firm and Extra Firm foam were tested in uniform compression.

6.2.1 Test Setup

Figure 16 shows one of these specimens in the Instron testing machine prior to testing. The 3-inch square by 2-inch thick specimens were cut out of a larger sample provided by the manufacturer. They were compressed between steel plates at loading rates ranging from 1.0 inches per minute to 50.0 inches per minute.

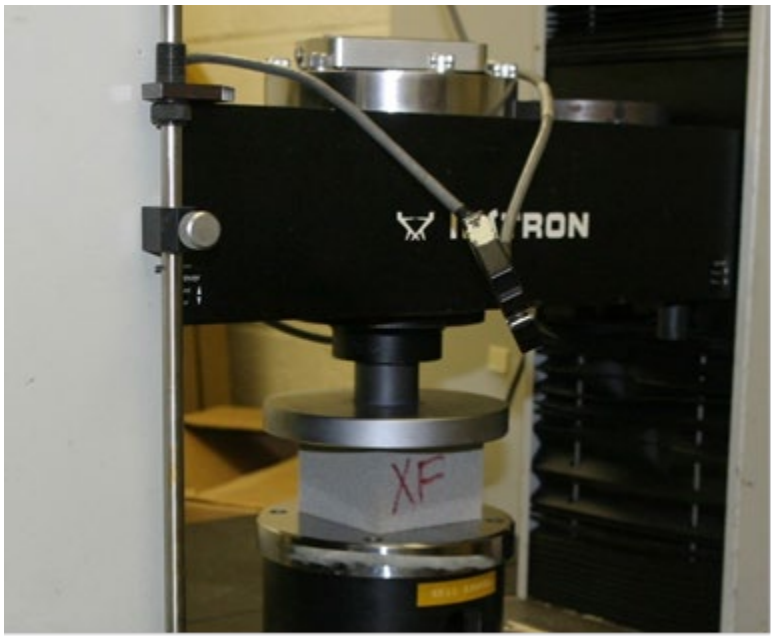

Figure 16. Test setup for headrest foam compression tests

6.2.2 Test Results

The results of the foam compression tests conducted at 1.0 inch/minute are summarized in Figure 17. As expected, the test results indicated that the compressive force in the foam increased with continued compression at a relatively small rate until the specimen was crushed by about 60 percent. From this point onward, the load began to increase rapidly due to consolidation of the foam. A comparison of the relative behavior of the two foams indicated that the Extra Firm foam was capable of absorbing about twice as much energy as the Firm foam after 1 inch of crush. Based upon these results, the Extra Firm foam was selected for use in the headrests. Data from the Extra Firm foam compression test conducted at 1.0 inch/minute was inserted into those finite element models that included the seat foam. Note that the tests conducted at higher loading rates were inconclusive as to the effect of the loading rate on the compressive behavior and may have been susceptible to local buckling of the foam and bulging due to friction between the foam and the plates.

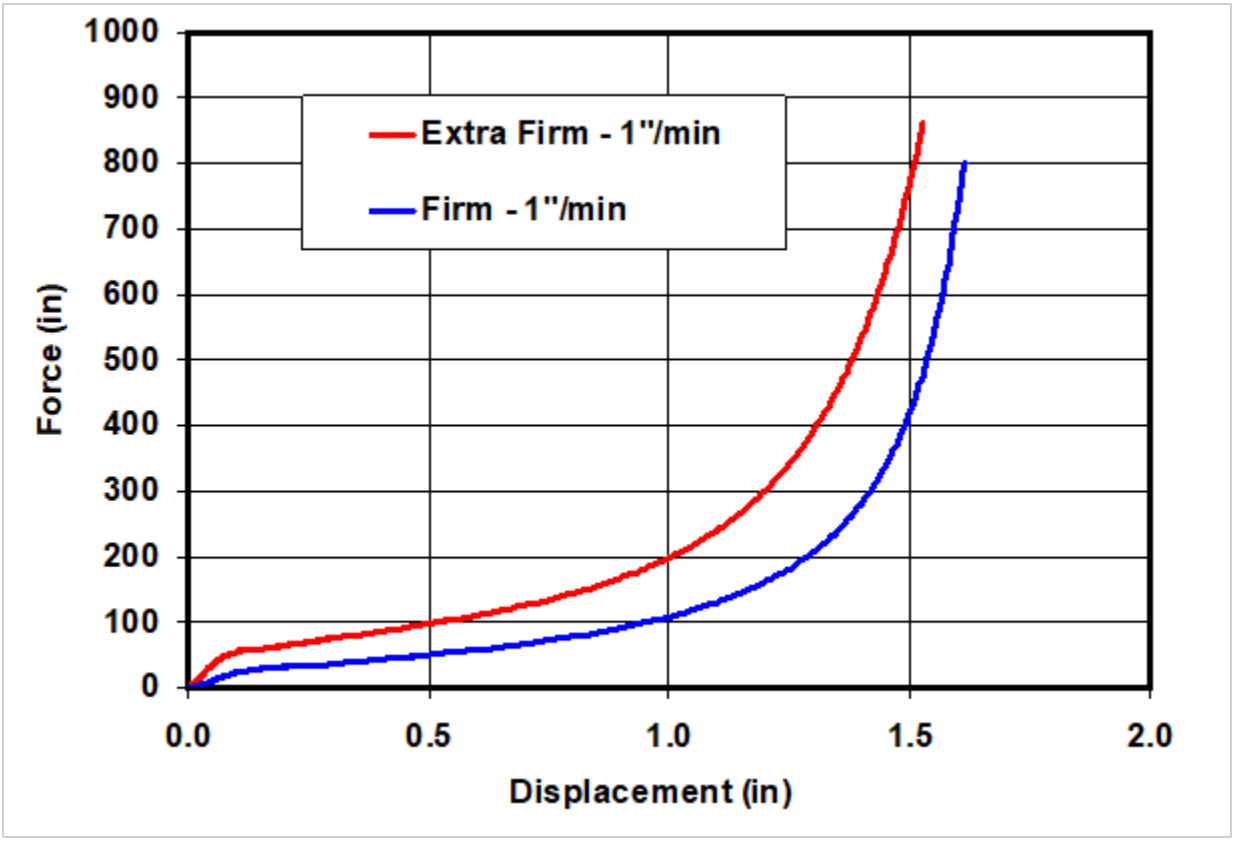

Figure 17. Results of headrest foam compression tests conducted at 1.0 inch per minute

7. Seat Design Analysis

In this section, the results of analyses supporting the design of the seating system are summarized. Two types of analyses were conducted: FEA, using Abaqus [7], and occupant dynamics analyses, using MADYMO (**MA**thematical **DY**namic **MO**del) [8].

FEA were used primarily to determine the force-crush characteristics of the seating system and to evaluate the structural integrity of the seat.

MADYMO analyses were performed to predict the behavior of the seat and its occupants during FF and RF collision scenarios and to evaluate occupant response relative to acceptable limits for a number of injury criteria.

7.1 Finite Element Analyses

Several FEA were conducted to help develop the design of the crashworthy seating system and ensure that it met performance requirements. FEA results were also used to characterize moment-rotation behavior of the seat back and headrest for input to subsequent MADYMO runs.

In the sub-sections below, the results of these simulations are summarized.

FEA models were developed in this program to simulate:

- Energy absorption behavior for a one-dimensional, single-degree-of-freedom (SDOF) dynamic system representing the collision between the occupant and the seat
- Bending of a seat tube specimen
- Bending of the headrest frame due to impact from behind
- Occupant impact loading of a single seat
- Multi-occupant loading of the full three-seat system

7.1.1 One-Dimensional Occupant/Seat Collision Model

To help address some questions that arose during the program regarding the amount of energy that is absorbed when an occupant is subjected to an 8g triangular pulse and collides with either the occupied seat back in a RF collision or the forward seat back in a FF collision, a series of one-dimensional SDOF analyses were performed using Abaqus. These analyses were focused on evaluating the mechanics of this collision and in particular the effect of applying an 8g acceleration pulse to the system as well as the effect of seat spring characteristics. A schematic of the model is shown in Figure 18.

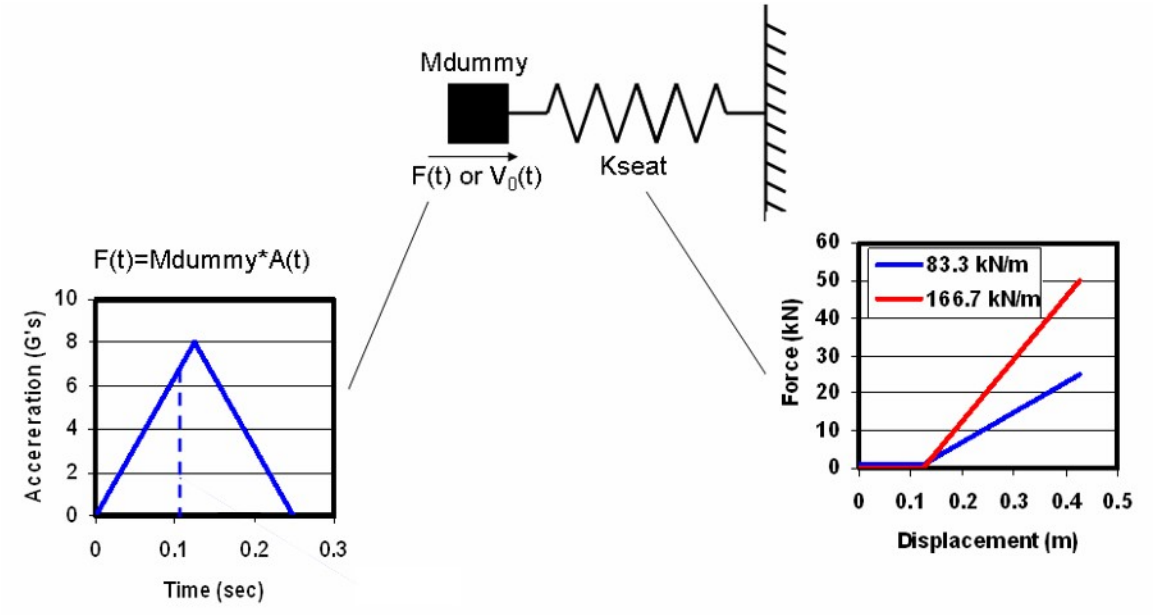

Figure 18. A schematic of the one-dimensional, SDOF dummy/seat model

The results of the one-dimensional analyses indicated that there were three primary determinants of the energy absorption requirements:

1. Crash pulse
2. Free-flight distance
3. Force-deflection characteristics of the system (occupant plus seat)

The results further suggested that the effective compliance of the occupant caused the total energy absorption requirements for the system (occupant plus seat) to increase, but at the same time the occupant absorbed a significant amount of energy itself, so that the energy absorption requirement for the seat actually decreased.

7.1.2 Tube Bending Model

The tube bending model was used to evaluate the moment-rotation behavior of the seat back. The results of the model were used to select tube sizes for testing.

The model for simulating the bending of a seat back tube forward is shown in Figure 19(a). The model was constructed to match the geometry, fixturing, and loading conditions of the tube bending tests described in Section 6.1. A similar model, with the rigid load application block repositioned to the underside of the end of the tube and reversed in its orientation (upwards relative to the tubes shown in Figure 19(a)) was also constructed.

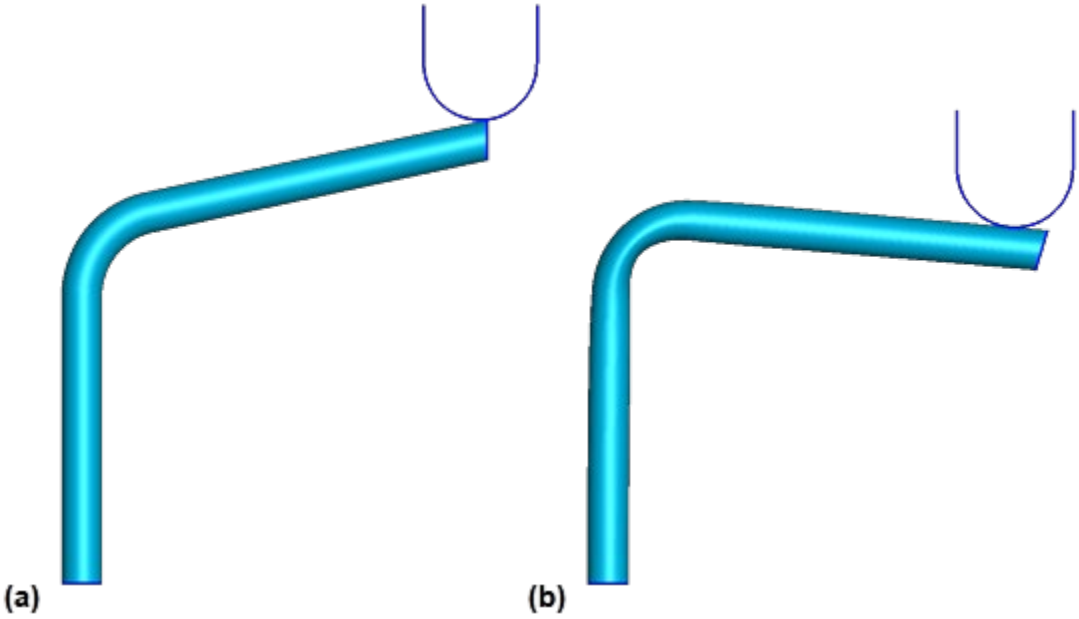

Figure 19. The seat tube *forward* bending FEA model
(a) undeformed; (b) deformed to 4.0 inches

Figure 19(b) shows the deformation of the tube predicted by the model for a load-point displacement of 4.0 inches for one of the tube thicknesses evaluated. In this analysis, a 0.083-inch tube thickness was modeled, with properties assigned based on the certification that came with the material (Sy=70 ksi) as opposed to the minimum value required by the specification for this material (Sy=50 ksi).

The predicted moment-rotation behavior for the 0.083-inch tube is shown in Figure 20.

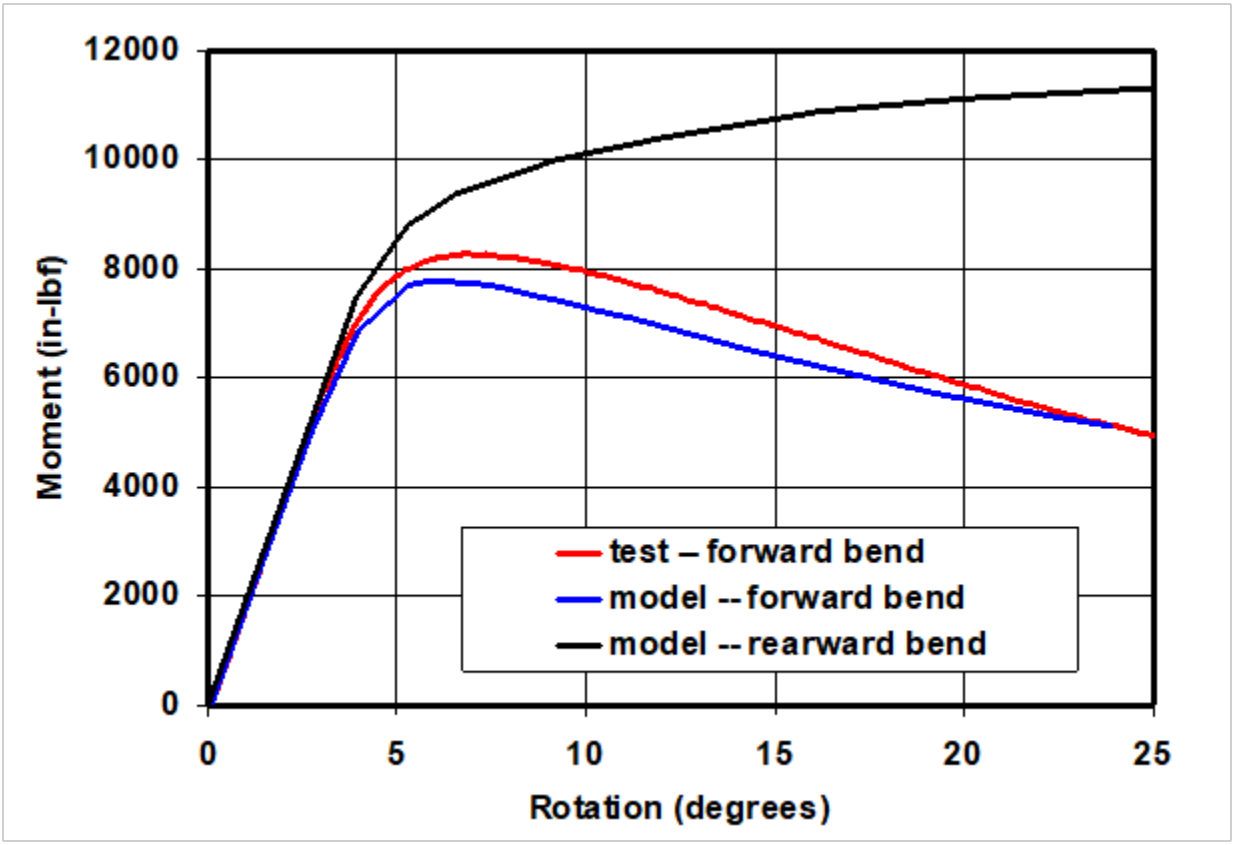

Figure 20. FEA predictions of seat tube moment-rotation behavior

For the forward bending of the seat tube, as illustrated in Figure 20, the FEA model predicted a peak moment about 5 percent lower than the value measured in the test. This difference was likely due to hardening that occurred when the seat tube was bent during manufacturing. Such hardening was not accounted for in the model.

For this same reason, FEA predictions of moment-rotation behavior in the *rearward* bending direction, also shown in Figure 20, were likely to be a few percent lower than measured values for rearward bending.

7.1.3 Headrest Models

Two FEA models were developed for the headrest: one to determine the moment-rotation behavior of the headrest frame and another to determine the force-displacement behavior of the headrest foam, both of which were later used in the MADYMO calculations.

7.1.4 Headrest Frame Bending

The headrest frame bending model is illustrated in Figure 21(a). In this analysis, a quasi-static load was applied to the back center of each of the two vertical support bars. The seat back tube was assumed to be fixed. The predicted moment-rotation behavior is shown in Figure 21(b), together with a simplified, multi-linear fit to the data.

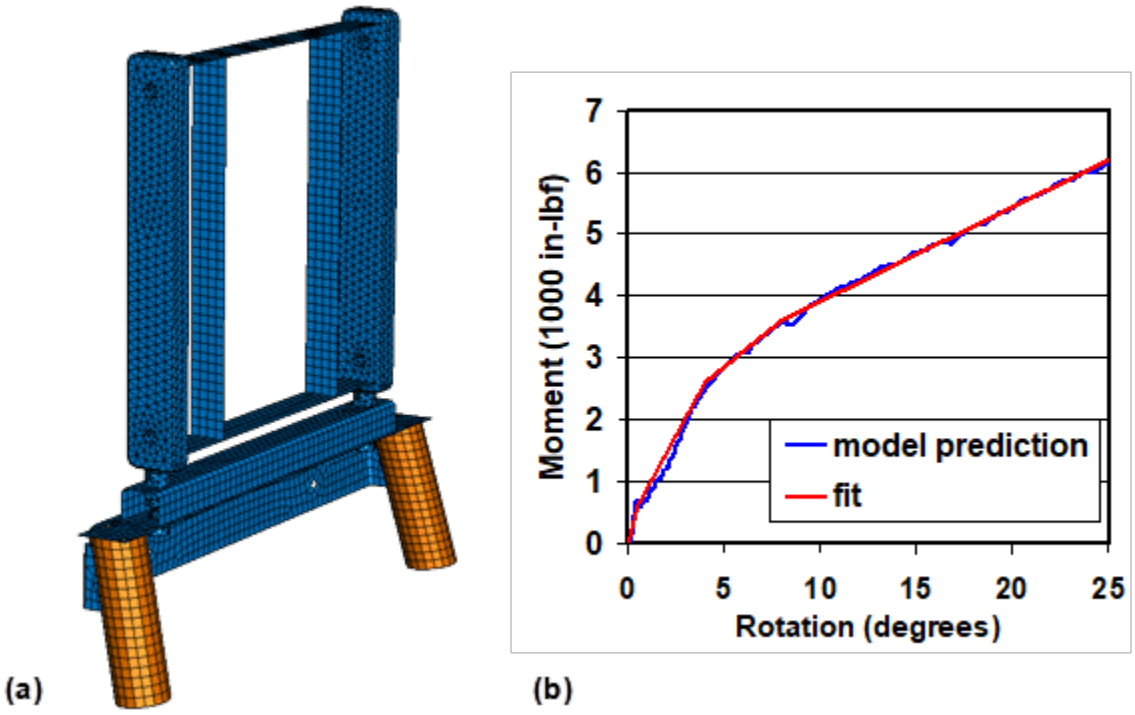

Figure 21. (a) FEA model for bending of the headrest frame; (b) predicted moment-rotation behavior of the headrest frame, including a simplified multi-linear fit supplied to MADYMO

7.1.5 Headrest Foam Crush

The compliance of the foam at the back of the headrest was determined for an impact loading of a rigid object with roughly the shape of a human head. The mesh for this model is shown in Figure 22(a). The model for the headrest included the headrest frame shown in Figure 21(a) plus the headrest foam and foam-to-frame support plate. The analysis was conducted using Abaqus/Explicit with a slow impact velocity of 10 in/sec (essentially quasi-static conditions). Properties for the foam were determined based upon the compression tests described in Section 6.2. Results for two impact locations that bound the likely head impact locations are shown in Figure 22(b).

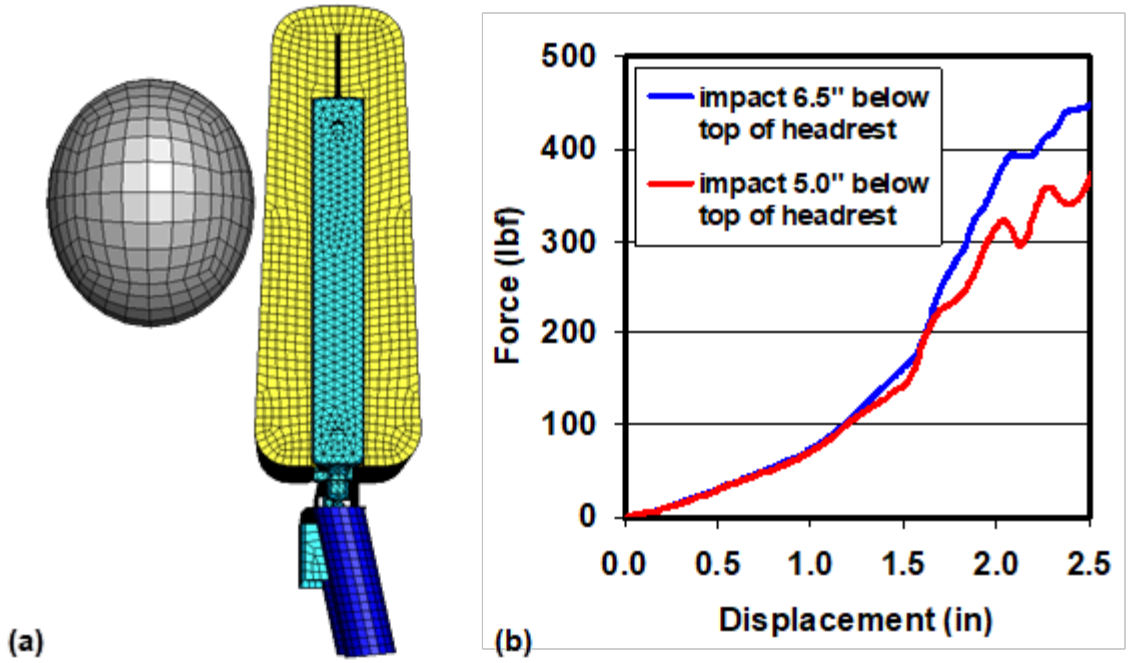

Figure 22. (a) FEA model for crush of the headrest foam; (b) predicted force-displacement characteristics for two impact locations

7.1.6 Single-Seat Models

Early in the program, a single-seat model was developed to evaluate some of the design alternatives developed through the concept generation process. Two examples of such models are shown in Figure 23. The one on the left (Figure 23(a)) used a square cross-section tube, as used in some existing commuter seats, instead of a round tube. The one on the right (Figure 23(b)) included an energy-absorbing mechanism at the attachment to the seat channel. Each model simulated the impact of a FF occupant just below the top of the seat back.

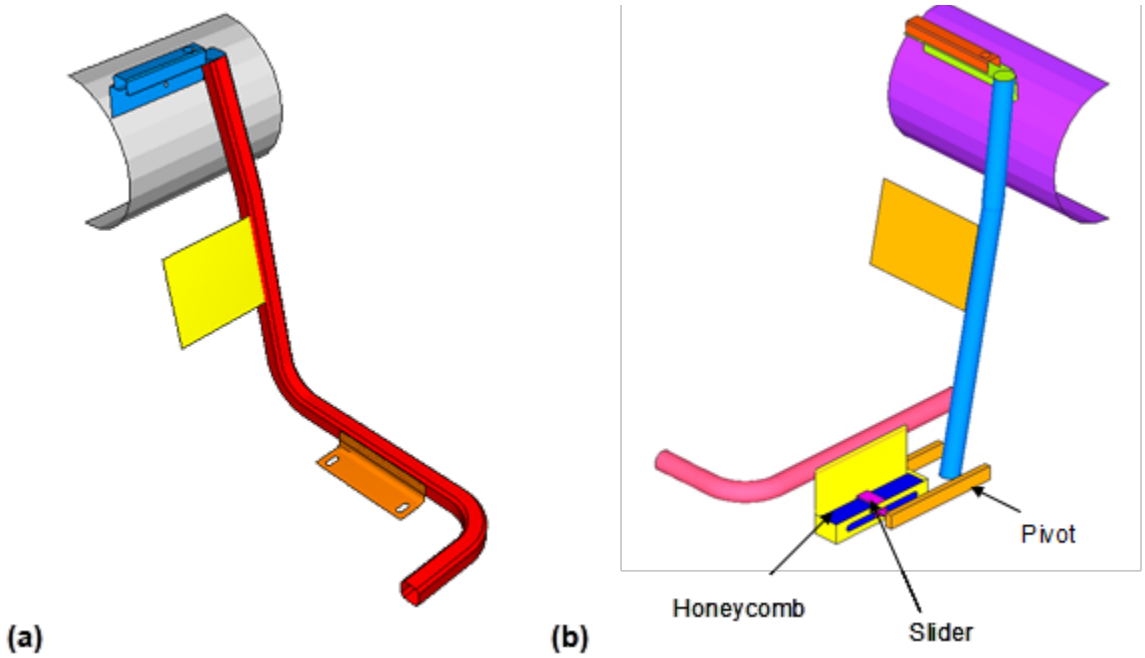

Figure 23. Example single-seat models: (a) square tubes; (b) energy-absorber at connection to seat channel

Another single-seat analysis included not only the seat frame but also the seat back plastic shroud. Much like the headrest foam impact analysis described in Section 7.1.5, this analysis was performed to provide seat back force-deflection behavior to the MADYMO program. Illustrations of the model prior to deformation and after 1.0 inch of knee displacement are shown in Figure 24. A plot of the force-deflection results for this model is shown in Figure 25. The seat back was fairly compliant until the gap between the shroud and the seat brace (approximately 0.25 inches) was overcome, at which point the response stiffened considerably.

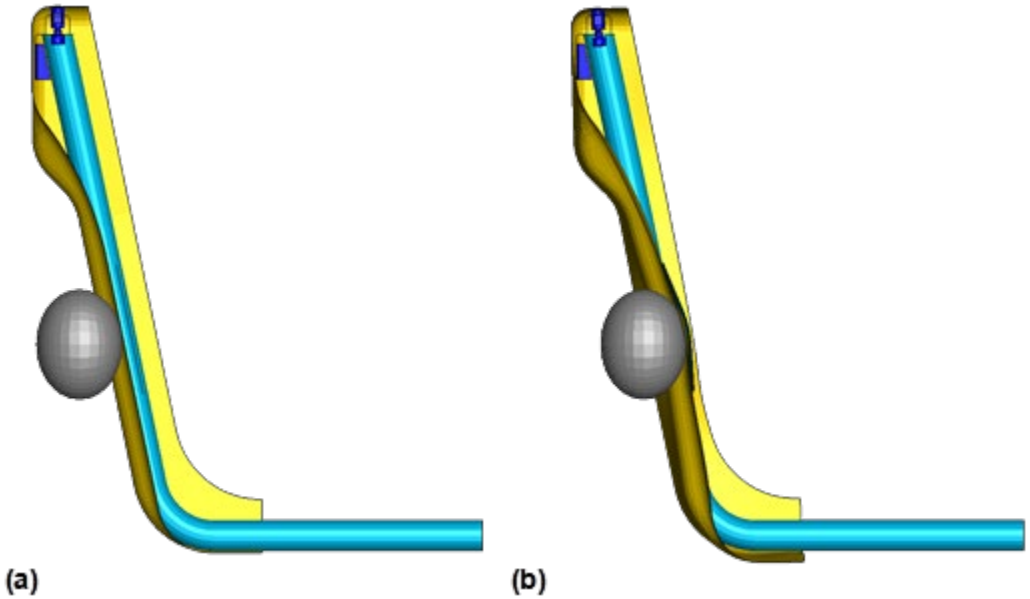

Figure 24. Single-seat with shroud model: (a) undeformed; (b) rigid "knee" moved forward by 1.0 inch

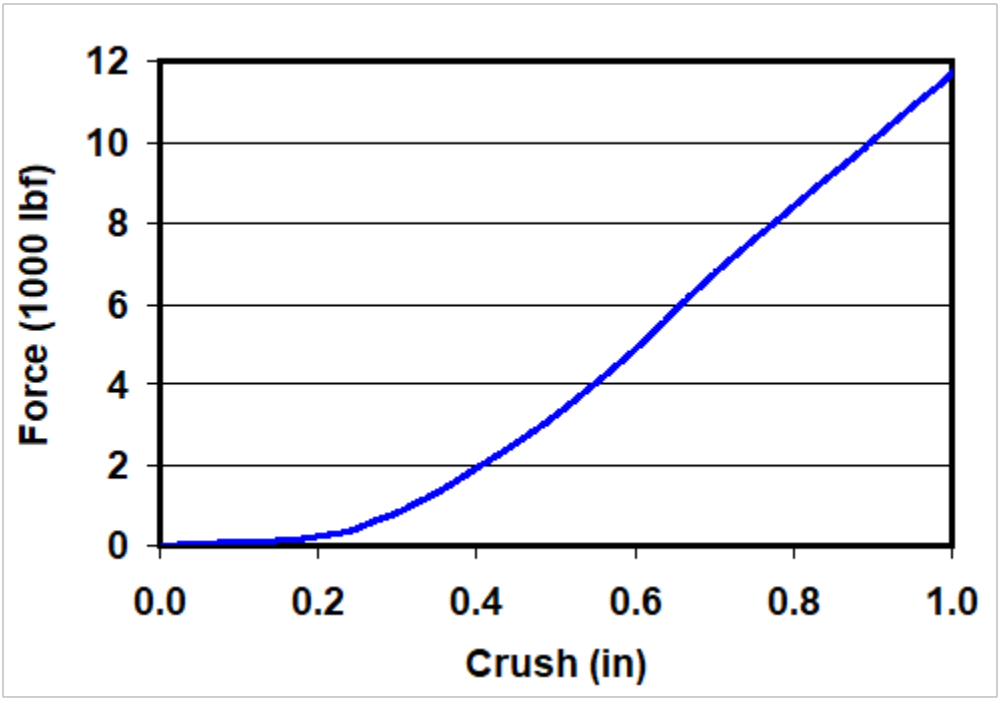

Figure 25. Force-deflection results for deformation of seat back shroud

7.1.7 Three-Seat Models

The single-seat model was eventually replaced by a more complete three-seat model that included the support channel and pedestal. Once the seating system design was determined, this model was used to conduct:

- Quasi-static analyses to determine the moment-rotation behavior of the seat back and evaluate the structural integrity of the various seating system components.
- Dynamic impact analyses to predict the extent of seat back rotation and the loads that arose at the connections to the floor and wall and at the connections between the seats and the seat channel for both the FF and RF occupant impact scenarios; the dynamic model was also used to further evaluate the structural integrity of the seat.

Initial versions of these models were used to evaluate the original seat design constructed for use in the CEM train-to-train collision test. The models were updated and repeated following each of the two design revisions discussed in Section 5.

A few selected results from the three-seat models are presented in the sub-sections below. Further discussion of model predictions is presented in Section 10, "Comparison of Tests and Analyses."

Forward-Facing Collision Scenario (Quasi-Static Analysis Only)

The model for the FF collision scenario is illustrated in Figure 26. This model included a total of approximately 170,000 elements. Due to the complexities associated with the dynamic impact of the occupants in a FF collision scenario, only the quasi-static loading scenario was modeled. (The dynamic loading scenario was analyzed in MADYMO.)

The load was applied to the back of each seat via rigid, semi-circular cylinders. For the scenario shown in Figure 26, they were positioned so that they struck the back of each seat back shroud at the center of the seat brace, about 10 inches above the horizontally-oriented seat bottom tubes. In another loading scenario, the rigid cylinders were raised so that they contacted the top of each seat back, about 20 inches above the seat bottom tubes.

The seating system was fixed to the floor at the bottom of the pedestal at the bolt locations. In addition, rigid surfaces representing the floor were added at these locations so that, if the pedestal deformed, downward motion of the end of the pedestal was constrained. Similarly, the channel was fixed at the bolt locations that fastened the channel to the wall, and a rigid plate was added to further constrain upward motion of the end of the channel. To simplify the model, the headrest foam was modeled as rigid, so that only its inertial properties affected the results of the analysis. (In the end, the inclusion of the headrest did not affect the calculations, because only the quasi-static crush of the seat back was modeled. They were primarily added for visualization purposes.)

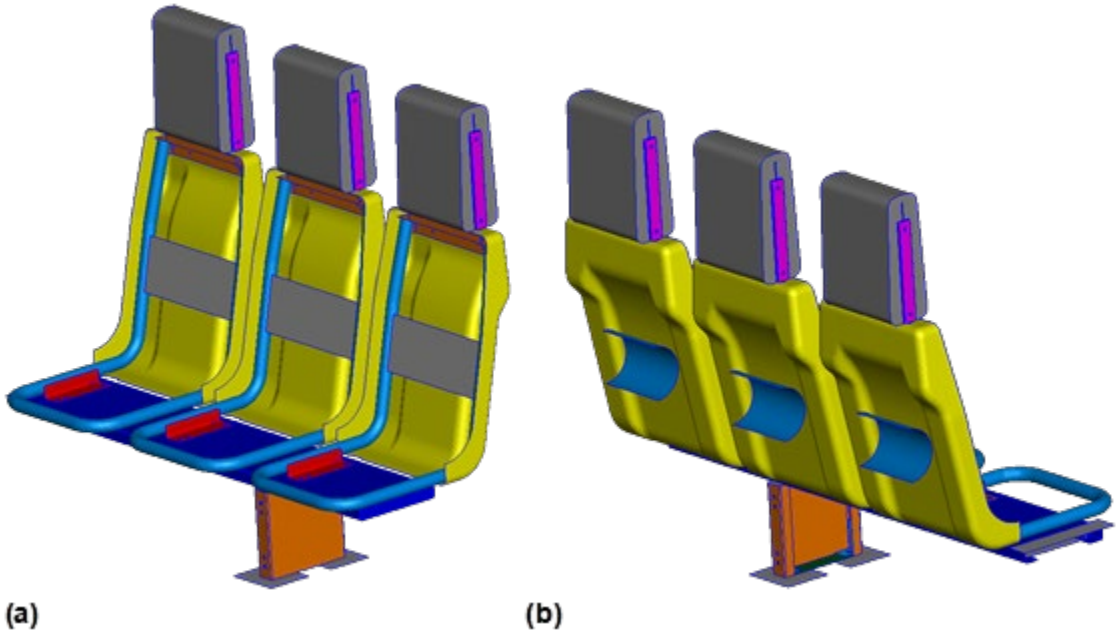

Figure 26. Three-seat model for FF collision scenario: (a) view from front; (b) view from behind

A constant displacement rate of 20 inches/second was applied to the loading cylinders, with both lateral and vertical motion of the impactors constrained. This displacement rate was chosen to increase the speed of the calculation as much as possible without introducing unwanted inertial effects. (Note: with explicit/dynamic FEA codes, the solution time is proportional to the time period of the simulation.)

Figure 27 shows contours of plastic strain superposed on the deformation of the three-seat system for a seat rotation of about 24 degrees. As is evident in the figure, most of the deformation occurred near the bend of the seat tubes.

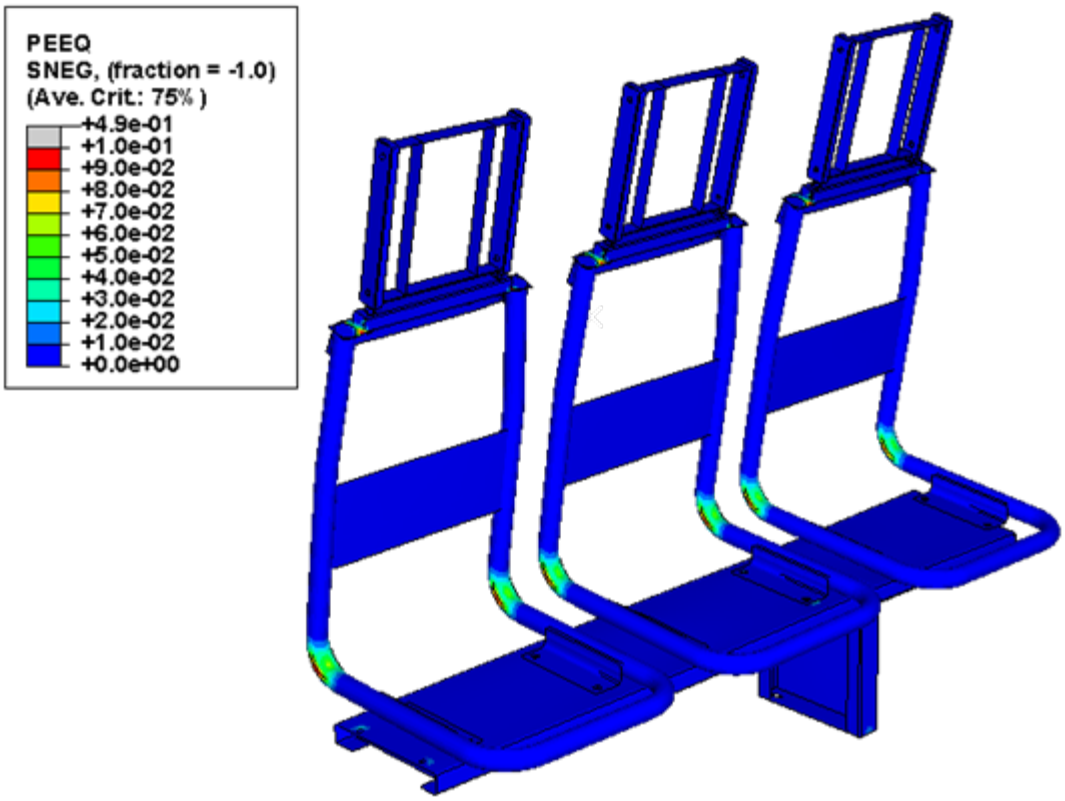

Figure 27. Plastic strain distribution for a seat back rotation of about 24 degrees

Results from preliminary versions of this model were used to evaluate the behavior of the seating system and identify potential weaknesses in the design. Figure 28 illustrates an example of how analysis results were used to improve the design. As is evident in the figure, the original design did not have any reinforcement of the channel near its connection to the wall. As a result of this analysis, the channel was reinforced in this region and the excessive deformation was eliminated.

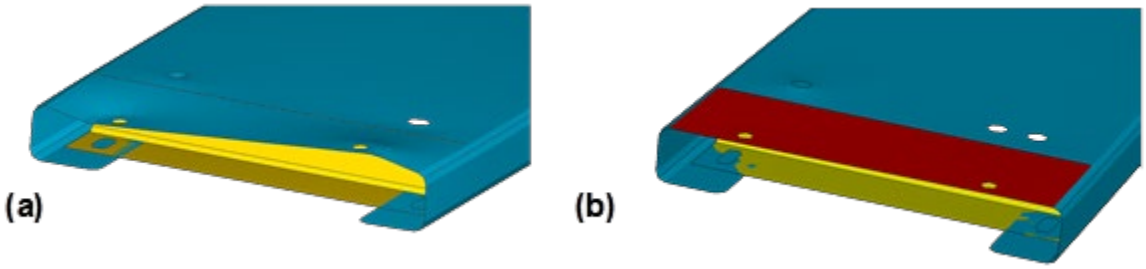

Figure 28. (a) Analysis of the original seat design indicated that the channel was deforming excessively near its connection to the wall (b) the addition of a stiffening plate eliminated the excessive deformation

The predicted moment-rotation curve for the FF seats loaded 10 inches above the bottom seat tubes is compared in Figure 29 with the behavior predicted in the single-tube analysis and with the single-tube test result. Also shown in this figure is the simplified moment-rotation curve provided as input to the MADYMO program. Note that, following quasi-static seat tests, the

assumed strength of the tubes was further increased by 10 percent to account for fabrication-induced hardening of the tubes. All of the modeling results reflected this change.

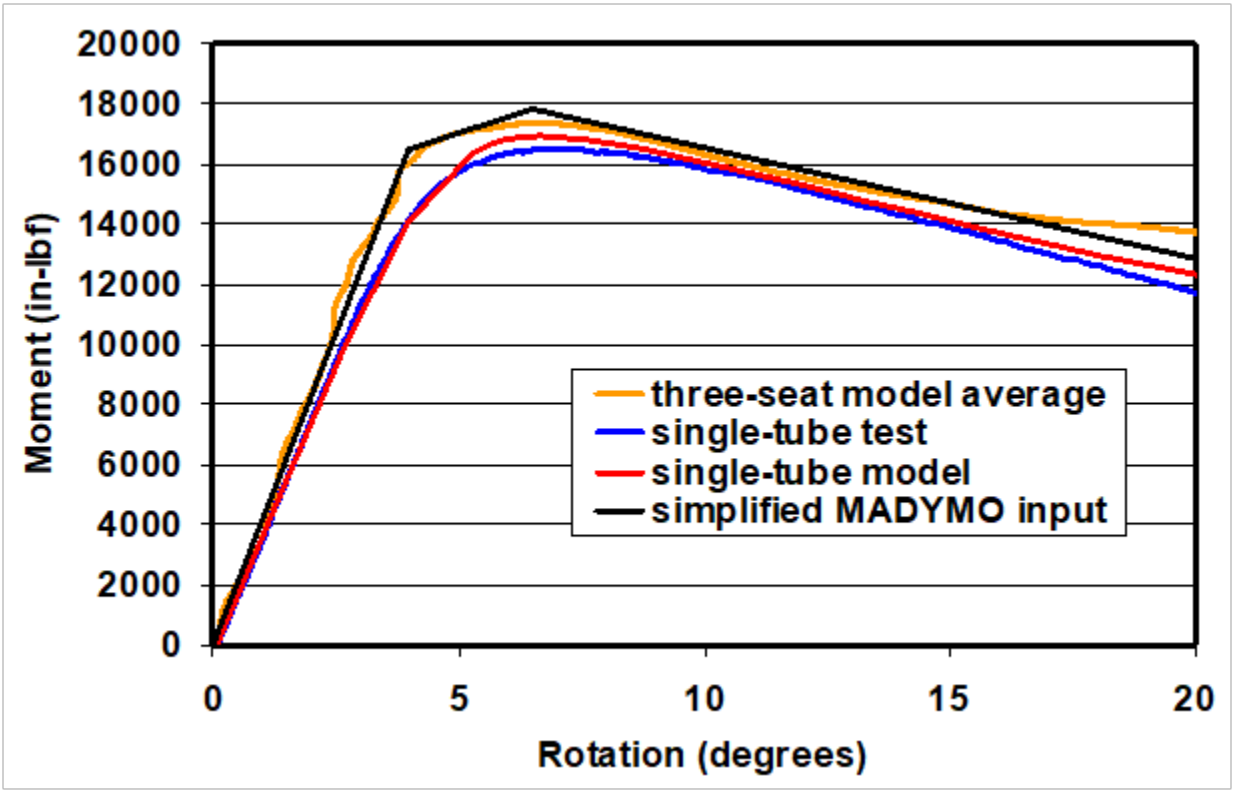

Figure 29. For FF seats, a comparison of predicted average moment-rotation behavior of seat backs with predictions and test results for single-seat tube analysis and the simplified moment-rotation curve provided as input to the MADYMO program

Rear-Facing Collision Scenario

The model for the RF collision scenario is illustrated in Figure 30. It differed from the model for the FF collision scenario in the following ways:

The loading cylinders were replaced by rigid bodies representing occupant torsos. Such torso blocks were used for quasi-static testing of the seating system for the RF loading scenario. Dimensions for the torso block were derived from drawings provided to TIAX by Armor Holdings.

A representation of the seat back foam was added to the model so that its compliance could be accounted for in the calculations.

The seat back shroud was not modeled, as it had little or no effect on seat behavior when loaded in the RF configuration.

The headrest was not explicitly modeled. Its inertial contribution was factored into the dynamic calculations by adding mass along the top of the seat back frame.

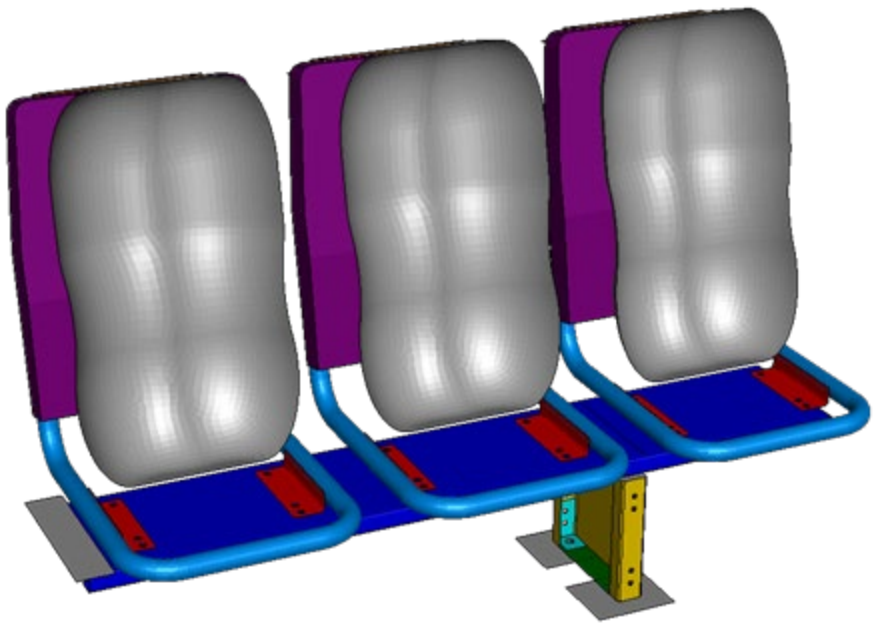

Figure 30. Three-seat model for RF collision scenario

The predicted moment-rotation behavior for the RF seat is shown in Figure 31. Results for the full RF seating system indicated that it was somewhat more compliant than the individual seat tubes. This was likely due to the additional compliance of the seat frame.

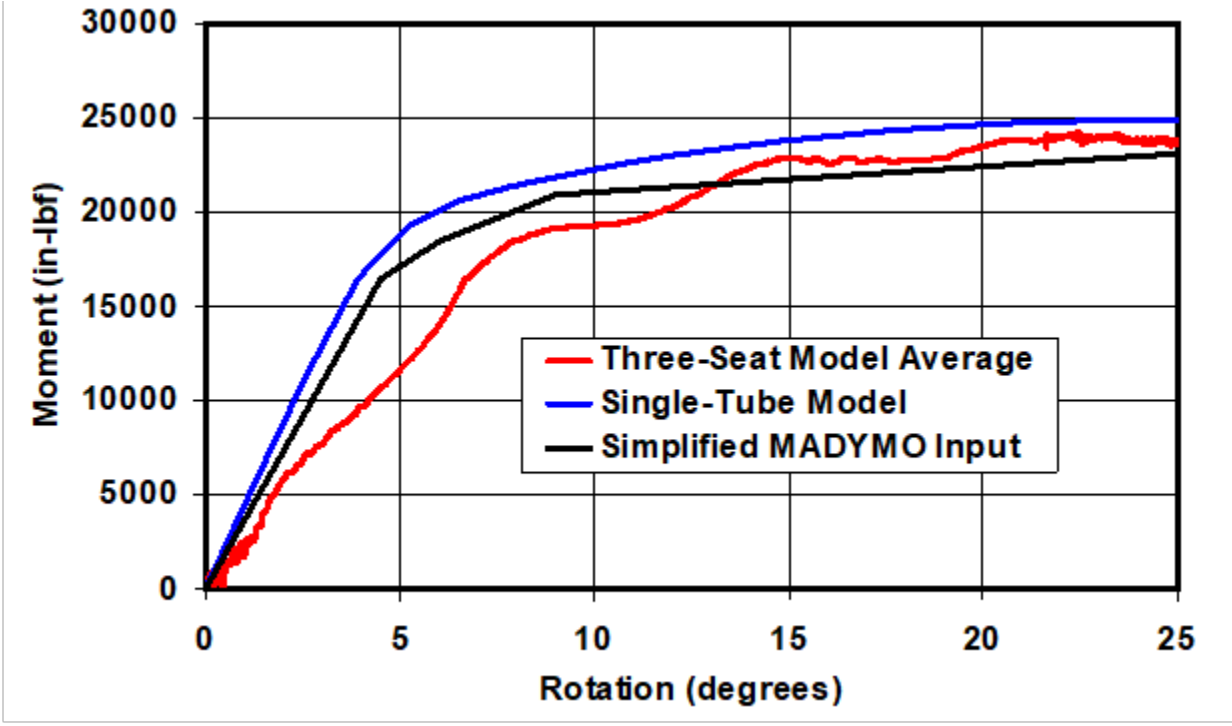

Figure 31. For RF seats, a comparison of predicted average moment-rotation behavior of the seat backs with results for single-seat tube analysis and the simplified moment-rotation curve provided to the MADYMO program

Results from a dynamic analyses of the RF seat subjected to a 12g triangular pulse indicated that, as was the case for the FF seat (see Figure 27), most of the plastic deformation of the seat structure occurred near the bend of the seat tubes. There were, however, a few additional locations in the seat support structure where plastic strains arose during the collision.

The highest plastic strain of 11.5 percent arose in the L-bracket where the pedestal was mounted to the channel, as is shown in Figure 32. The channel saw slightly smaller strain levels of about 8.6 percent arising near the rivnut connections of the seats to the channel (Figure 33). Analysis results suggested that the redesigned pedestal experienced plastic strains of only about 4.0 percent, arising near the location of the forward floor bolt (Figure 34).

Reaction forces at the floor and the wall were captured during the analysis. These were compared to the tensile strength of the bolts in Table 7 and indicated that the bolt strengths were sufficient to withstand the predicted loads. In addition, the forces transmitted through the rivnuts from the seats to the channel were captured via the use of connector elements. The maximum predicted pull-out load of 1,700 lbf was well below the specified minimum pull-out strength of the rivnut of 3,600 lbf (for a 1/8-inch plate).

Table 7. Comparison of predicted reaction loads to specified bolt strength levels

Location	Bolt Diameter (in)	Predicted Vertical Force (lbf)	Tensile Strength (lbf)	Predicted Longitudinal Force (lbf)	Shear Strength (lbf)
Floor	5/8	13,500	36,500	2500	27,900
Wall	1/2	3,000	22,650	2500	17,850

Based upon the predicted plastic strain levels and reaction forces, the redesigned seat system appeared to have sufficient structural integrity to withstand the 12g impact of the three RF seated occupants.

Some of the three-seat model predictions are compared with test results in Section 10.

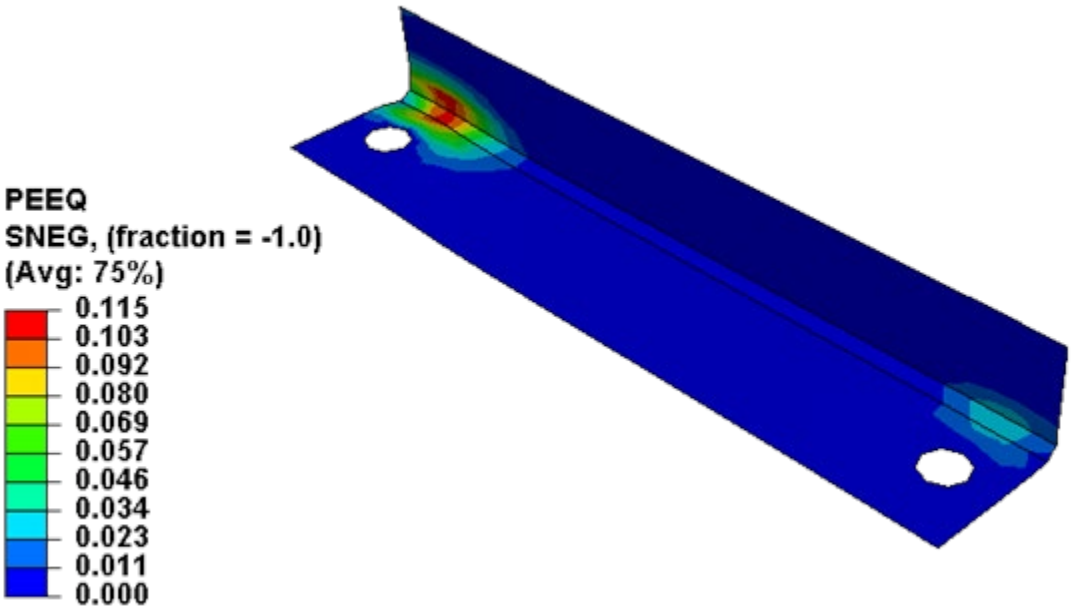

Figure 32. The highest plastic strains arose in the L-bracket where the pedestal was mounted to the channel

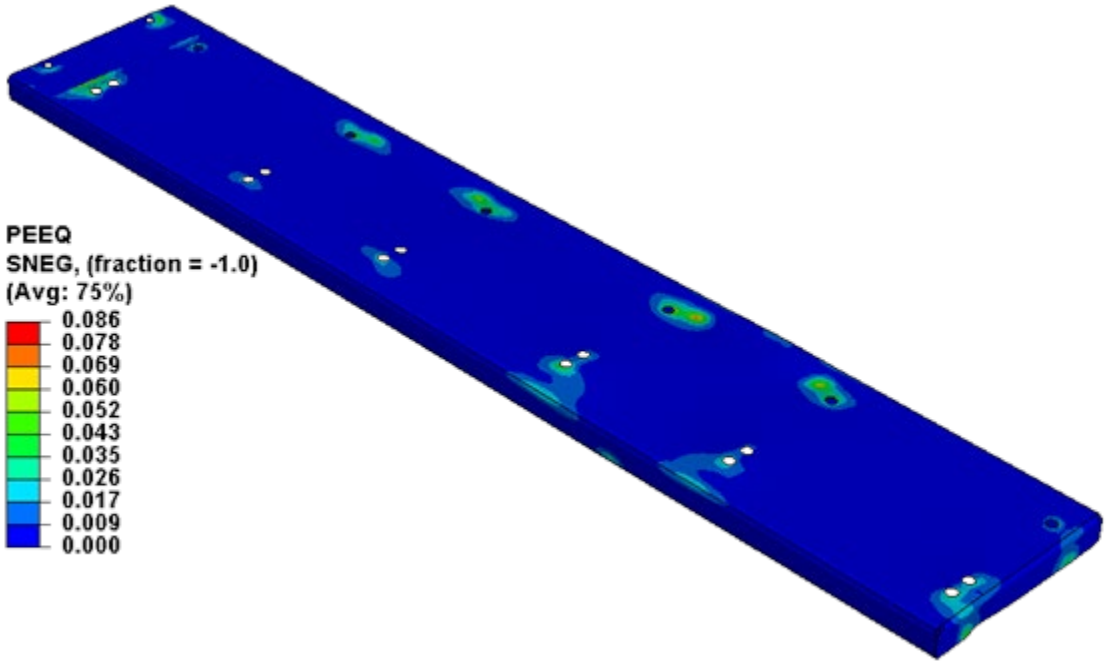

Figure 33. Plastic strains of 8.6% arose in the channel

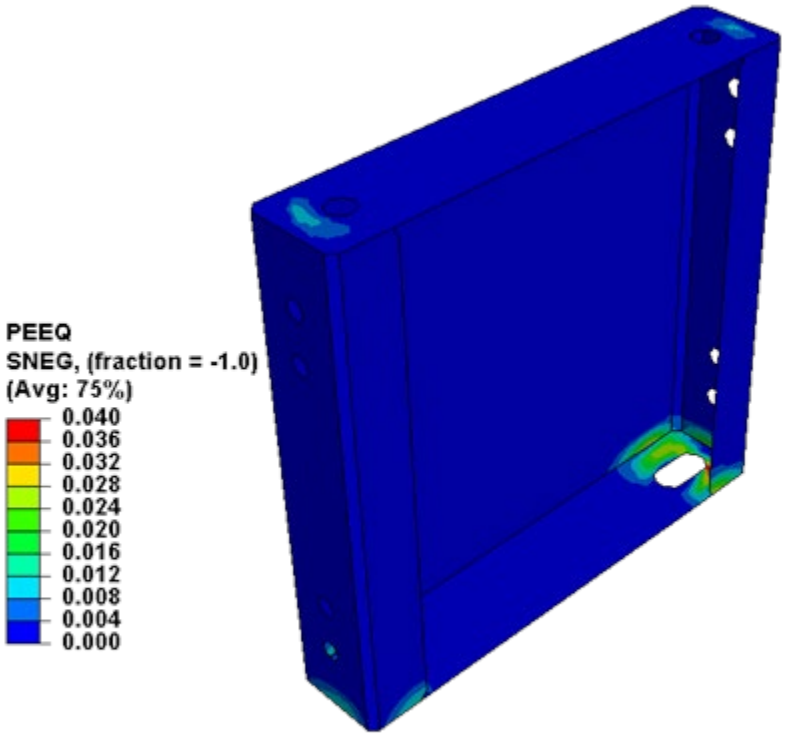

Figure 34. Plastic strains of only 4.0% arose in the pedestal

7.2 MADYMO Analyses

The MADYMO software package was used to simulate the collision behavior of seated passengers for both the FF and RF seating configurations. MADYMO is a general-purpose numerical code employing rigid body dynamics and finite element technology for solving the Newtonian equations of motion. It is the leading occupant safety software program and is widely used in the transportation, aerospace, and military industries. In these analyses, the rigid body dynamics capabilities of MADYMO were employed to evaluate seat and occupant behavior when subjected to an 8g (FF) or 12g (RF) acceleration pulse.

7.2.1 Model Description

Figure 35 shows a side view of the MADYMO model. The seating system was modeled as a collection of rigid masses representing the seat support channel, the pedestal, and the three individual seat modules for each of two rows of seats. Each of the individual seats was modeled as having three primary components: a seat bottom, a seat back, and a headrest. As is evident in the figure, each of these key seat components was further made up of a number of individual planes, ellipsoids, and cylinders that described the geometry of that component. These surfaces were also used to model contact with other system components.

Figure 35. MADYMO model for the seating system occupied by three passengers

The compliance of the seating system was characterized in a simplified manner by specifying a limited number of degrees of freedom:

- A nonlinear rotational spring and damper that characterized the bending of the seat back with respect to the seat bottom.
- A nonlinear rotational spring and damper that characterized the bending of the headrest with respect to the seat back.
- A nonlinear translational spring that characterized the compliance of the seat back cushion.
- Nonlinear translational springs that characterized the compliance of both the front and the back of the headrest cushions.
- Bilinear, three-dimensional translational springs that characterized the seat attachments at the floor and wall.

The characteristics of each of the various springs were based upon the results of the finite element models described in Section 7. In some cases, minor adjustments were made to reach better agreement with the test data. Figure 36 shows the moment-rotation characteristics for the rotational springs used in the respective models for the FF and RF configurations and for the headrest pivot rotational spring. The finite element predictions have been simplified into multi-linear characterizations of the behavior. Similarly simple representations of spring behavior have been defined to represent the nonlinear compliance of the seat back cushions, the headrest, and the plastic shroud that covers the back of the seat, as shown in Figure 37. Damping elements have been added in parallel to each of these springs, approximately equal to 10–20 percent of critical damping.

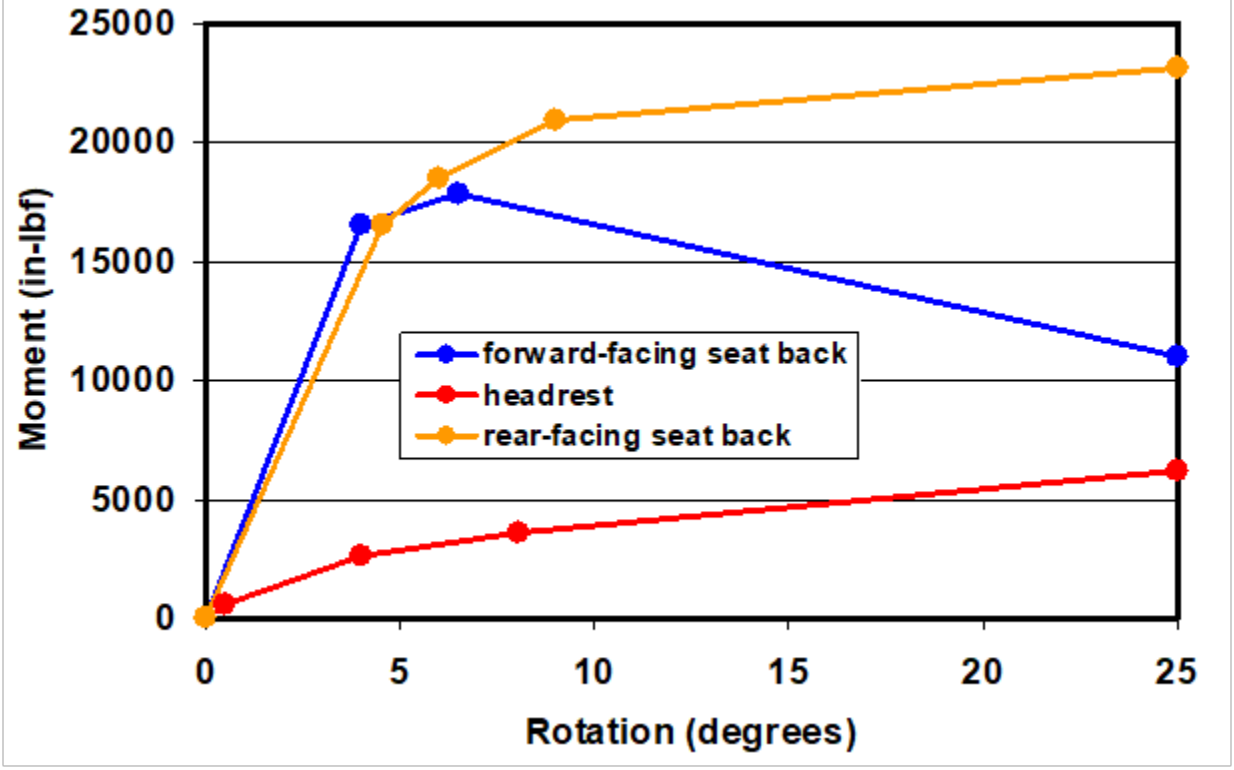

Figure 36. Simplified moment-rotation behaviors for the seat back in both the FF and RF orientations, and for the headrest

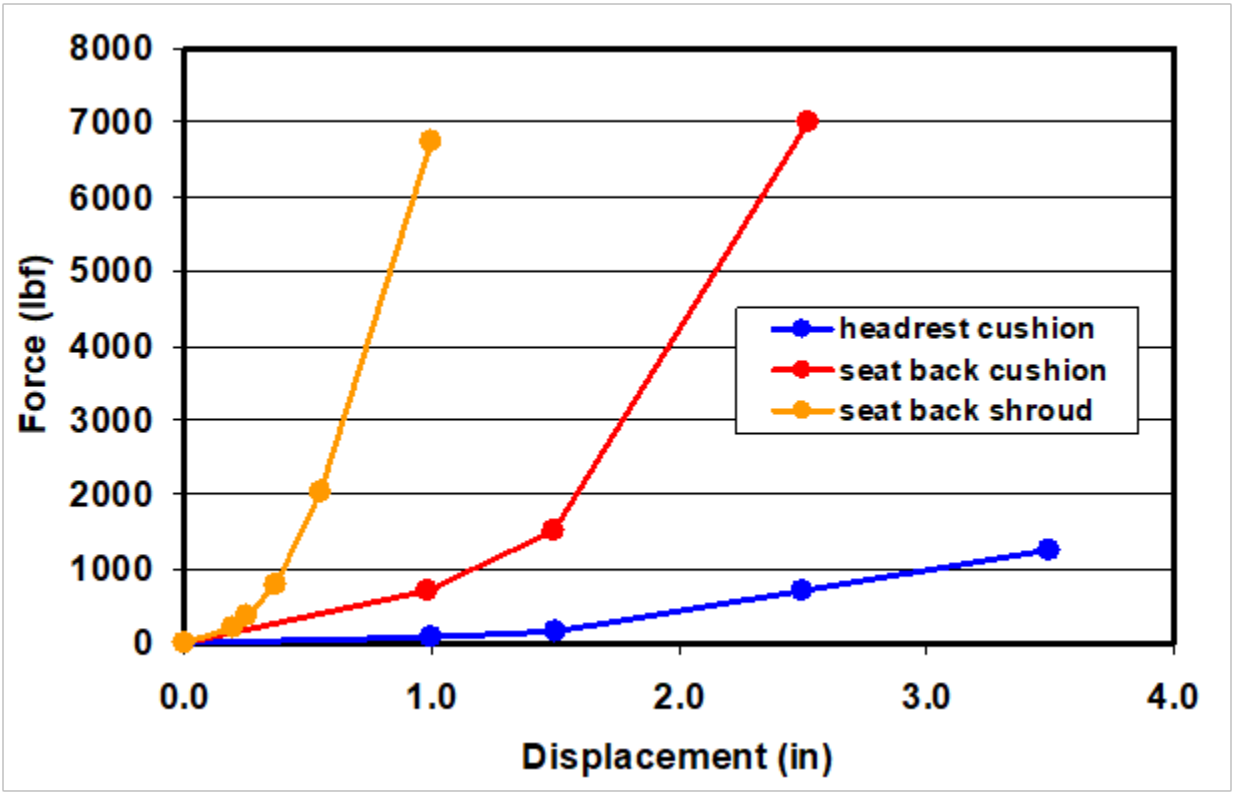

Figure 37. Simplified force-displacement behaviors for the headrest and seat back cushions, and for the seat back shroud

The representation of each individual seated passenger was based on a MADYMO library of ATD models that allows the user to configure the passenger as desired – in this case in a seated position. A 50th percentile male ATD model (m=170 lbm) was selected to represent the seated occupants. The geometry of the ATD was represented as a collection of connected ellipsoidal shapes, each with a prescribed mass. Some of these shapes were rigidly connected to one another; others were connected with spring and damper elements that model articulation at knee joints, elbow joints, the neck, etc. The ellipsoids also included translational compliance to model compression. All of the elements allowed for interaction of their surfaces with impacting objects. In addition to these structural elements, the MADYMO ATD models also had embedded in them the mathematical algorithms necessary to calculate the various injury criteria used to assess the severity of a collision.

For this program, the starting point of the model was an existing Volpe model based on a three-passenger M-Style commuter seat. This model was modified by Altair Engineering to include the specific seat components and geometry associated with the new seat design, based on CAD drawings. Additional modifications to the model and final calculations were performed by Kristine Severson of the Volpe Center.

The model evolved over time and many calculations were performed as the model and the design of the seat itself were modified. In the sub-section below, predictions from the model in its final form are summarized.

7.2.2 Analysis Results

MADYMO simulations were conducted for two collision scenarios:

- Seats in a FF orientation subjected to an 8g crash pulse.
- Seats in a RF orientation subjected to a 12g crash pulse.

The results of these simulations are summarized below.

Forward-Facing Orientation

The motion of the seat and occupants is shown in Figure 38 at four points in time. Upon impact, the occupants slid forward until their knees struck the backs of the seats in front of them approximately 0.11 seconds after impact (Figure 38(b)). The ATDs then translated forward and rotated about their knees until their faces impacted the back of the headrests of the forward seats, and their chests impacted the tops of the seat backs about 0.22 seconds after impact (Figure 38(c)). With their forward motion blocked at two locations, the ATDs then slid upward, with the extent of rotation at both the knees and the waist becoming smaller. At 0.40 seconds, they essentially reached a standing position (Figure 38d). They then proceeded to fall back into the seat.

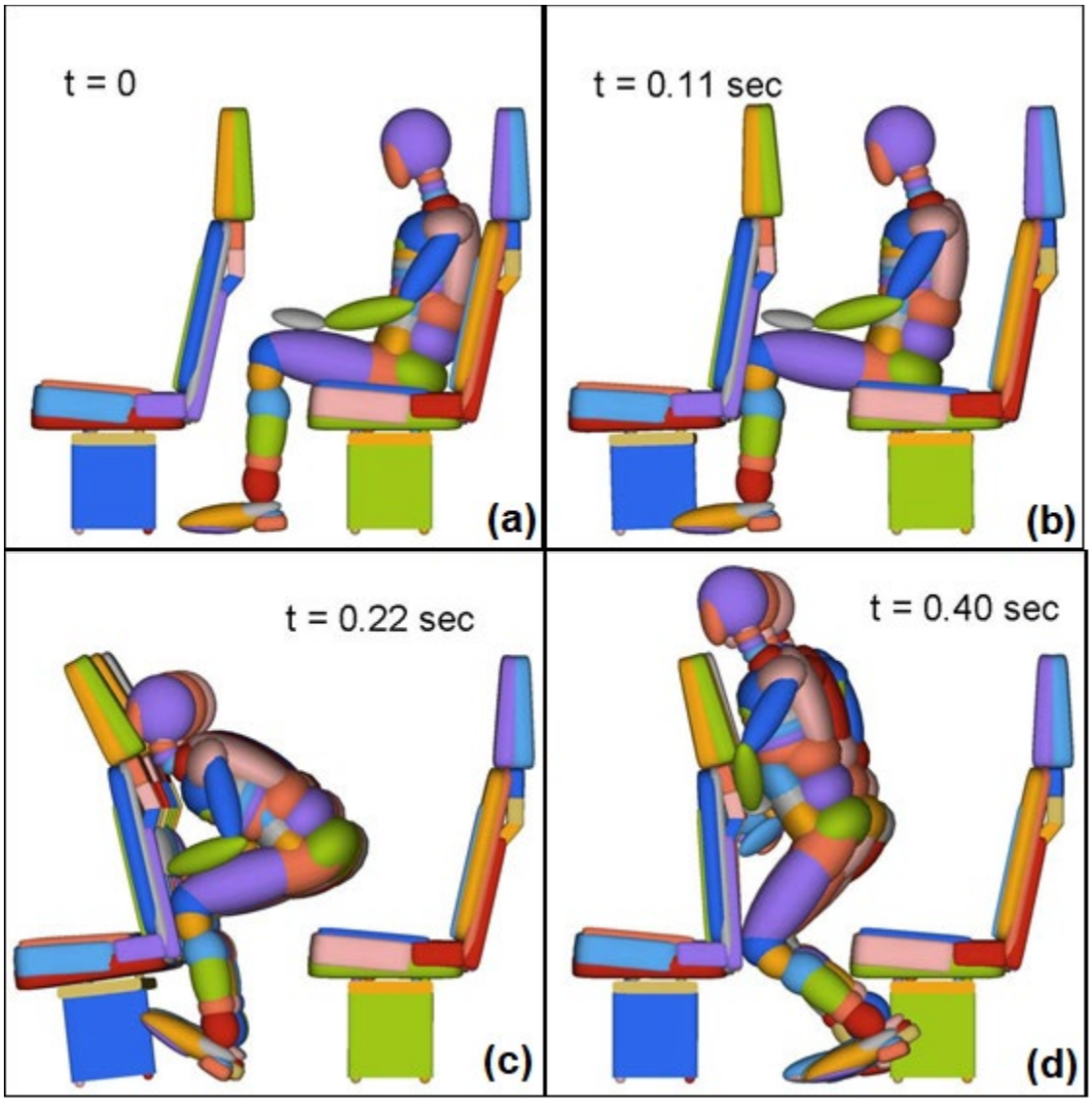

Figure 38. Predicted occupant and seat motion at four points in time following impact: (a) t=0, (b) t=0.11 sec, (c) t=0.22 sec, and (d) t=0.40 sec

The predicted moment-rotation behaviors of the seat backs for this scenario are shown in Figure 39. The seat rotated about 8 degrees due to impact of the knees, and then began to unload. The moment increased again when the face and chest impacted, with the rotation increasing to almost 12 degrees. The seat back then unloaded, and the rotation decreased to a final extent of about 8 degrees. The moment reached its maximum value of approximately 20,500 in-lbf (2,320 Nm) after about 6 inches of rotation, and then gradually dropped to about 15,000 in-lbf (1700 Nm) at 14–17 degrees of rotation.

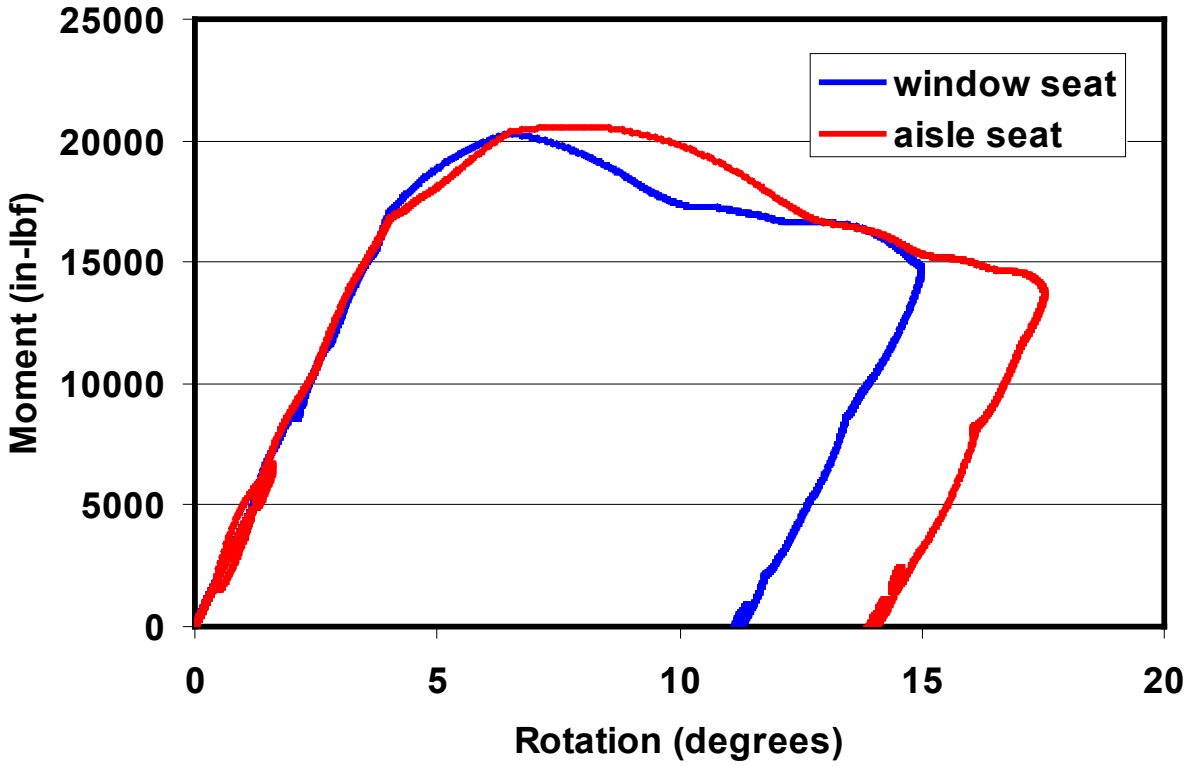

Figure 39. Predicted moment-rotation behaviors for the aisle and window seat backs for the FF, 8g crash pulse

The predictions of injury parameter values are summarized in Table 8, and indicate that the HIC15 values for both aisle and window occupants were sizable, but below the allowable limit.

Table 8. Predicted injury results for the FF 8g collision scenario

Criterion	Injury Threshold [9]	50th Percentile Male, Aisle Seat	50th Percentile Male, Window Seat
HIC15	700	**590**	650
Nij	1.0	0.69	0.65
Peak Neck Fz, lbf	+940/-900	140/-290	140/-330
Chest Accel., g	60	18	17
Femur Load, lbf	2,250	1300	1770

Rear-Facing Orientation

The motion of the seat and occupants for the RF orientation is shown in Figure 40 at four points in time. Upon impact, the occupants pushed back against the seat backs. The loads on the seat frames built, causing the seat backs to rotate with respect to the seat bottoms. At 0.21 seconds (Figure 40(b)), the seat back rotated to its fullest extent of approximately 30 degrees. The ATDs then rebounded forward, with their knees striking the facing seat at about 0.5 seconds (Figure

40(c)). The torsos of the ATDs then rotated forward, with their heads not quite reaching the facing seat backs after 0.7 seconds (Figure 40(d)).

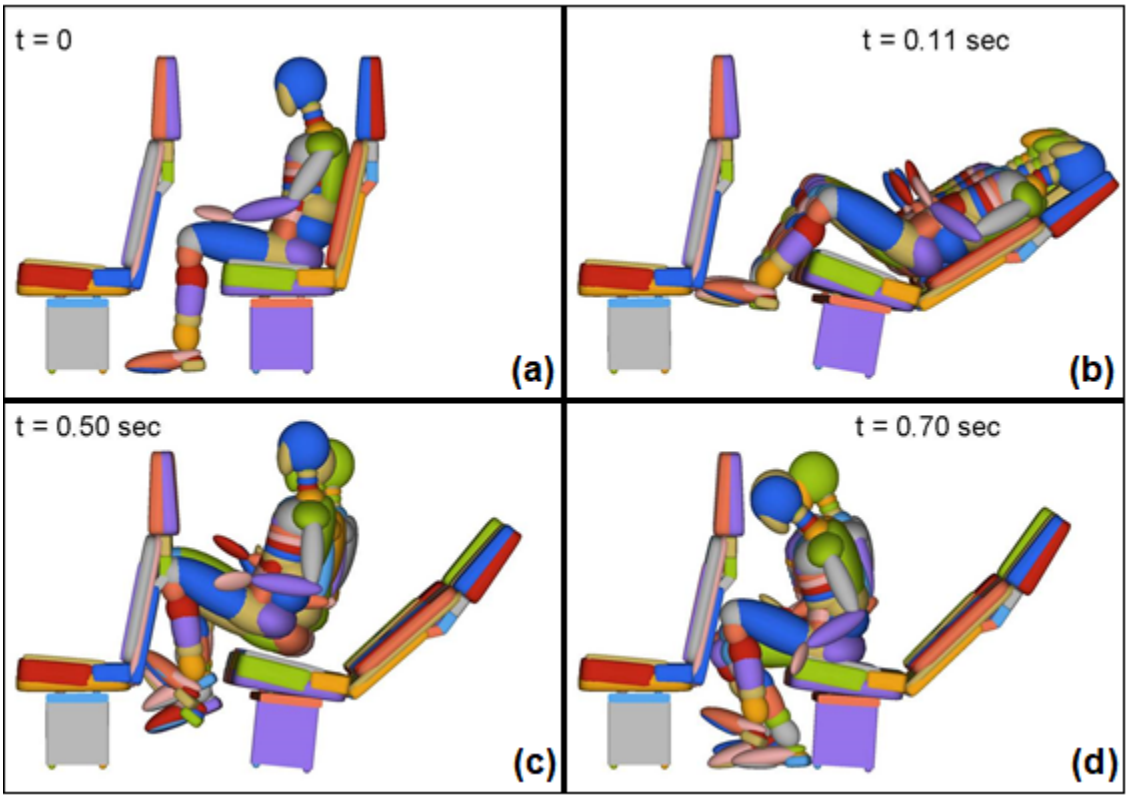

Figure 40. Predicted occupant and seat motion at four time points following impact for the RF configuration: (a) t=0, (b) t=0.21 sec, (c) t=0.50 sec, and (d) t=0.70 sec

The predicted moment-rotation behaviors of the aisle and window seat backs for this scenario are shown in Figure 41. The seat backs rotated a total of about 30–35 degrees, and then unloaded, with about 5 degrees of elastic recovery. The moment reached a peak of about 25,000 in-lbf (2260 Nm) after 24 degrees of rotation.

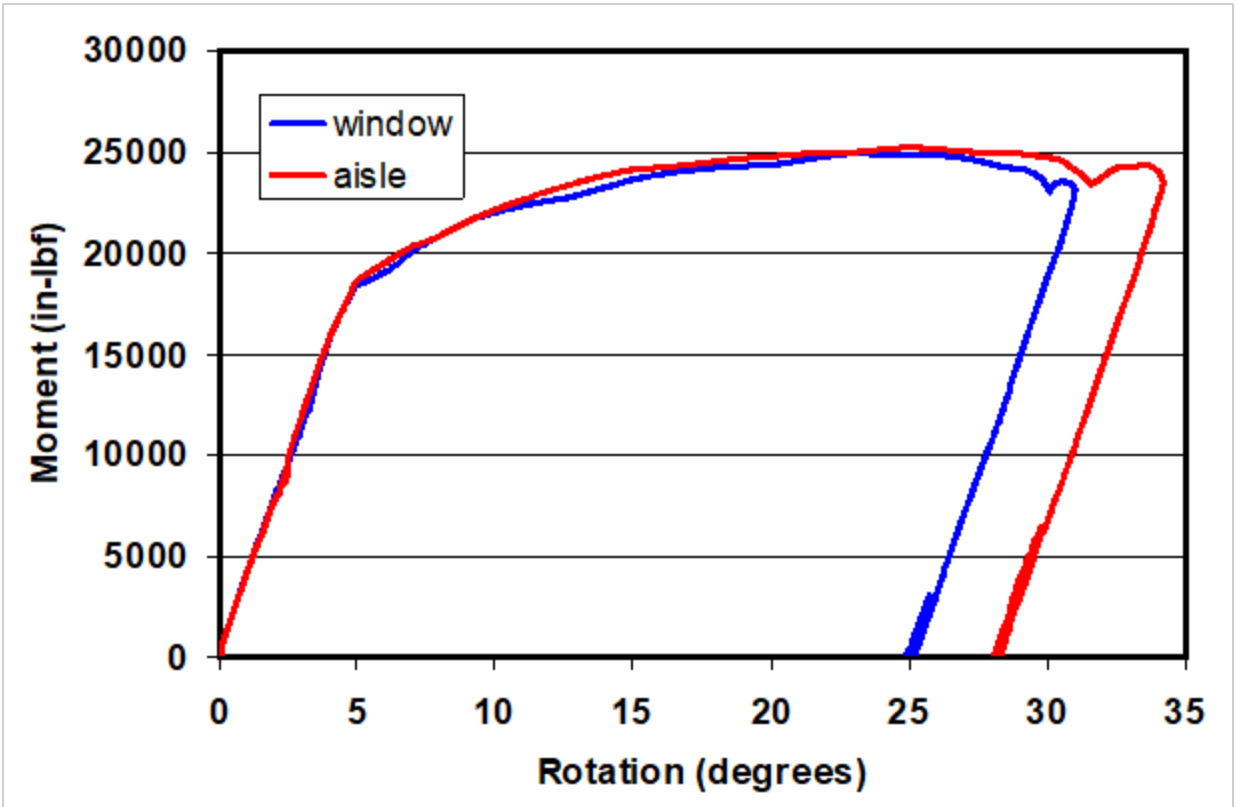

Figure 41. The predicted moment-rotation behavior of the seat back for the RF, 12g crash pulse

The predictions of injury parameter values are listed in Table 9. Due to the large rotation of the seat back and the support of the ATDs against the seat and head cushions, the injury results are much smaller than they are for the FF case, with all values well below the acceptable limits.

Table 9. Predicted injury results for the RF 12g collision scenario

Criterion	Injury Threshold [9]	50th Percentile Male, Aisle Seat	50th Percentile Male, Window Seat
HIC15	700	79	72
Nij	1.0	0.27	0.25
Peak Neck Fz, lbf	+940/-900	230/-50	240/-40
Chest Accel, g	60	14	14
Femur Load, lbf	2,250	580	240

8. Fabrication

This section includes a brief description of the steps required to fabricate the seats. It is arranged according to subassembly and then individual materials and components. The fabrication was performed by TMS. All of the welding was performed by welders qualified to AWS standards. The materials were specified, ordered, and received at TMS facilities, and eight, three-person seating systems were fabricated. Four seating systems were shipped to TTCI in Pueblo, Colorado, so they could be included in the CEM train-to-train test, and the other four were sent to Armor Holdings in Phoenix, Arizona, to perform quasi-static testing and dynamic sled testing.

8.1 Seat Bucket Subassembly

The seat bucket consisted of a seat frame and back and bottom plastic shrouds, as shown in Figure 42.

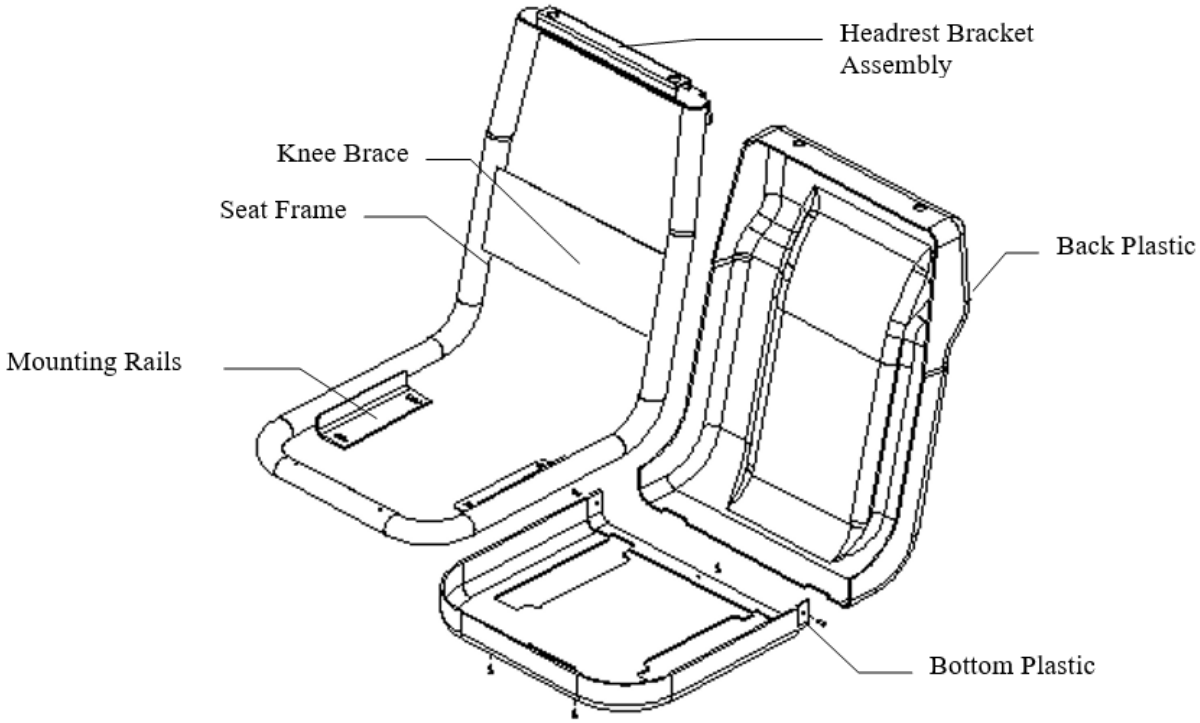

Figure 42. Seat frame and shrouds

8.1.1 Seat Frame

The seat frame was a powder coated welded structure made from steel plates, sheets, and tubing. The tubing was formed using special bending dies and was made of 1.5-inch OD by 14 gauge (0.083-inch) wall ASTM A513 Type 5 material with a yield strength of 70 ksi, based on material testing. The tubing was selected to provide optimal energy absorption during a crash. Mounting rails were welded to the frame tubing at the bottom of the frame and were made of 7 gauge (0.180-inch) hot rolled steel.

A bracket assembly for headrest attachment was welded to the top of the frame. The bracket consisted of a channel and a bent plate that were welded together. Both the channel and the bent plate were made of 12 gauge (0.120-inch) hot rolled steel. The bent plate was laser cut from CAD geometry and formed into shape. The channel was formed into a "U" shape. The bent plate had a slot for accepting the upper tab on the back seat cushion, as well as holes for accepting the headrest. The bent plate had bracing features so that loads from the head impacting the headrest were distributed into the seat frame tubing. The holes in both the upper and lower brackets were aligned during welding.

A thin knee brace plate was welded to the frame tubing at the midpoint of the seat back. The plate was designed to transfer the impact load from a passenger's knees into the seat frame, and to protect the seat back cushion from being forced out of the seat during a train collision. Without the plate, the knees of a passenger seated behind the impacted seat could deform the seat back plastic shroud enough to damage the seat back cushion pan and cause it to become disengaged from the seat frame. The knee brace plate was 14 gauge (0.075-inch) hot rolled steel.

The seat frame was welded in a specially designed and fabricated weld fixture (Figure 43). On the left in Figure 43 is one of the two welded mounting rails and on the right is the headrest bracket assembly welded to the top of the seat back frame.

Figure 43. Seat frame welding and fixture

8.1.2 Back and Bottom Plastic shrouds

The seat back and seat bottom plastic shrouds were made of thermoformed plastic (Kydex 6200) which meets the flame and smoke requirements given in 49 CFR Part 238, Appendix B. The seat back plastic shroud was contoured to closely fit the seat frame and provide maximum knee space for the passenger seated behind.

Both parts were made from production tooling specific to the thermoforming process. The tooling fabrication process began with CAD files. Wooden patterns (male) were cut from the CAD files using computer numerical control (CNC) equipment. Cast aluminum production tools were then made from the patterns. The cast aluminum tools were water cooled to improve production cycle time and part consistency. A sheet of the plastic material was placed onto the cast aluminum tool and both were inserted into a thermoforming machine. The machine heated the plastic sheet, causing the material to form around the shape of the tool. Vacuum ports located

on the production tool aided in this process. Once the part was cooled it was removed from the tool and trimmed. The trimming was done by using CNC routing equipment that provided part consistency.

The sheet stock used to make the seat back and seat bottom plastic shrouds had a specified color, finish, and thickness. The color and finish can be varied, if desired, to suit the project. During the thermoforming process, the plastic sheet became thinner as it was formed. The sheet stock thickness was selected so that the finished parts were a minimum of 0.060-inch thick.

The seat back and seat bottom plastic shrouds were fastened to the seat frame by means of blind, aluminum, large-flange rivets.

8.2 Seat Back Cushion

The seat back cushion consisted of back foam, a back pan subassembly, and a sewn upholstery cover, as shown in Figure 44. During the upholstery process, the back foam was bonded to the back pan to insure it remained centered on the pan.

8.2.1 Back Foam

Back foam was fabricated from post-treated material meeting the flame and smoke requirements given in 49 CFR Part 238, Appendix B. The foam was cut from raw blocks of material and built up by bonding pieces together so as to provide passenger comfort and appropriate contouring. Foam stiffness, or IFD, was approximately 35 lbf, when measured at 25 percent deflection of a 2-inch thick specimen, according to ASTM D3574 Test B1. The manufacturer and brand of the foam was Chestnut Ridge Safeguard.

8.2.2 Back Pan Subassembly

The back pan subassembly consisted of a formed aluminum pan, an upper clip, and two lower clips. The aluminum pan was made from 0.063-inch thick aluminum sheet 3003-H14. The edges of the pan were formed into a channel shape for the upholstery cover attachment. The flat pan was cut from an aluminum sheet using a CNC turret punch with appropriate tooling for cutting and boring holes.

The upper clip was designed to provide attachment to the seat frame. The lower clips were designed to retain the bottom cushion where it meets the seat back. Each of these clips was made of 0.050-inch thick 1074 spring steel. After forming to their respective shapes, the clips were heat-treated to 40–45 Rockwell C hardness, zinc-plated and baked to relieve hydrogen embrittlement.

Both upper and lower back clips were attached to the back pan by means of blind, aluminum, large-flange rivets.

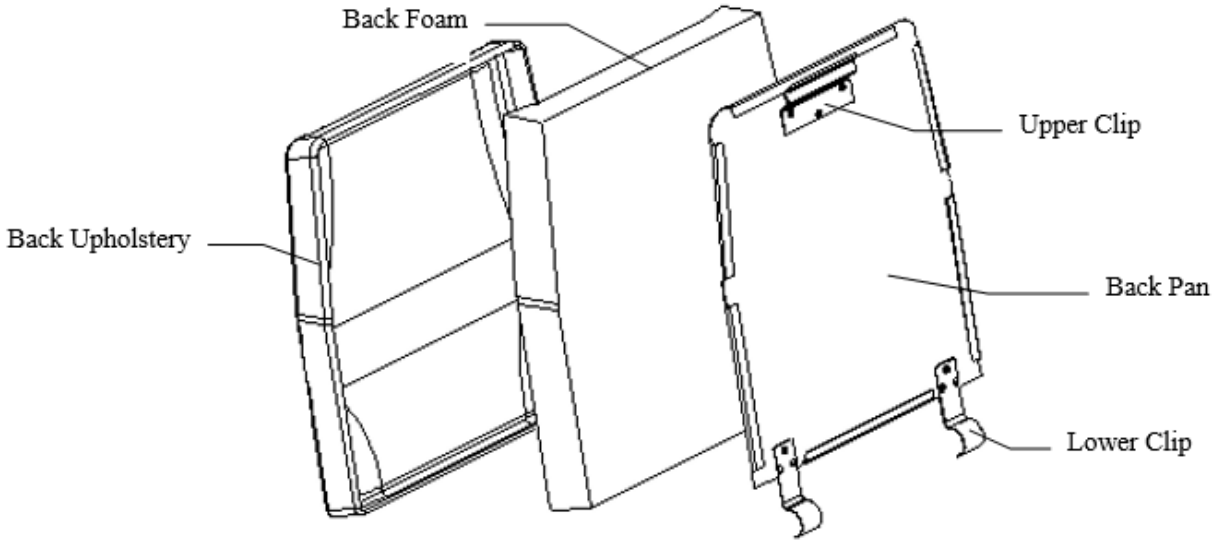

Figure 44. Seat back cushion components

8.2.3 Back Upholstery Cover

The back upholstery cover was made of fabric meeting the flame and smoke requirements given in 49 CFR Part 238, Appendix B. A vinyl coated fabric was used for this project. The cover was cut from fabric using patterns specifically designed for the seat. The edges of the upholstery cover were sewn with polypropylene strips to provide attachment to the back pan.

8.3 Seat Bottom Cushion

The bottom cushion consisted of bottom foam, a bottom pan subassembly, and a sewn upholstery cover, as shown in Figure 45. During the upholstery process, the bottom foam was bonded to the back pan to insure it remained centered on the pan.

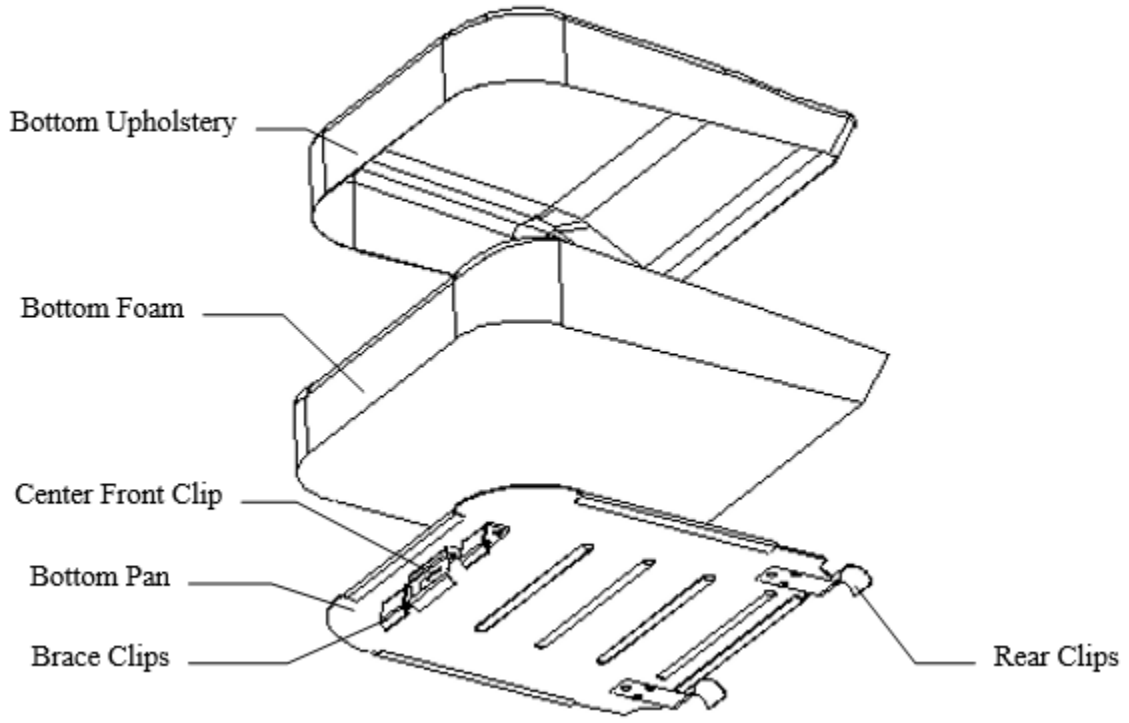

Figure 45. Seat pan bottom cushion components

8.3.1 Bottom Foam

Bottom foam was fabricated from post-treated material meeting the flame and smoke requirements given in 49 CFR Part 238, Appendix B. The foam was cut from raw blocks of material and built up by bonding pieces together so as to provide passenger comfort and appropriate contouring. Foam stiffness, or IFD, was approximately 55 lbf, when measured at 25 percent deflection of a 2-inch thick specimen, according to ASTM D3574 Test B1. The manufacturer and brand of the foam was Chestnut Ridge Safeguard XL.

8.3.2 Bottom Pan Subassembly

The bottom pan subassembly consisted of a formed aluminum pan and a clip attachment system. The aluminum pan was made from 0.090-inch thick aluminum sheet 3003-H14. The edges of the pan were formed into a channel shape for upholstery cover attachment. The center of the pan was stiffened by means of ribs formed into the pan. The flat pan was cut from aluminum sheet using a CNC turret punch with appropriate tooling for cutting, boring holes, and forming ribs.

The clips at the rear of the pan were designed to engage with the clips at the bottom of the seat back pan. The center front clip was designed to retain the bottom cushion to the seat frame by means of a hole engaging a protruding block on the frame. Each of these clips was made of 0.050-inch thick 1074 spring steel. After forming to their respective shapes, the clips were heat-treated to 40–45 Rockwell C hardness, zinc-plated and baked to relieve hydrogen embrittlement.

On either side of the center front clip were brace clips. These clips were designed to locate the bottom cushion assembly on the seat frame and brace the cushion against the seat frame during a

collision. The brace clips were made of 0.125-inch thick aluminum 3003 H-14 formed into shape.

All of the clips were attached to the back pan by means of blind, aluminum, large-flange rivets.

8.3.3 Bottom Upholstery Cover

The bottom upholstery cover was made of fabric meeting the flame and smoke requirements given in 49 CFR Part 238, Appendix B. A vinyl coated fabric was used. The cover was cut from fabric using patterns specifically designed for the seat. The edges of the upholstery cover were sewn with polypropylene strips to provide attachment to the back pan.

8.4 Headrest Assembly

The headrest assembly consisted of a headrest cushion, a headrest frame, and a headrest attachment system, as shown in Figure 46. The headrest cushion consisted of the headrest pan, headrest foam, and a sewn headrest upholstery cover.

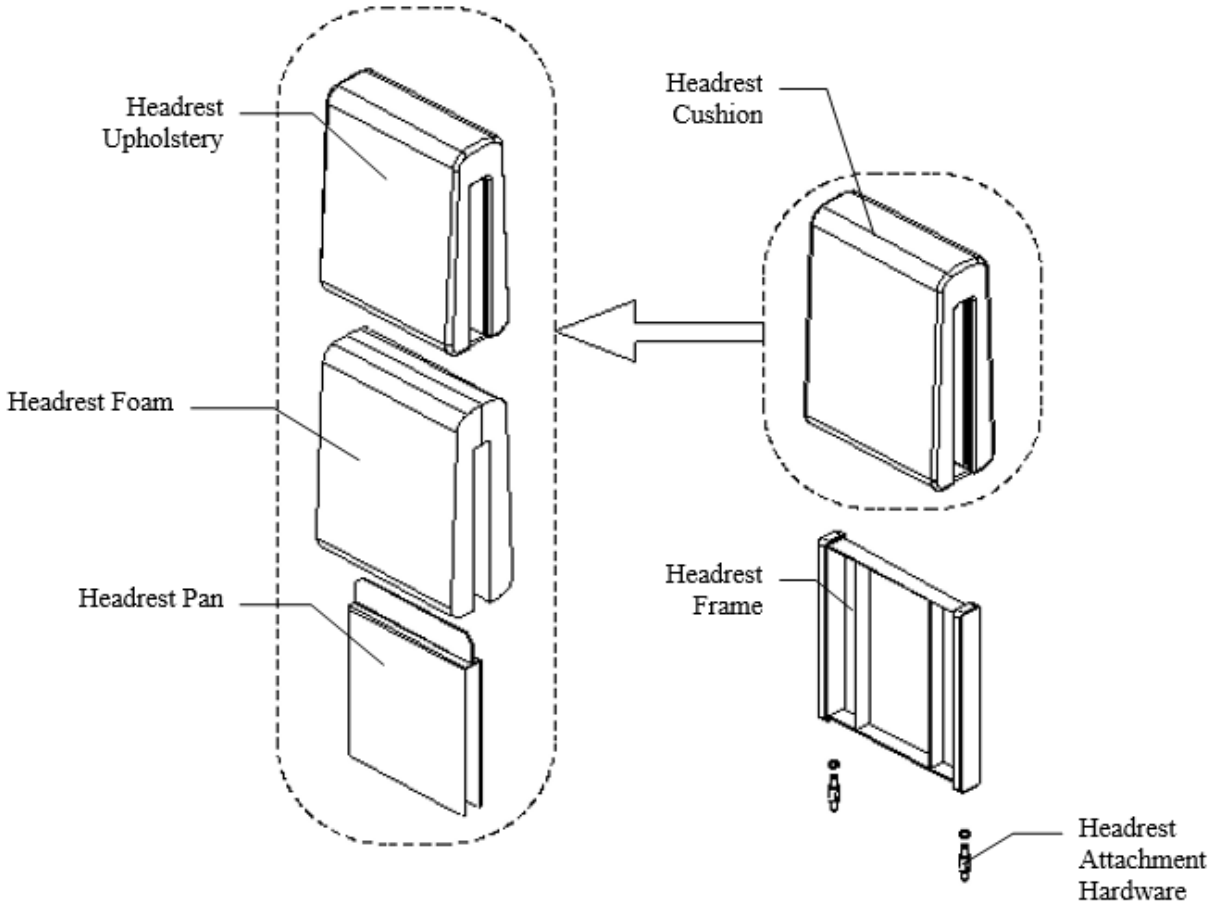

Figure 46. Headrest components

8.4.1 Headrest Cushion

The headrest cushion consists of a headrest pan, headrest foam and headrest upholstery cover. The headrest pan is made of 0.063-inch thick aluminum 3003 H14 and was formed into shape from a single flat sheet.

The headrest foam was fabricated from material that has been treated to meet the flame and smoke requirements given in 49 CFR Part 238, Appendix B. The foam IFD was approximately 75 lbf, when measured according to ASTM D3574 Test B1. The manufacturer and brand of the foam was Chestnut Ridge Safeguard. Stiffer foam was used for the new design compared to the baseline design to provide additional protection for passengers seated behind, should a collision occur.

8.4.2 Headrest Frame

The headrest frame was a weldment consisting of two vertical posts, two vertical braces, and two horizontal frame members, as shown in Figure 47. The two vertical posts were made of 5/8-inch thick by 1.50-inches wide 1018 cold-rolled steel. These posts had tapped holes on one end to accept the attachment system.

The two vertical braces and two horizontal frame members were made of 11 gauge (0.120-inch) thick by 1.00-inch wide low carbon, hot-rolled steel. After welding, the frame was powder-coated black. The vertical length of the headrest frame had been increased to 10.63 inches.

8.4.3 Headrest Upholstery Cover

The headrest upholstery cover was made of fabric meeting the flame and smoke requirements given in 49 CFR Part 238 Appendix B. A vinyl coated fabric was used. The cover was cut from fabric using patterns specifically designed for the headrest. The edges of the upholstery cover were sewn with hook and loop strips to provide attachment to the headrest pan.

8.5 Seat Support Channel Assembly

The seat support channel assembly consisted of a formed and welded stainless steel channel, special rivet nuts, and stiffener angles, as shown in Figure 47 (the bottom plate is not included in this figure). The entire assembly was provided with a brush finish after welding.

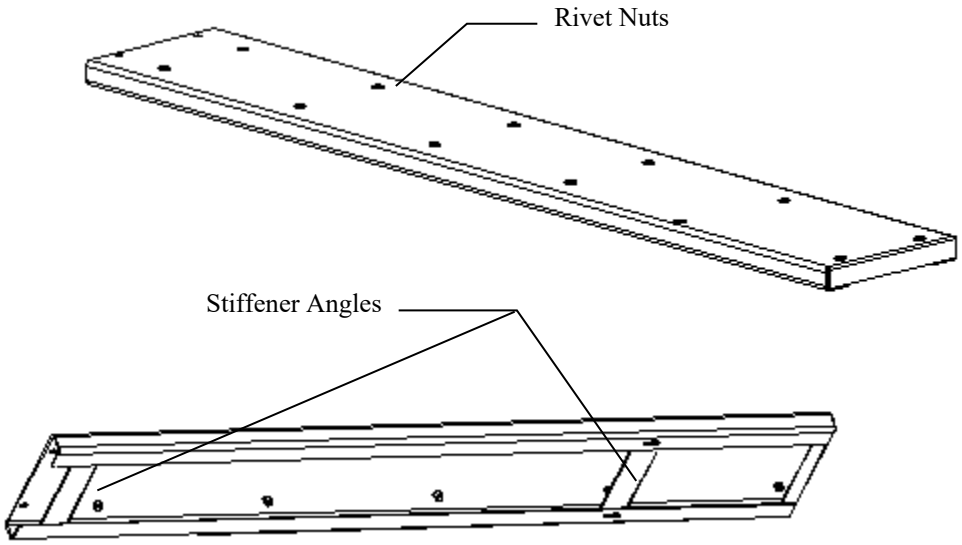

Figure 47. Seat support channel weldment

8.5.1 Support Channel Weldment

The support channel was made of 11 gauge (0.120-inch) thick 304 stainless steel. The channel was laser-cut in the flat and then formed into a channel shape, with a closed, boxed end. The boxed end was welded closed and was at the aisle end of the channel. Hexagonal holes were cut into the material for rivet nuts. The hexagonal shape prevented the nuts from rotating. Holes were provided in the wall end of the channel for attachment to the car wall structure. Slots were provided in the lower return edges of the channel for pedestal attachment.

The weldment included two stiffener angles – one located near the wall attachment holes and one at the pedestal attachment slots. These angles were welded to the channel. The photographs in Figure 48 show the welding of the stiffener angles to the support channel.

After welding, the entire exposed portion of the support channel was given a brush finish equal to a 100–120-grit finish.

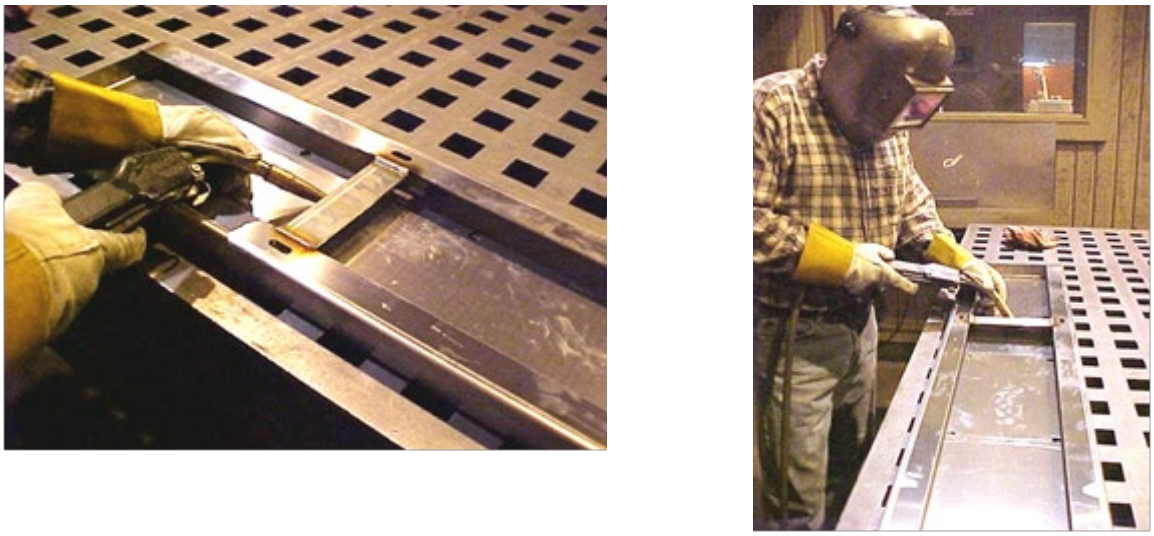

Figure 48. Support channel stiffener welding

8.6 Seat Support Pedestal

The seat support pedestal consisted of a pedestal weldment and pedestal cover with screws (Figure 49 and Figure 50).

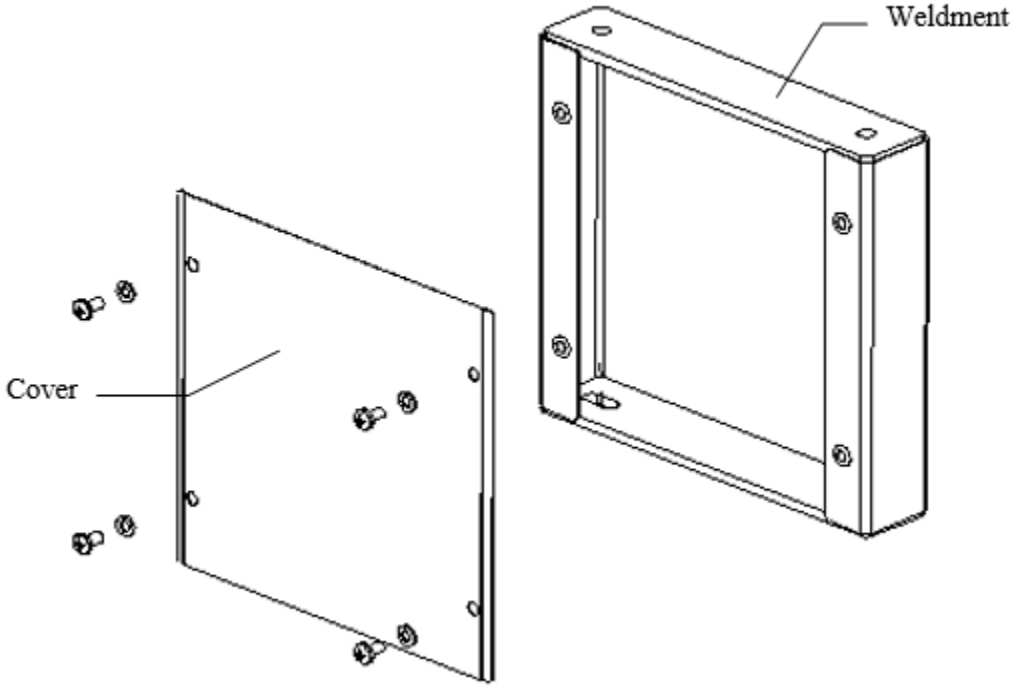

Figure 49. Seat support pedestal assembly

Figure 50. A photograph of the pedestal weldment

8.6.1 Pedestal Weldment

The pedestal weldment consisted of upper and lower plates and a wrapper skin. The upper and lower plates were made from 0.25-inch thick, type 304 stainless steel. Originally, the upper plate had two 0.416-inch diameter holes for mounting to the support channel. The lower plate had two 0.532-inch by 1.00-inch slots for mounting to the car floor. The modifications in design revision #2, as described above in Section 5.6.1, increased the diameter of the holes in the upper and lower plates to 0.532 inch and 0.656 inch, respectively.

The wrapper skin was made of 16 gauge (0.06-inch) thick 304 stainless steel sheet, formed into a channel shape. Four hexagonal holes were punched into the short legs of the channel to accept special rivet nuts.

The wrapper skin and upper and lower plates were welded together. After welding, the entire exposed portion of the pedestal was given a brush finish equal to 100–120-grit finish.

8.6.2 Pedestal Cover

The pedestal cover was made of 18 gauge (0.048-inch) thick, type 304 stainless steel. The material was pre-finished with a mill standard #3 finish on one side. Holes with 0.312-inch diameter were punched near the four corners for mounting the cover to the channel weldment. The edges of the cover were offset slightly to provide a rattle-free fit to the pedestal weldment. The pedestal cover was fastened to the pedestal weldment by means of four Phillips head stainless steel screws, 0.25-20 by 0.50-inch long, complete with 0.25-inch stainless steel lock washers.

8.7 Modifications

As described in Sections 5.5 and 5.6, modifications were made to the seat design on two occasions: following the CEM full-scale train-to-train test, and following the first set of dynamic sled tests. In each case the modifications were made primarily to strengthen the seat, particularly at its connection to the floor.

Figure 51 shows the assembled seat pedestal that was fabricated based on the first set of modifications. The installed corner brackets in the pedestal are shown in Figure 52.

Figure 51. Revised pedestal design showing the continuous weld and the mounting holes on the side of the pedestal channel for the additional corner brackets

Figure 52. Assembled corner brackets in the revised pedestal

Figure 53 shows the bottom of a seat channel with the cover plate welded to it to increased its torsional stiffness. The cover plate was a 0.125-inch (3.2-mm) thick stainless steel plate welded at its sides to the channel. The cutout for the pedestal attachment is located on the left side of the photograph. The portion of the seat channel that mounts to the wall is shown on the right side of the photograph.

Figure 53. Seat channel with welded bottom cover plate

A 3-inch wide strip of 0.125-inch (3.2-mm) thick stainless steel was welded to the underside of the seat channel at the wall end. Bolt holes were match-drilled to accommodate attaching the seat channel to the wall. This doubler plate was used to reinforce the wall attachment to ensure the bolts would not pull out during the 12g RF sled test. Figure 54 shows the doubler plate welded to the bottom side of the seat channel.

Figure 54. Welded doubler plate

During the CEM full-scale train-to-train collision test, the seat bottom and seat back cushions of the seats tested in the experiments came loose and separated from the seats in both the FF and RF seat experiments. It was hypothesized that accelerations during the test had caused the bottom seat cushion to come dislodged from its retention block, allowing it to separate from the seat. To keep the bottom seat cushion from sliding backward, a hard rubber block was bonded to the inside surface of the plastic shroud, allowing less than a 0.10-inch (2.5-mm) gap between the back of the cushion and the rubber block. A photograph of the block bonded in place on the seat back shroud is shown in Figure 55.

Figure 55. Rubber stop bonded to the plastic shroud

The seat cushions remained attached during the FF sled test. However, during the first RF sled test, some of the cushions did become detached. For this reason, an additional retention device was inserted to augment the rubber blocks.

Specifically, two C brackets were welded to the seat frame, as shown in Figure 56 (top photograph) to capture the bottom cushion pan brackets (bottom photograph), and thus kept the seat bottom cushion from translating backward under the 12g acceleration pulse.

Figure 56. Two "C" brackets welded to the seat frame (top photograph). Bottom seat cushion and seat frame assembly

9. Seat Testing

Several quasi-static and dynamic sled tests of the seating system were conducted to demonstrate its mechanical behavior and validate model predictions. Three quasi-static tests were conducted – two with the seats oriented in a FF configuration, and one with the seats oriented in a RF configuration. Three dynamic sled tests were also conducted – one with the seats oriented in a FF configuration, and two with the seats oriented in a RF configuration.

9.1 Quasi-Static Seat Testing

In October 2006, three quasi-static tests of the seating system were conducted at the facilities of Armor Holdings Aerospace and Defense Group (formerly Simula Technologies, Inc., subsequently BAE Systems, Inc.) in Phoenix, Arizona. As described in Section 8.7, the seats used in these tests were modified subsequent to the full-scale, train-to-train test of CEM equipment conducted in March 2006, and revealed that the seats were not adequately attached to the carbody. The seat channel, pedestal, and pedestal attachments were all strengthened.

The quasi-static tests were conducted for two purposes:

- To measure the force versus displacement behavior of the seat back (from which the moment versus rotation of the seat back can be estimated)
- To verify that the seats remained attached to the test fixture under these loading conditions

The results of the tests were subsequently used to fine-tune finite element models of the seat, and, in particular, the strength of the seat tube material used in the model.

For each of these destructive tests, a new seat was fastened to the test fixture. The seat was instrumented to measure triaxial reaction loads at the floor and wall attachment points as well as uniaxial displacement at several hard points on the seat. The load was applied to each seat back via three hydraulic rams. Three uniaxial load cells and three string potentiometers were in place to measure the force and displacement of the loading ram at the individual seat backs during each test.

In the first test, with the seats oriented in the RF direction, the load was applied to the seat back cushions via three effectively rigid torso blocks positioned in the seats to represent the body of a RF occupant. In the second and third tests, with the seats oriented in the FF direction, loads were applied via cylindrical rams to the backs of seats. In the second test, the loads were applied at the height of the knee bolster to represent loading due to knee impact. In the third test, the loads were applied to the back of the headrests to represent head impact of a FF occupant.

Results indicated that all of the test objectives were met in all three tests. The reaction forces were measured, and the moment versus rotation of each seat back was calculated. The failure mode in each test was determined to be plastic hinge formation near the bend in the steel seat frame tubes; no failures of the seat attachments were observed.

For each of the quasi-static tests, the moment versus rotation behavior of the seat back was estimated based on the measured axial load and displacement, and an estimated moment arm. The moment arm was estimated as the vertical distance between the seat bottom and the load under the assumption that the seat hinges at the bend in the seat tube. As illustrated in Figure 57, the angle was estimated as $\theta = \arctan(Z/X)$.

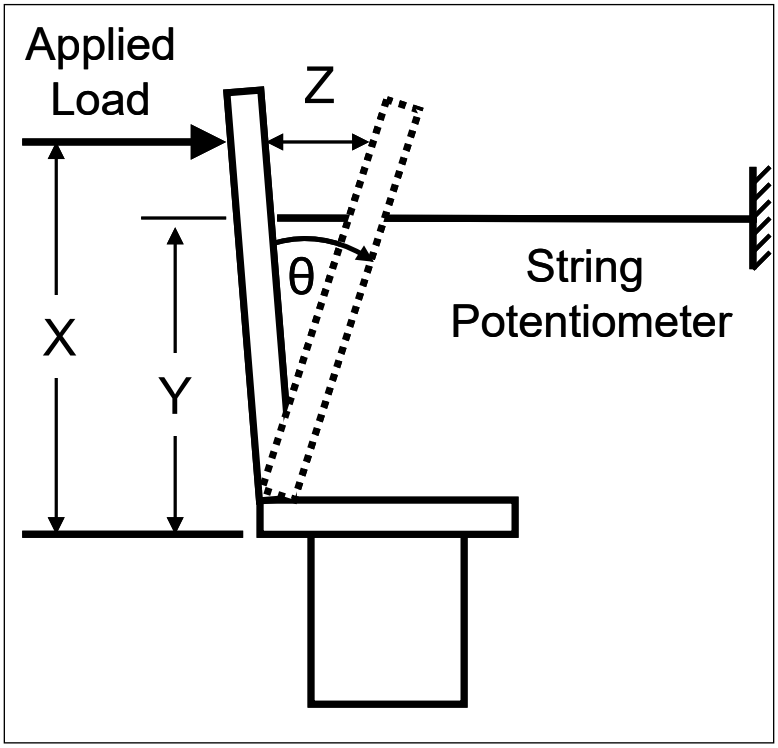

Figure 57. Schematic illustration of the estimate of seat back rotation angle from displacement measurement

9.1.1 Rear-Facing Body Load Test

Figure 58 shows photographs of the seats before and after the RF body load test. In this test, the load was applied to the seat back via effectively rigid torso blocks at a height of 14.5 inches above the seat bottom.

Figure 58. Pre- and post-test photographs of the RF body load test

A plot of the measured moment versus rotation for each seat, approximated from the measured force versus displacement, as described above, is shown in Figure 59. Each seat back in this test exhibited similar moment-rotation behavior. The seat backs rotated from 17 to 22 degrees, with peak moments ranging from 27,000 to 32,000 in-lbf.

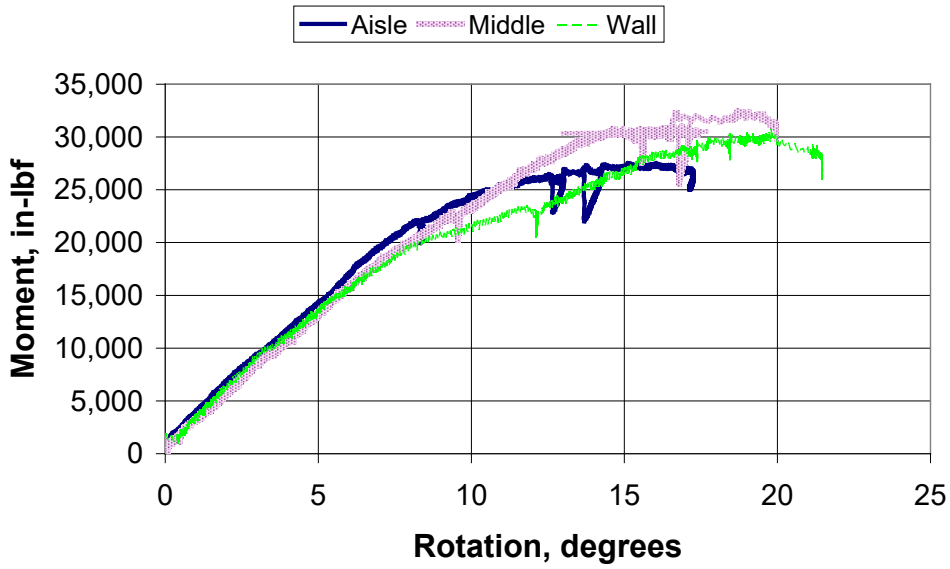

Figure 59. Moment versus rotation behavior measured during RF body load test

The largest reaction loads occurred at the vertically-oriented load cells under the floor pedestal, which reached a peak of 12,500 lbf in compression and 11,500 lbf in tension at the aft and fore floor load cells, respectively. The largest reaction loads at the wall mounts also occurred in the vertical direction, which reached a peak of 2,700 lbf in compression and 2,200 lbf in tension at the aft and fore floor load cells, respectively.

9.1.2 Forward-Facing Knee Bolster Load Test

Figure 60 shows the seats before and after the FF knee load test. The load was applied to the plastic shroud covering the back of the seat at a height of 9.5 inches above the seat bottom, in-line with the knee bolster.

Figure 60. Pre- and post-test photographs of the FF knee load test

A plot of the moment versus rotation for each seat back is shown in Figure 61. The middle and aisle seats rotated nearly 15 degrees, reaching a moment of over 20,000 in-lbf before a plastic hinge developed in the seat tubes at the angle between the seat bottom and seat back. The window seat exhibited a slightly smaller peak moment of 17,500 in-lbf. This difference may be attributed to the constraint of the wall attachment, the vertical location of the load application relative to the channel, and the method used to calculate rotation. There was more torsion of the seat channel during this test than during the other two quasi-static tests because the height of the load application was the nearest to the seat channel. The torsion of the seat channel to which the seat tubes were mounted resulted in some rotation of the seat bottom tubes of the middle and aisle seats, while the seat bottom tubes of the window seat did not experience appreciable rotation due to the proximity of the wall mount. The rotation calculation did not account for any rotation of the seat bottom tubes.

The largest reaction loads in this test occurred at the vertically-oriented load cells under the floor pedestal, which reached a peak of 10,200 lbf in compression and 9,800 lbf in tension at the fore and aft floor load cells, respectively. The largest reaction loads at the wall mounts also occurred in the vertical direction, which reached a peak of 1,900 lbf in compression and 1,700 lbf in tension at the fore and aft floor load cells, respectively.

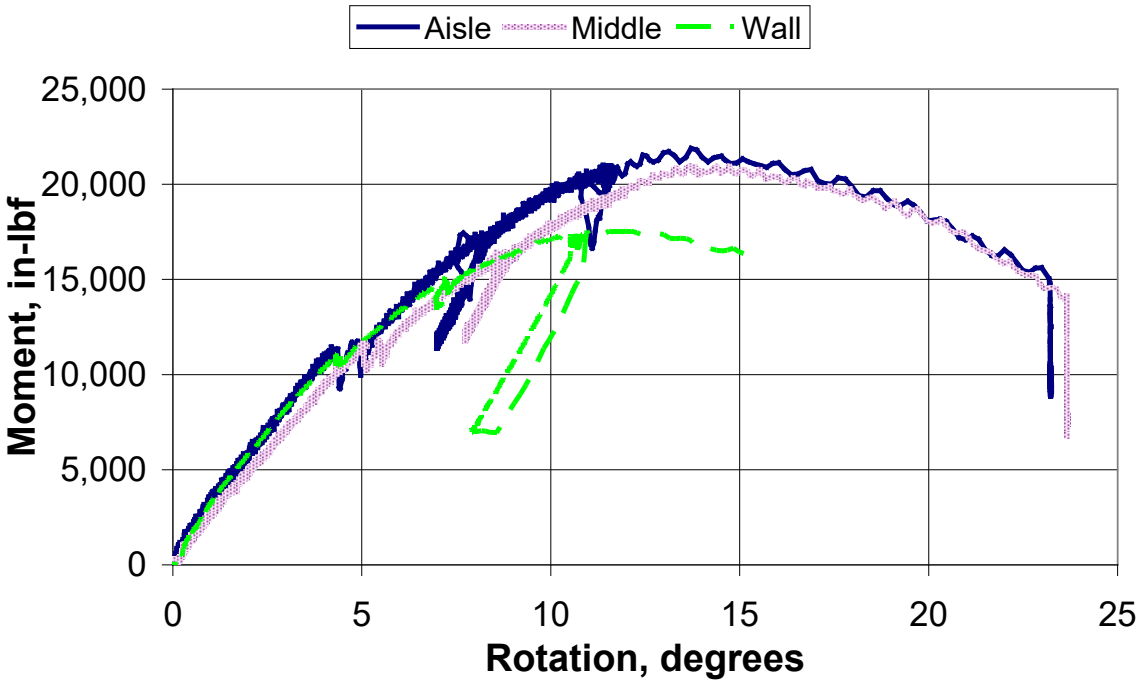

Figure 61. Moment vs. rotation behavior from FF knee load test

9.1.3 Forward-Facing Head Load Test

Figure 62 shows the seats before and after the FF head load test. In this test, the load was applied to the middle of the headrest at a height of 32.5 inches above the seat bottom.

A plot of moment versus rotation behavior for each seat back is shown in Figure 63. All of the seat backs exhibited similar moment-rotation behavior. They rotated forward 10–12 degrees with moments reaching 18,000–20,000 in-lbf before plastic hinges developed in the seat tubes.

The largest reaction loads in this test occurred at the vertically-oriented load cells under the floor pedestal, which reached a peak of 5,600 lbf in compression and 5,200 lbf in tension at the fore and aft floor load cells, respectively. The largest reaction loads at the wall mounts also occurred in the vertical direction, which reached a peak of 1,000 lbf in compression and in tension at the fore and aft floor load cells, respectively.

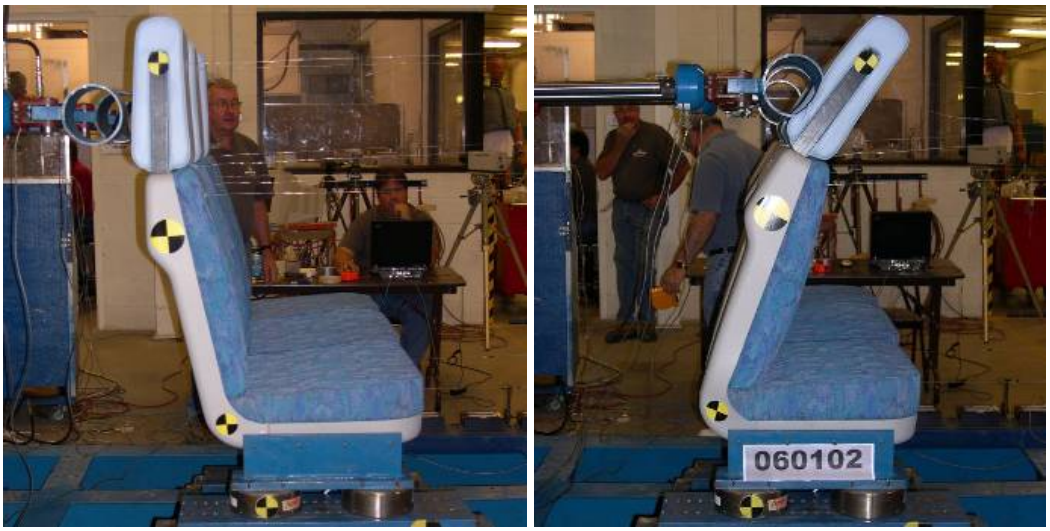

Figure 62. Pre- and post-test photographs of the FF head load test

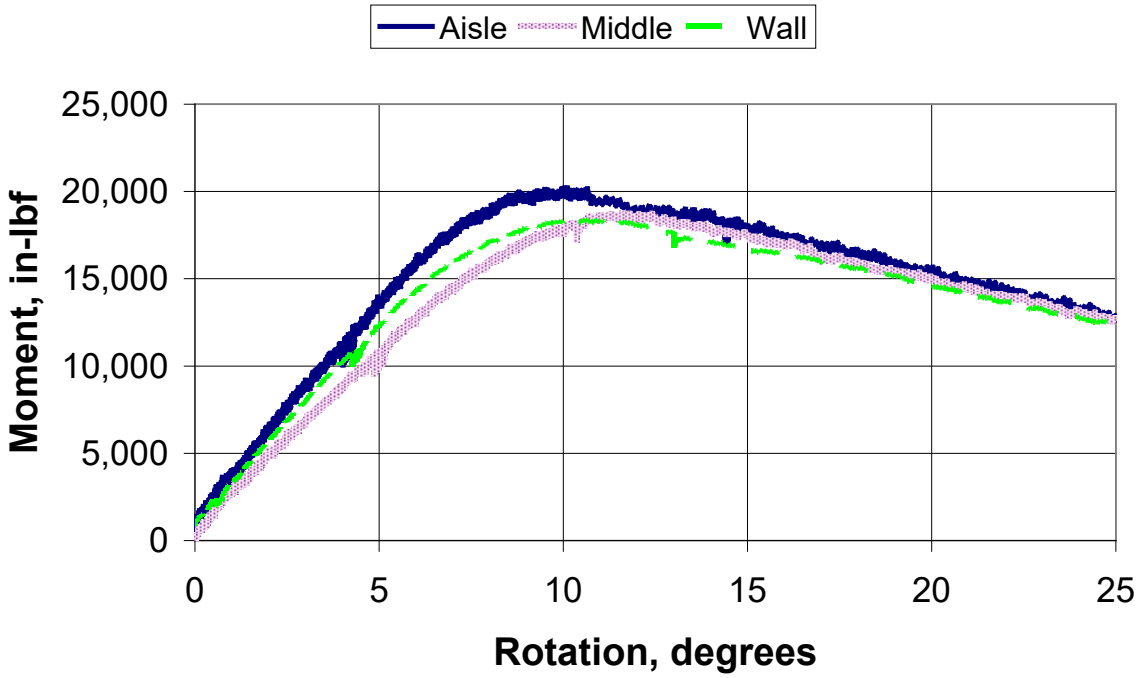

Figure 63. Moment vs. rotation behavior from the FF head load test

9.2 Dynamic Seat Testing

In October 2006, two dynamic sled tests of the seating system were conducted. The seats used in these tests were identical to the seats used in the quasi-static tests – they included the first set of design improvements that were incorporated following the CEM train-to-train test.

In the first dynamic sled test, the seats were oriented in the FF direction and were subjected to an 8g crash pulse. In the second test, the seats were oriented in the RF direction and were subjected to a 12g crash pulse. Each test included three 50th percentile Hybrid III male ATDs. The ATDs

in the aisle and window positions were instrumented to measure triaxial head and chest accelerations, uniaxial (front-to-back) moment and biaxial forces on the upper neck and axial femur loads. The ATD occupying the middle seat was not instrumented due to instrumentation constraints. The face, chest, and knees of each ATD were chalked in different colors to identify contact locations between each body part and the impacted seat.

For each test, two rows of seats were mounted to the test sled at a 32-inch seat pitch. The seat pitch is defined as the longitudinal distance between like features of two seats facing the same direction in consecutive rows. The seats were instrumented to measure triaxial reaction load time-histories at the floor and wall attachment points. Accelerometers were placed on the test sled to measure longitudinal acceleration.

The longitudinal sled system is operated by connecting the front of the sled to a drop weight through a pulley and cable system. The rear end of the sled is connected to a haul-back winch via a cable system. By pulling the sled back a calculated distance and locking it to a release mechanism, the drop weight is raised, storing the potential energy required to accelerate the sled down the track toward a cardboard honeycomb stack placed directly in front of a rigid impact barrier. A “dozer” plate is mounted on the front of the sled to impact the stack of honeycomb cardboard, which is shaped in a predetermined configuration so as to decelerate the sled in a manner that produces the desired deceleration time-history, or crash pulse.

9.2.1 Forward-Facing 8g Sled Test

The target triangular crash pulse and the actual crash pulse measured during the FF 8g sled test are shown in Figure 64. The area under the curve, which is the total change in velocity, is 22.0 mph for the idealized pulse and 21.9 mph for the actual pulse. The test crash pulse was deemed acceptable in that it met the requirements specified in SAE AS8049, Performance Standard for Seats in Civil Rotorcraft, Transport Aircraft, and General Aviation Aircraft [10].

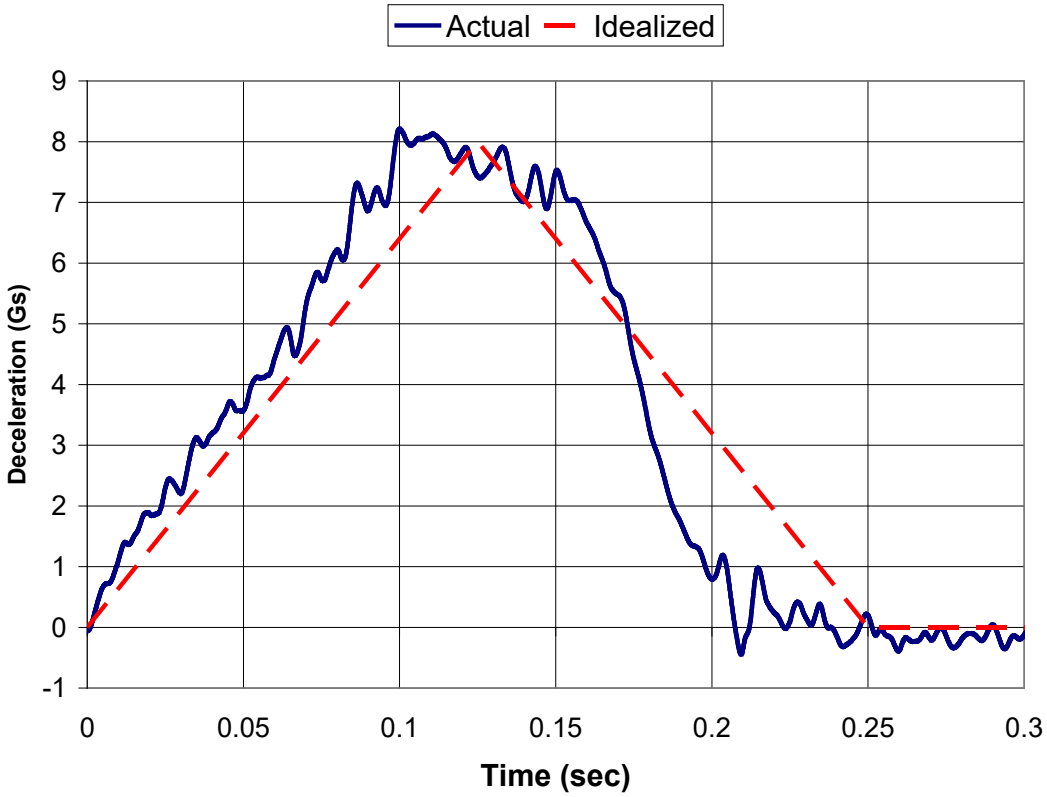

Figure 64. Comparison of target triangular 8g crash pulse and actual measured crash pulse for FF sled test

Figure 65 shows the seats before and after the FF sled test. Results indicated that all of the test objectives were met. The seats remained attached to the test sled with no visible deformation at the seat attachments. The ATDs were compartmentalized. The aisle dummy fell off the sled following the impact, but was effectively compartmentalized per the definition in the APTA Standard for Row-to-Row Seating in Commuter Rail Cars [1]. All injury criteria were below the maximum thresholds and all cushions remained attached.

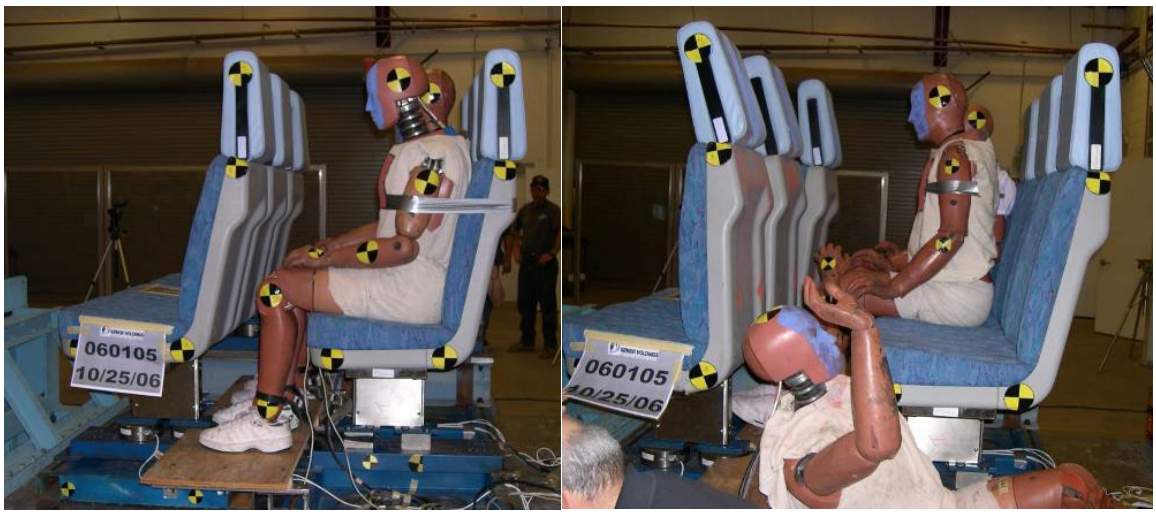

Figure 65. Seats and ATDs before and after the FF 8g sled test

Once the test sled impacts the cardboard honeycomb stack, it begins to decelerate. The ATDs continue to translate forward with respect to the seats at the velocity just prior to impact. In this test, the ATDs' knees impacted the seat backs first, loading and slightly deforming the knee bolsters. This transferred the load into the seat back frames, initiating plastic deformation of the seat tubes. The ATD heads then impacted the headrests and their chests impacted the top of the seat backs. The seat backs deformed plastically, experiencing a permanent rotation between 6 degrees (window seat) and 15 degrees (aisle seat), as determined from pre- and post-test angle measurements of the seat back.

The headrests provide a compliant impact surface that helps to minimize head deceleration. The foam padding deforms and transfers load to the aluminum support plate. Figure 66 shows the permanent set in the back of the headrest, which was accompanied by permanent deformation of the support plate.

All test data were recorded, and all data channels appeared to function properly, with the exception of the left femur load transducer and the upper neck flexion/extension (My) moment transducer in the aisle ATD. Consequently, the Nij dataset is not complete. Based on the upper neck shear (Fx) and axial (Fz) load-time histories alone, and the injury results of the ATD in the window seat, which were slightly more severe, it is nearly certain that the maximum Nij for the aisle ATD would have been lower than the 0.50 maximum Nij measured for the window ATD, and well below the maximum allowed value of 1.0.

Figure 66. Impacted headrests following the FF dynamic sled test

The injury results for the FF 8g test are listed in Table 10. All of the calculated values were below the maximum allowable thresholds, which were taken from the Federal Motor Vehicle Safety Standards [9]. The injury results were modestly higher for the ATD in the window seat

position. The effective stiffness of the aisle seat was lower than that of the window seat due to the torsional compliance of the seat channel.

Table 10. Injury results for FF 8g sled test

Criterion	Injury Threshold [9]	50th Percentile Male, Window Seat	50th Percentile Male, Aisle Seat
HIC15	700	560	260
Nij	1.0	0.50 (Ntf) 0.31 (Nte) 0.46 (Ncf) 0.20 (Nce)	*
Peak Neck Fz, lbf	+940/-900	+480/-280	+140/-180
Chest Accel, g	60	28	19
Femur Load, lbf	2,250	970 920	* 700

* As a result of transducer failure, these quantities were not calculated.

The peak reaction loads for each load cell are listed on a schematic representation of the seat shown in Figure 67. (Note that a negative load value is indicative of a force opposite the direction of the arrow.) The critical load was assumed to be the vertical tensile load in the load cell under the rear pedestal-to-floor bolted connection, since this was where the failure initiated in the FF occupant experiment in the CEM train-to-train test. The peak load measured at this position in the train-to-train test was 6,830 lbf, at which point the attachment failed. The peak load measured at the same position in the sled test was 9,850 lbf. The results of this sled test indicated that the modifications to the pedestal attachment provided a significant improvement in the attachment strength.

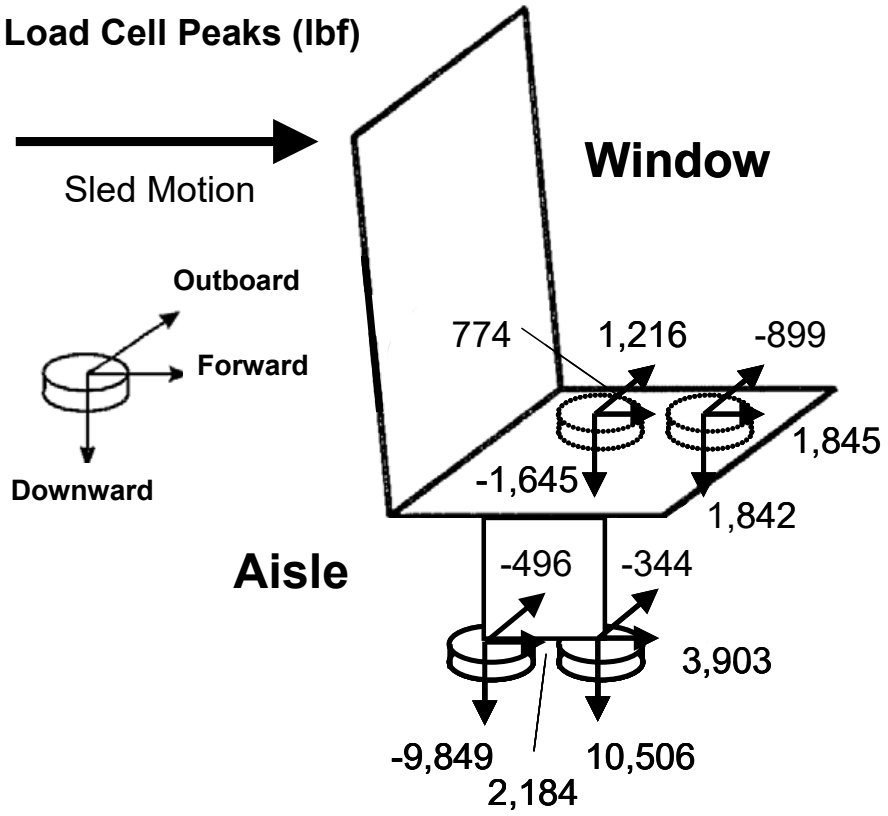

Figure 67. Schematic of peak reaction loads measured during the FF 8g sled test

9.2.2 Rear-Facing 12g Sled Tests

The first of two sled tests with the seats oriented in the RF configuration and subjected to a 12g crash pulse was conducted in October 2006. Like the seats used in the quasi-static test, the pedestal was strengthened for this test. However, despite these changes, the pedestal became detached during this test, with the forward pedestal bolt failing by fracture. Prior to failure, the maximum vertical tensile load in the pedestal reached almost 13,500 lbf, nearly twice the load measured during the full-scale train-to-train collision test. Despite this significant increase in connection strength between the pedestal and the floor, the large vertical tensile load that arose during the RF crash test was enough to overcome the additional strength. One contributing factor was that the actual test pulse was significantly more severe than the 12g target pulse that was the basis for the design. The test pulse, as shown in Figure 68, increased to 12g after only about 0.105 seconds instead of 0.125 seconds. At 0.125 seconds, the calculated kinetic energy of the system was about 60 percent higher than it would have been if the target 12g triangular pulse had been followed exactly. (Note that, despite this large difference in kinetic energy, this pulse met the minimum requirements of SAE AS8049). After 0.125 seconds, the pulse went even higher – to over 15gs – but this was likely due to the failure of the seat pedestal.

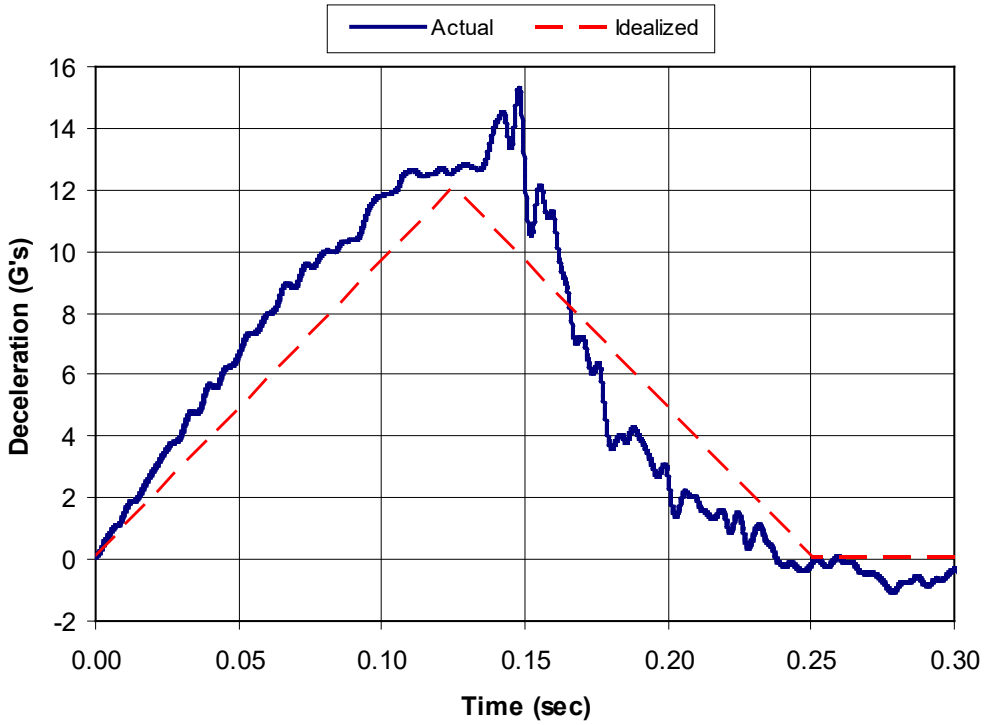

Figure 68. Comparison of target and actual measured crash pulses for the first RF 12g sled test

Subsequent to this first test, the seat design was further analyzed and additional modifications to the pedestal and channel were prescribed. The additional modifications, as noted in Section 5.6, included larger bolts at the floor and wall connection points to prevent seat attachment failure. Two additional rivet nuts per seat module were also added to ensure that the seat-to-channel attachment would not fail. An additional cushion retention clip was added to each seat frame to ensure cushion securement during the 12g test.

The newly modified seats were successfully tested under the RF 12g conditions in August 2007. All test conditions were identical to the previous RF test. Figure 69 shows the idealized triangular crash pulse and the actual crash pulse measured during the RF 12g sled test. The area under the curve, which is the total change in velocity between 0.0 and 0.25 seconds, is 32.9 mph for the idealized pulse and 32.7mph for the actual pulse. The test crash pulse was deemed acceptable in that it met the requirements specified in SAE AS8049 [10].

Figure 70 shows pre- and post-test photographs from the second RF sled test. The seats remained attached to the test sled with no visible deformation at the seat attachments. The ATDs were clearly compartmentalized. All injury criteria were below the maximum thresholds and all cushions remained attached.

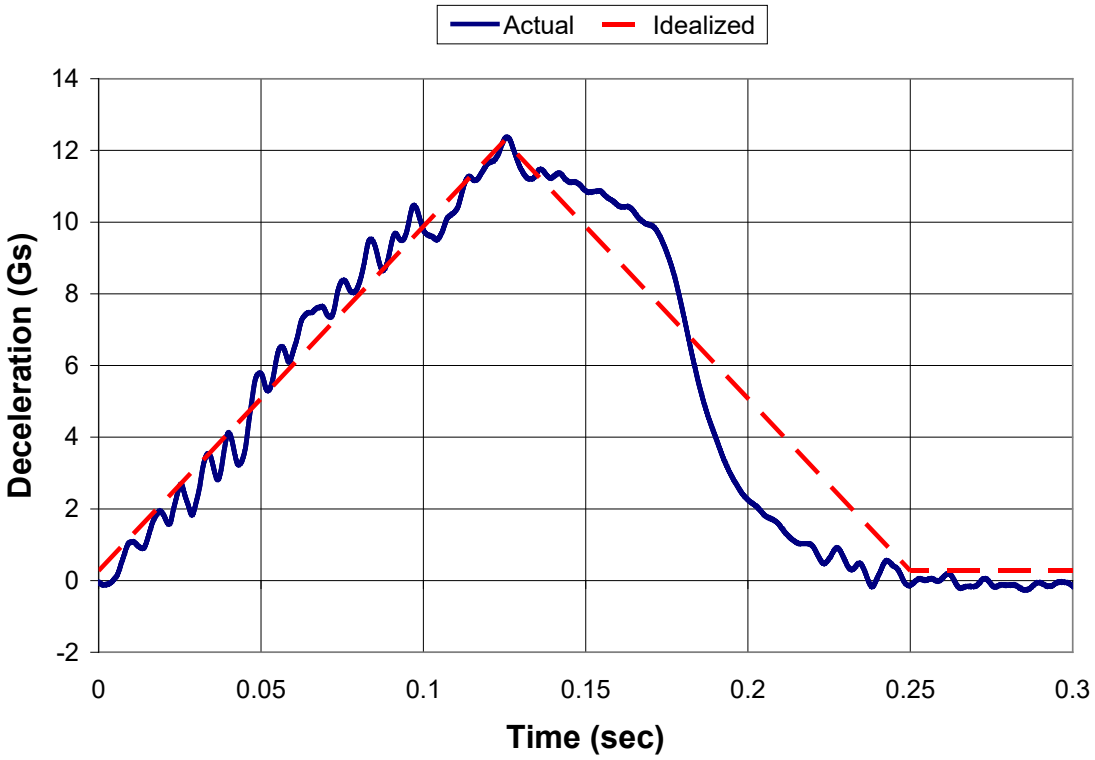

Figure 69. Comparison of target and actual measured crash pulses for the second RF 12g sled test

Figure 70. Pre- and post-test photographs of the RF 12g sled test

Immediately after impact, the ATDs translated backwards into the seat back cushions, with minimal vertical displacement. The heads appear to have been well-supported by the headrests. The seat backs then began to deform, reaching a permanent rotation between 22 and 28 degrees, as determined from pre- and post-test angle measurements of the seat back. The ATDs rebounded away from the seat backs with minimal velocity relative to the test sled and seats. They came to a stop with their heads resting against the adjacent seat back. They slid forward on

the bottom cushion a few inches, but not enough for their knees to make contact with the adjacent seat.

The injury results for the RF 12g test are listed in Table 11. All the measured values were less than 25 percent of the maximum allowable thresholds. The results from this sled test indicated that the RF seating configuration provided a high degree of occupant protection under extremely severe collision conditions. All injury criteria in this test were below the injury criteria measured in the FF 8g test, even though the collision energy was over 100 percent higher.

Table 11. Injury results for RF 12g sled test

Criterion	Injury Threshold [9]	50th Percentile Male, Window Seat	50th Percentile Male, Aisle Seat
HIC15	700	20	70
Nij	1.0	0.10 (Ntf) 0.14 (Nte) 0.03 (Ncf) 0.10 (Nce)	0.15 (Ntf) 0.22 (Nte) 0.03 (Ncf) 0.17 (Nce)
Peak Neck Fz, lbf	+/-	+130/-2	+2300/-10
Chest Accel, g	60	1	15
Femur Load, lbf	2,250	50 940	n/a*

*The ATD in the aisle position was not equipped with femur load cells.

The peak reaction loads for each load cell are listed on a schematic illustration of the seating system shown in Figure 71. The RF 12g collision environment was much more severe than those of any of the previous occupant experiments conducted under the FRA's Railroad Equipment Safety Program. In the first RF 12g sled test and the RF occupant experiment on the CEM train-to-train test, the critical load path was through the rear load cell of the pedestal-to-floor attachment, as this was where both seat detachments initiated. In the train-to-train test the peak load at this position was 6,420 lbf when the attachment failed. In the first RF 12g sled test the peak load at this position was 13,600 lbf when the attachment failed. In the successful RF 12g sled test, the peak load measured at this position was 14,070 lbf. This load was nearly 50 percent higher than the largest vertical tensile load measured in the FF 8g sled test. Attention has been drawn to the large reaction loads associated with these extreme collision conditions such that car builders and seat manufacturers designing for similar conditions can be alerted to the high strength requirements. Note that the loads can be expected to be about one-third smaller for two-seat systems.

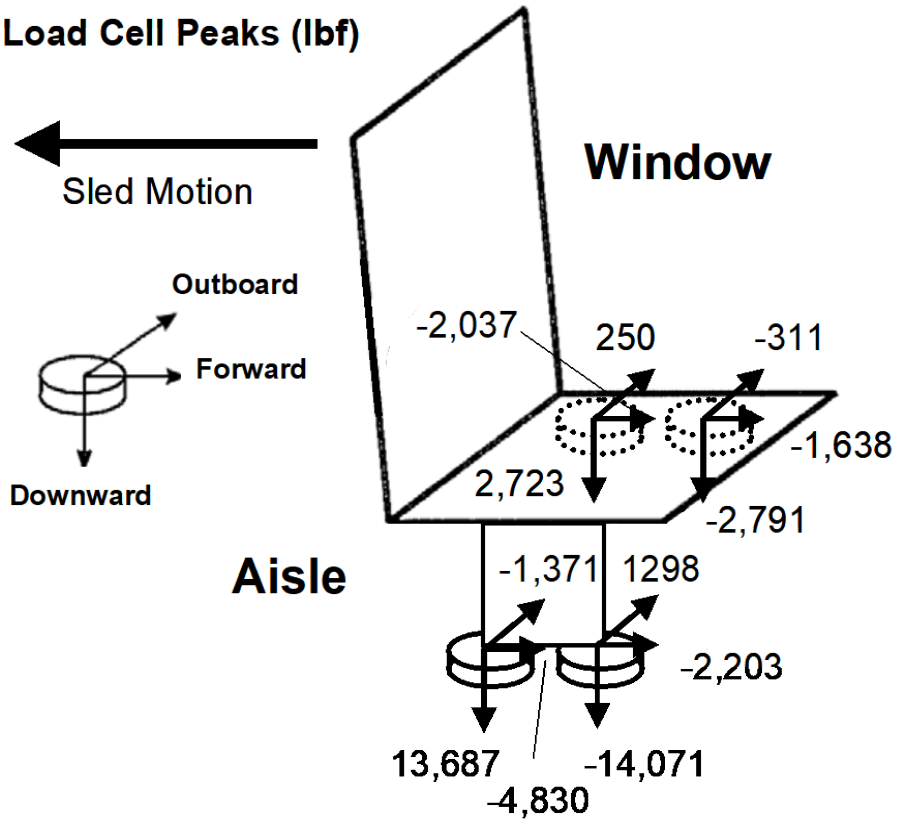

Figure 71. Schematic of peak reaction loads in RF 12g sled test

10. Comparison of Tests and Analyses

In this section, the predictions of the FEA and MADYMO models described in Section 7 are compared with the results of quasi-static and dynamic sled tests described in Section 9.

10.1 Quasi-Static Tests

The quasi-static tests were characterized by two primary results:

- Reaction loads at the seat support channel and pedestal attachment points
- Force-displacement characteristics (from which moment-rotation characteristics can be estimated)

Peak values from load cell measurements for the three quasi-static tests were compared to Abaqus predictions in Table 12. Note that the Abaqus results presented in this table do not include a 10 percent increase in tube strength that was later added to the model to account for hardening of the tubes during manufacturing. Note also that the sign convention was based upon the orientation of the load cells in the test – positive values indicate that the load cell was in tension. For vertical loads, this implies that positive values represent upward loads. Total loads in the longitudinal and vertical directions are compared in Table 13. Also shown in Table 13 are the calculated moments about the aft pedestal connection point for the three load cases. These moments were taken about a lateral axis, i.e., and were due to forces in the longitudinal and vertical directions.

The vertical loads on the pedestal appeared to be consistent with the moment results. These two results can be viewed as key indicators of the degree of consistency between the model and test results, and are indicated in bold.

A comparative review of the key results from the quasi-static FEA models and tests, as summarized in Table 12 and Table 13, indicates the following:

- Model and test results appeared to agree best for the FF head load test. For this case, the various measures of peak load and moment indicated that the model under-predicted the results of the test by 3 to 15 percent.
- The difference in agreement for the FF knee load case appeared to be greater, ranging from 16 to 22 percent.
- The difference in agreement for the RF case appeared to be highest, ranging from 15 to 32 percent. Note that, with the exception of the longitudinal load, the differences were all less than 30 percent.
- The model appeared to do a good job predicting the distribution of *total* reaction load between the wall and the pedestal.
- The model also appeared to be consistent in its predictions of the individual vertical reaction loads, i.e., the degree of under-prediction tended to be the same at the wall and at the pedestal.
- The model was not, however, able to correctly predict how the longitudinal reaction loads were split between the forward and aft connections at either the wall or the pedestal. This was not surprising, given the difficulty of correctly modeling the compliance of the system between either of these two points.

Table 12. Comparison of FEA model predictions and test measurements of peak longitudinal (L) and vertical (V) load cell forces from the three quasi-static tests

Test	Load Cell	Test (L) [lbf]	Analysis (L) [lbf]	% diff (L)	Test (V) [lbf]	Analysis (V) [lbf]	% diff (V)
FF knee load	cylinder-window	-1850	-1720	-7			
	cylinder-middle	-2210	-1530	-31			
	cylinder-aisle	-2300	-1710	-26			
	pedestal fwd	3810	1440	*	**-10240**	**-8570**	**-16**
	pedestal aft	750	1790	*	**9830**	**7860**	**-20**
	pedestal total	4560	3230	-29			
	wall fwd	1280	1325	*	-1880	-1650	-12
	wall aft	400	450	*	1720	1450	-16
	wall total	1680	1775	6			
FF head load	cylinder-window	-570	-550	-4			
	cylinder-middle	-590	-560	-5			
	cylinder-aisle	-640	-560	-13			
	pedestal fwd	520	680	*	**-5643**	**-5500**	**-3**
	pedestal aft	770	710	*	**5161**	**4870**	**-6**
	pedestal total	1290	1390	8			
	wall fwd	310	430	*	-1020	-1350	32
	wall aft	150	-190	*	960	1110	16
	wall total	460	240	-48			
RF load	cylinder-window	-1900	-1370	-28			
	cylinder-middle	-2260	-1350	-40			
	cylinder-aisle	-2140	1410	-34			
	pedestal fwd	-950	-1550	*	**11580**	**9640**	**-17**
	pedestal aft	-3480	-1170	*	**-12530**	**-10650**	**-15**
	pedestal total	-4430	-2720	-39			
	wall fwd	-540	920	*	2180	2510	15
	wall aft	-1240	-2250	*	-2700	-2890	7
	wall total	-1780	-1330	-25			

Table 13. Comparison of FEA model predictions and measurements for total loads and moments (moments taken about aft pedestal connection) for the three quasi-static tests

Test	Load	Test Result	Analysis Result	% diff
FF knee load	longitudinal-cylinders (lbf)	-6140	-4970	-19
	longitudinal-load cells (lbf)	**6220**	**4960**	**-20**
	vertical load (lbf)	-920	-1280	39
	moment (in-kip)	**126**	**98**	**-22**
FF head load	longitudinal-cylinders (lbf)	-1760	-1620	-8
	longitudinal-load cells (lbf)	**1740**	**1640**	**-6**
	vertical load (lbf)	-740	-1140	54
	moment (in-kip)	**65**	**55**	**-15**
RF load	longitudinal-cylinders (lbf)	-6151	-4090	-34
	longitudinal-load cells (lbf)	**-6130**	**-4140**	**-32**
	vertical load (lbf)	-1510	-1450	-4
	moment (in-kip)	**141**	**108**	**-23**

It was not surprising that the agreement between model predictions and test results was best for the FF head load test. For this case, the seat back was essentially loaded in bending and the deformation of the pedestal, the channel, and the connections between the channel and pedestal and between the channel and the seat were minimal. For the other two cases, the lower load application point introduced much more shear loading into the system, and the deformation of the seat back tube with respect to the remainder of the seat system became more complex and, for that reason, more difficult to model. For example, for both the forward knee and rear loading cases, the deformation of the connections between the channel and the seat base appeared to be much greater than the model predicted. This deformation complicated the load path and affected the reaction loads, making it less likely that the model and test would agree.

For the forward knee-loading case, there was another difference between model and test that likely affected the comparisons. It was evident that in the test the seat back shroud formed a buckle on its side. This buckle was a clear indication that the shroud was experiencing a significant load and contributing to the overall resistance of the seat back. The model did not capture this effect, as the seat back shroud was assumed to rotate freely as the seat back bent.

For the RF case, there was an even larger potential difference between the model and the test. Inspection of the test photographs indicated that the point of application of the load to the body block appeared to be a few inches lower than in the model. This difference of a few inches can easily affect the resulting loads by 20 to 30 percent or more. Much of the discrepancy between model predictions and test measurements for the longitudinal load can be attributed to this difference.

Another factor that likely contributed to differences between the model and the test is the level of friction acting between the load applicator and the seat, the seat back, or the head rest (the seat models assume coulomb friction with a coefficient of 0.3). Additional calculations performed on the single-tube model originally used to predict the moment-rotation behavior of the seat back indicated that the moment-rotation behavior was quite sensitive to this value. The original single-tube calculations were made without friction. Subsequent calculations indicated that using a coefficient of 0.3 increased the peak load by 7 percent. Given this effect, it seemed quite likely that the effective friction coefficient also played a role in the differences.

Figure 72 through Figure 74 show sample comparisons of FEA model predictions and test results for the three quasi-static load cases. Note that, due to the under-prediction of forces that was highlighted in Table 12 and Table 13, the yield and ultimate strength of the A513 tube material was eventually increased by 10 percent to account for the hardening due to forming of the bend in the tubes. Some of the analyses described below, as noted, include this increase in strength.

Figure 72 is a comparison of the force-displacement characteristics for the head load test. This figure shows results for the center seat. The model under-predicted the load by a little less than 10 percent for this case. Note that this model *did not* include the 10 percent increase in strength.

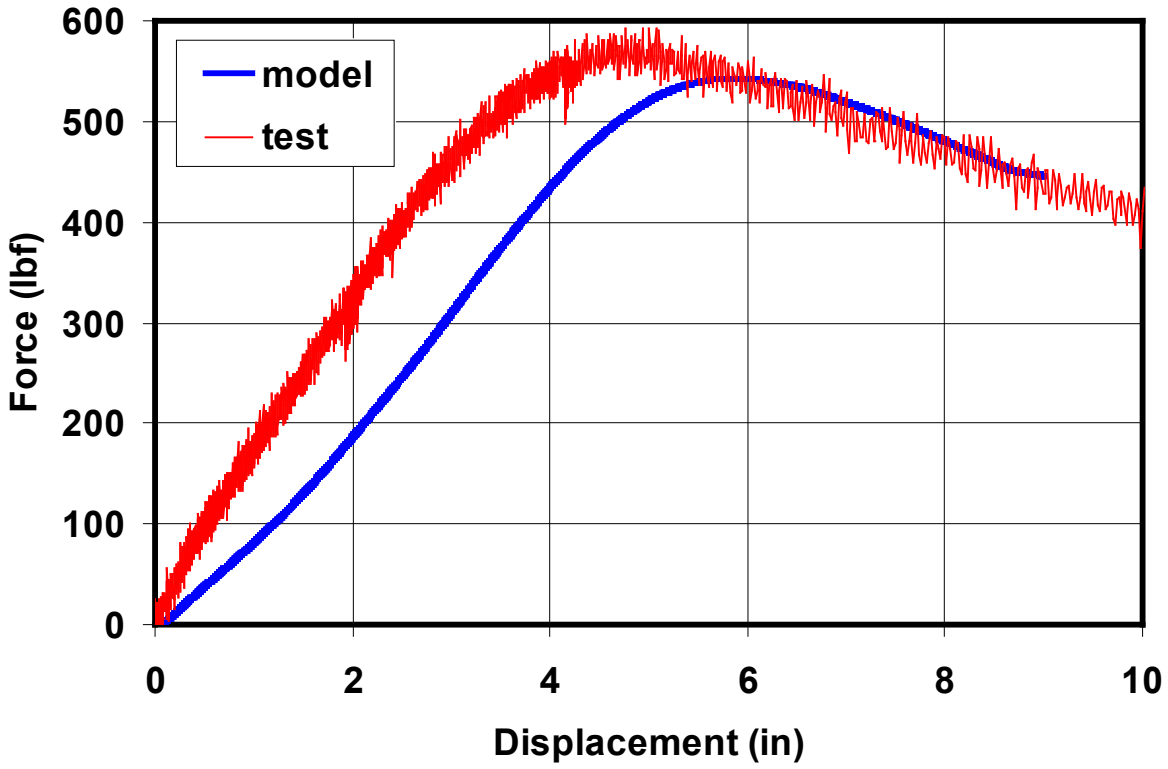

Figure 72. A comparison of FEA model predictions and test measurements for the force-displacement characteristics of the center seat for the FF head load test

Figure 73 compares test and model predictions of force-displacement characteristics for the window seat for the knee-load test. For this analysis, the results are presented *with and without* the 10 percent increase in tube strength. As is evident in the figure, the 10 percent increase in

strength, not surprisingly, led to about a 10 percent increase in predicted force. Note that the slope of the predicted force-displacement curve was steeper than the slope for the test curve. This was likely due to rotational compliance between the seat channel and the individual seat modules that was not picked up in the model.

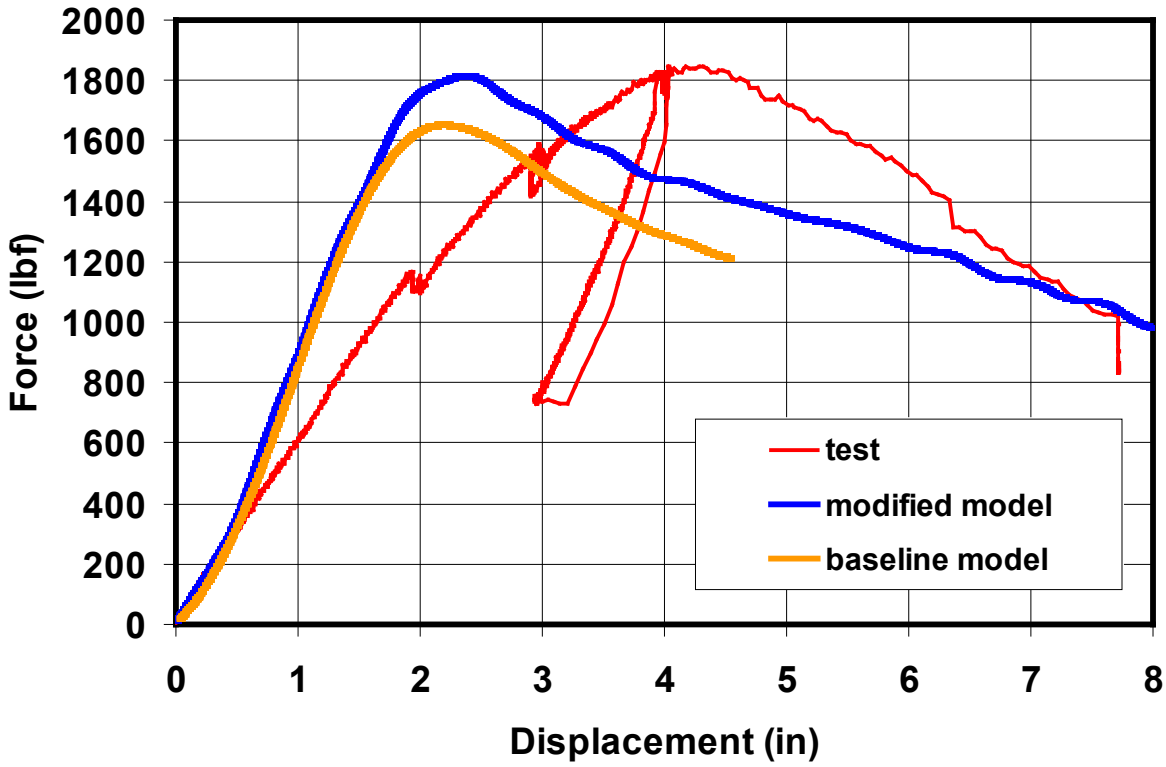

Figure 73. A comparison of FEA model predictions and test measurements for the force-displacement characteristics of the window seat for the FF knee load test

Figure 74 shows a comparison of model and test results for the RF torso load test. For this analysis, only the modified material model for the tubes, with a 10 percent higher strength, was used. As is evident, the additional strength improved the consistency between the model and the test. The initial slopes of the curves did not quite match, but that was likely due to the manner in which the seat back cushion compliance was modeled, as well as friction and other factors.

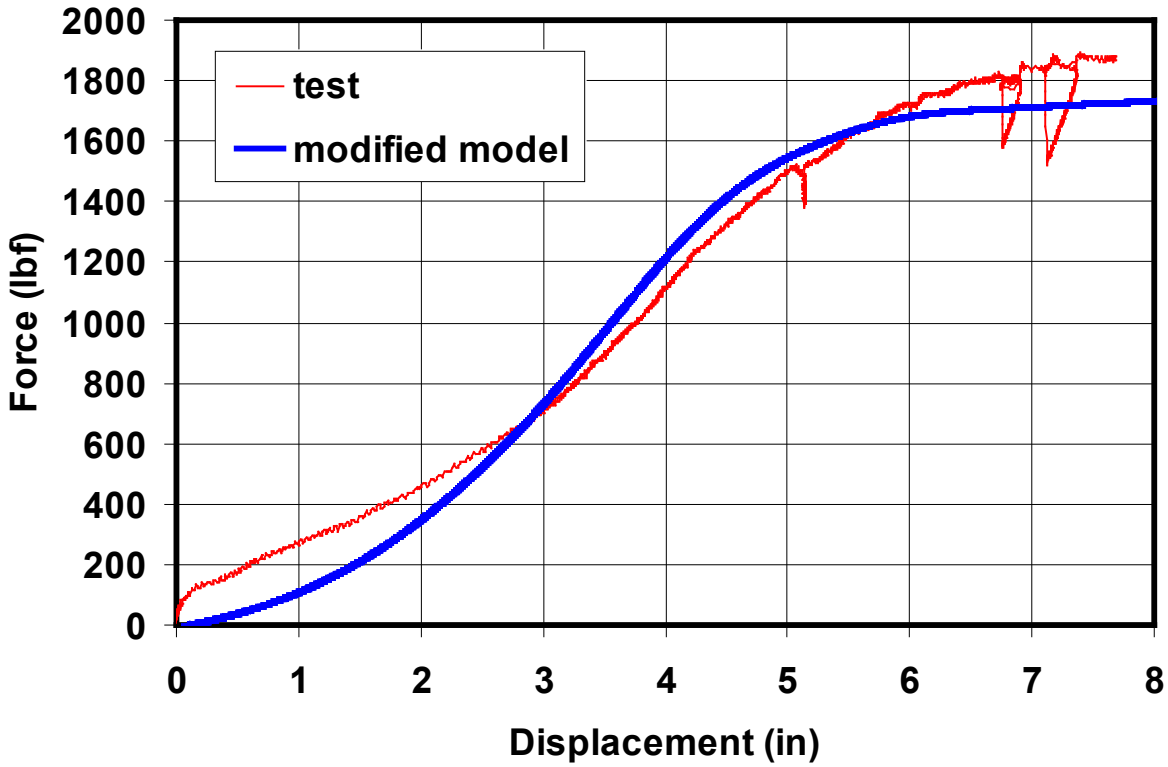

Figure 74. A comparison of FEA model predictions and test measurements for the force-displacement characteristics of the window seat for the RF torso load test

10.2 Dynamic Tests

Comparisons between model predictions and test measurements for the FF and RF dynamic sled tests are summarized below. Note that for the FF, 8g sled test, due to the complex interaction between the ATDs and the seat back, only the MADYMO predictions of dynamic behavior are compared with test measurements. For the RF, 12g sled test, where the load transfer from the ATD to the seat cushion is less complex, Abaqus predictions are also be compared with measured values.

10.2.1 Forward-Facing 8g Sled Test

The MADYMO model predicted that the seat backs rotated 15 degrees (window) to 17.5 degrees (aisle). Test results indicated that the seat backs rotated 6 degrees (window) to 15 degrees (aisle), with the middle seat rotating a little less than the aisle seat. Clearly there was much more variation in rotation than the model predicted. Since the individual seat modules and the ATDs were identical, this difference must be attributable to compliance in the seat pedestal and channel. In the MADYMO model, some compliance was defined at the connection between the pedestal and the floor and between the channel and the wall, but the channel was considered to be rigid. In the test, it appeared that twisting of the channel about the connections to the wall and the pedestal was significant enough to affect the total seat back rotation. The rotation at the window was much less because of its proximity to the very stiff wall mounting location.

Figure 75 shows a comparison of predicted longitudinal force-time histories calculated by adding the longitudinal reactions at the four attachment points. The total force calculated in the test was about 7,700 lbf. The MADYMO model predicted a peak force of about 8,000 lbf and captured the time-history of force quite well.

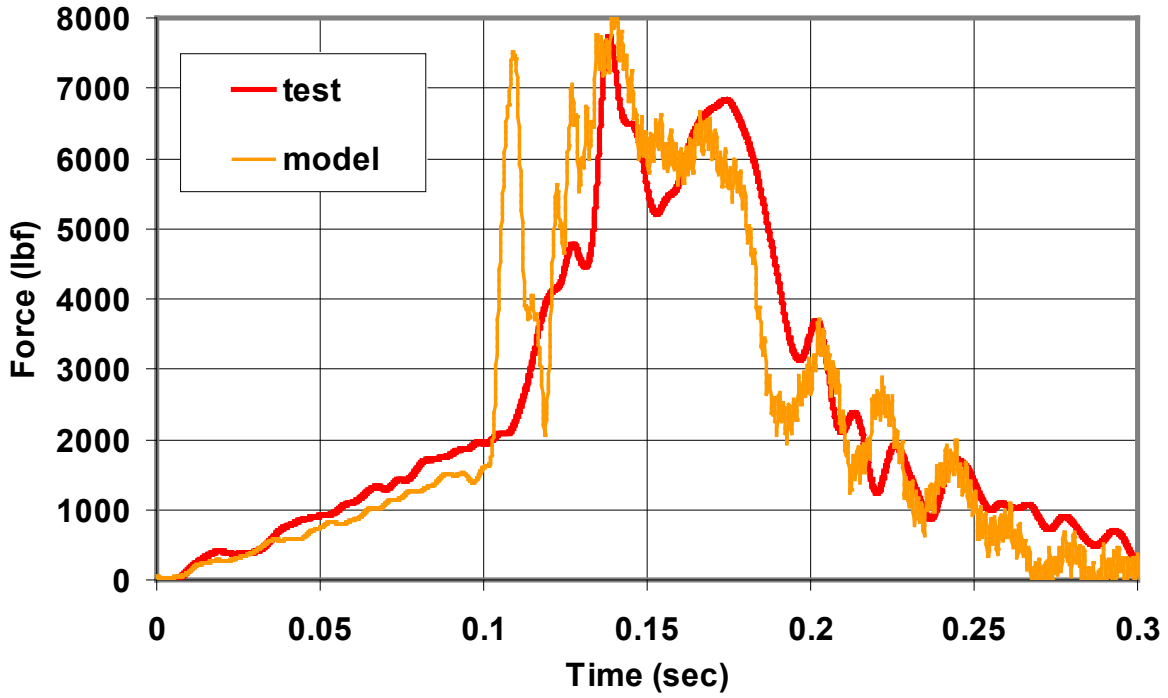

Figure 75. A comparison of total longitudinal reaction force-time histories predicted by MADYMO and measured in the FF sled test

A comparison of vertical reaction forces in the floor of the pedestal are shown in Figure 76. Once again the agreement between model and test results was quite good. For the critical tensile reaction at the back of the pedestal, the MADYMO model predicted a peak force of about 9,680 lbf at the back of the pedestal. The value measured in the test was 9,850 lbf. At the wall, the agreement was also quite good – the model predicted a peak tensile force of 1,700 lbf compared to a measured value of 1,650 lbf.

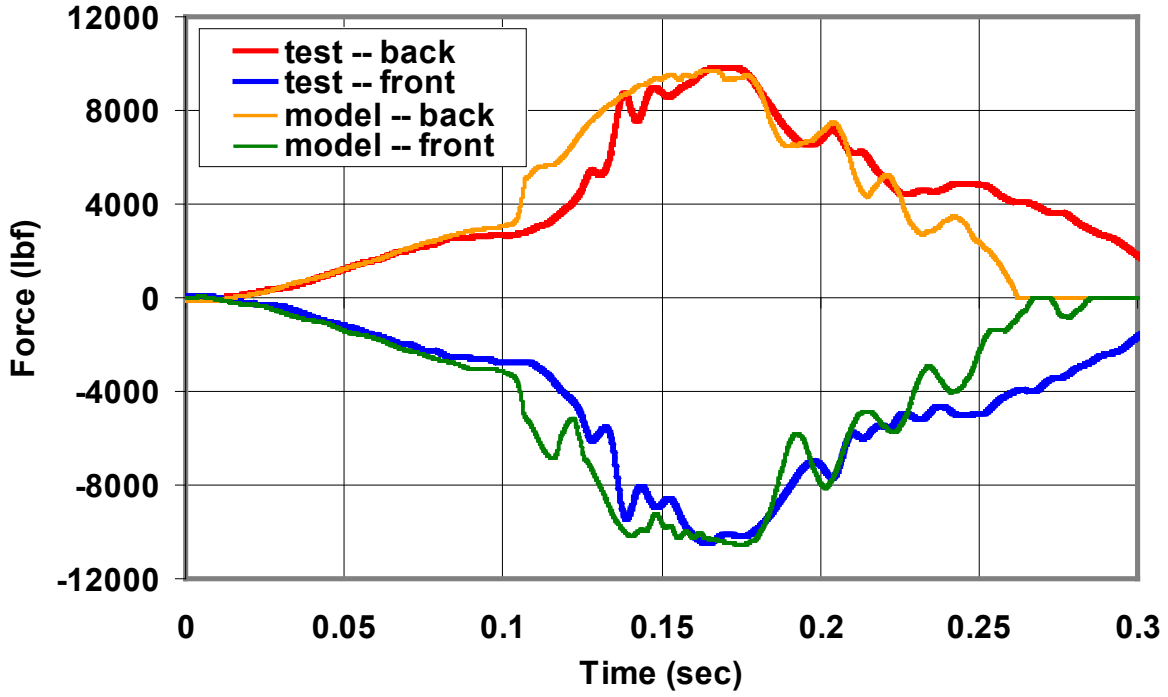

Figure 76. A comparison of vertical reaction force-time histories predicted by MADYMO and measured in the FF sled test at the front and rear pedestal connections

Comparisons of injury parameters for this scenario are presented in Table 14. As one might expect based on the seat rotation results, the test measurements indicated that the window seat ATD exhibited higher injury levels than the aisle seat ATD, whereas the MADYMO model predicted similar injury levels. Overall, the MADYMO predictions were conservative relative to the measured values, except for the chest acceleration parameter for the window ATD. The predicted value was about 50 percent higher than the predicted value. This result was consistent with the much smaller rotation relative to the model prediction that occurred during the test. The test result was still much less than the maximum allowable of 60g.

Table 14. Comparison of MADYMO model predictions with measurements for the Window (W-ATD) and Aisle (A-ATD) ATD injury parameters for the FF 8g sled test

Injury Criterion	Threshold [9]	MADYMO (W-ATD)	Test (W-ATD)	MADYMO (A-ATD)	Test (A-ATD)
HIC15	700	650	560	590	260
Nij	1.0	0.65	0.50	0.69	0.28
Peak Neck Fz, lbf	+940/-900	+140/-290	+480/-280	+142/-330	+140/-180
Chest Accel., *g*	60	17.0	27.5	17.8	18.8
Femur Load, lbf	2,250	1,770	970	1,300	700

10.2.2 Rear-Facing 12g Sled Test

For this scenario, the MADYMO model predicted that each of the seat backs would rotate about 27 degrees. Test results indicated that the seat backs rotated between 22 degrees (window seat) and 28 degrees (aisle seat). As noted, the differences in measured values were likely due to the twisting of the channel.

Abaqus predictions of reaction force versus time are compared to test results in Figure 77. Model predictions were quite consistent with test measurements, with the test peaks coming about 0.015 seconds later than model predictions. This was not unreasonable, given that the Abaqus model was based on the target crash pulse, not the measured pulse. The peak longitudinal load was predicted to be approximately 9,500 lbf, and was measured during the test to be 10,500 lbf. The MADYMO model predicted a peak total longitudinal reaction load of 9,000 lbf, as shown in Figure 78.

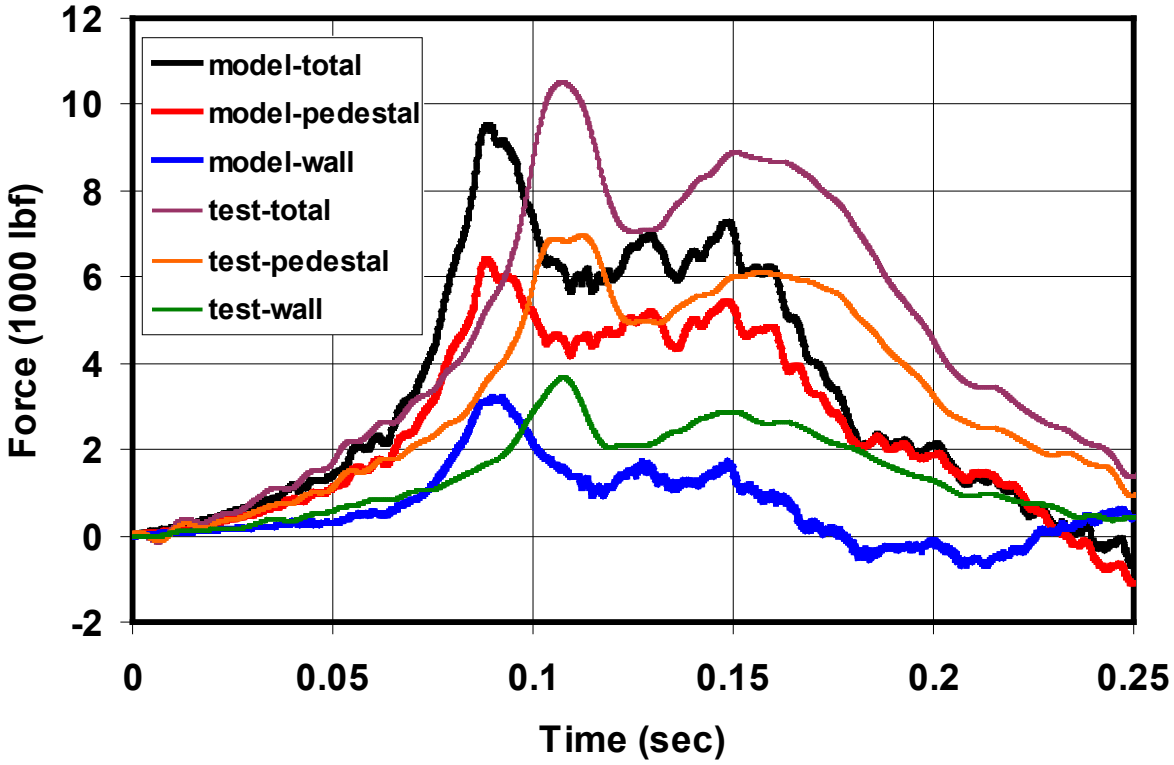

Figure 77. Comparison of Abaqus model predictions and test results for longitudinal reaction forces for the RF sled test

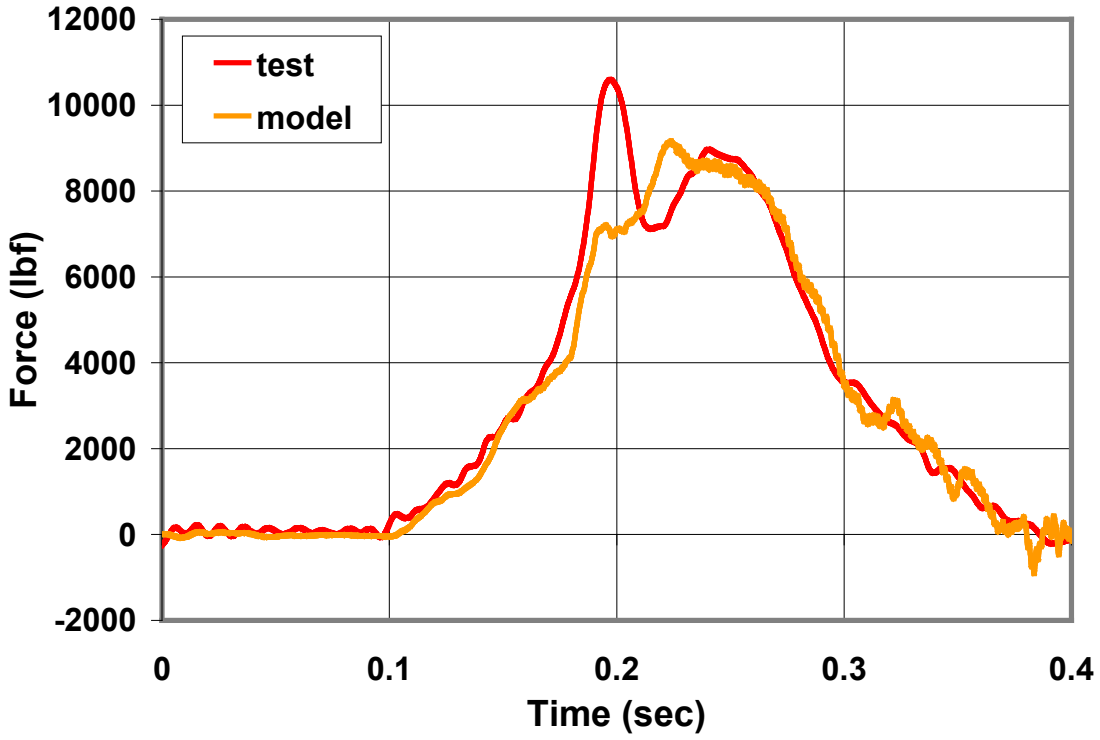

Figure 78. A comparison of total longitudinal reaction force-time histories predicted by MADYMO and measured in the RF sled test

Comparisons of both Abaqus and MADYMO results for the vertical reaction loads in the pedestal and wall attachments are shown in Figure 79 and Figure 80. Once again, the model predictions were very consistent with the test measurements, with the MADYMO models doing a better job of capturing the timing of the peaks. The maximum vertical tensile load in the pedestal (Figure 79), which has turned out to be a key attribute of this loading scenario, was predicted by Abaqus to reach 13,600 lbf and predicted by MADYMO to reach 14,800 lbf. Test measurements indicated that the peak actually reached 14,100 lbf.

At the wall (Figure 80), the reaction loads were much smaller, and again the agreement between the predictions of both models and the test results was quite good. The Abaqus model predicted peak loads of +3,500/-2,700 lbf, the MADYMO model predicts peak loads of +3,100/-3,700 lbf, and the measured test peak values were +2,700/-2,800.

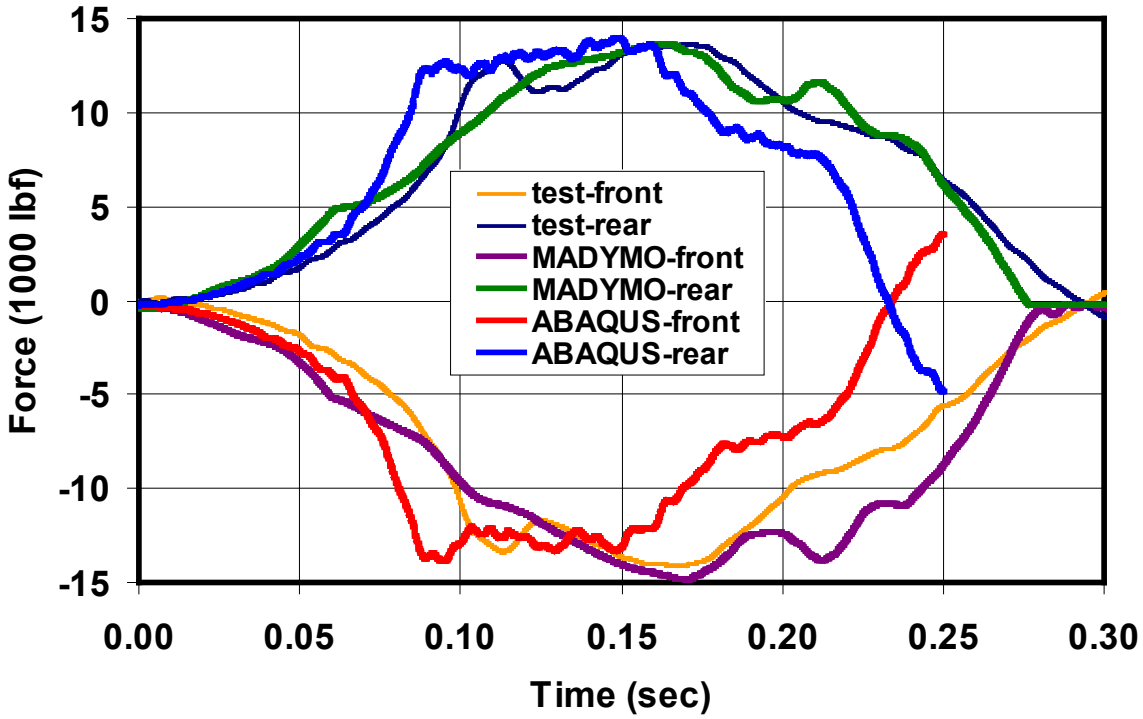

Figure 79. Comparison of Abaqus and MADYMO model predictions and test results for vertical reaction forces at the pedestal for the RF sled test

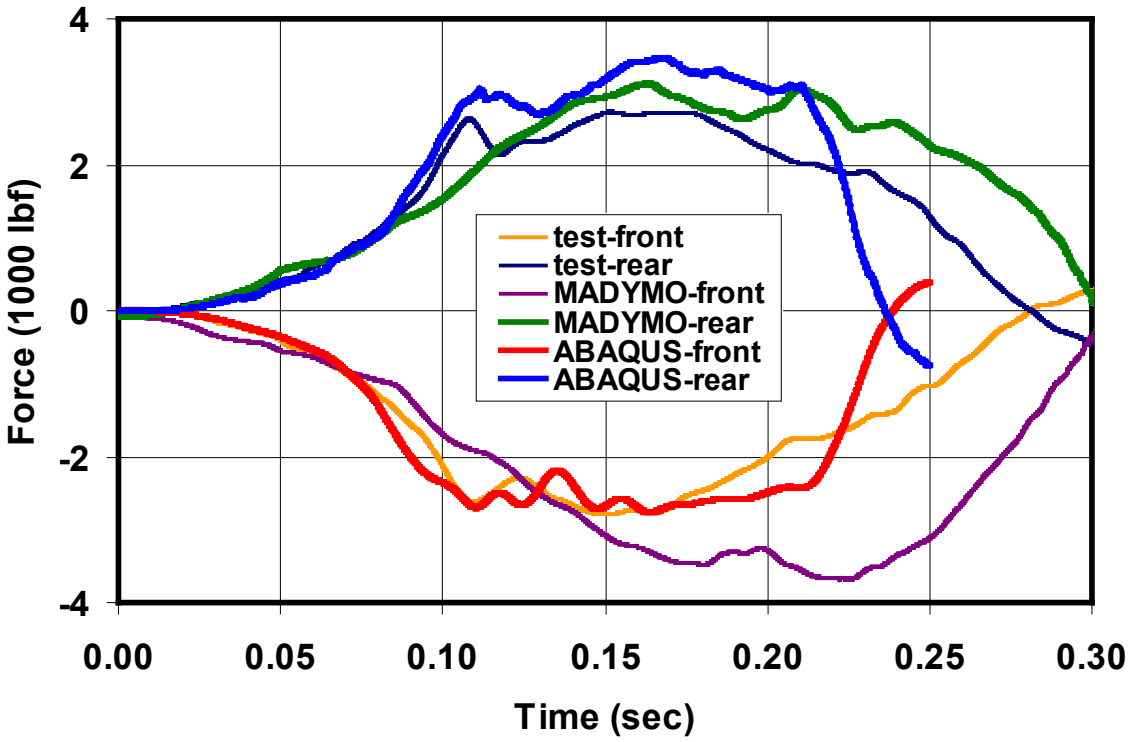

Figure 80. Comparison of Abaqus and MADYMO model predictions and test results for vertical reaction forces at the wall attachment for the RF sled test

Injury parameters predicted by MADYMO models for this scenario are compared with measured values in Table 15. In general, both the predicted and measured injury parameter values were quite low relative to the threshold values. For the most part, the MADYMO predictions were again conservative, with the exception of the chest acceleration for the aisle ATD, which was slightly higher than the predicted value, but well below the threshold value. The generally low injury parameter values were consistent with the very large rotation of the seat that was used to gradually absorb the impact energy of the collision.

Table 15. Comparison of MADYMO model predictions with measurements for the Window (W-ATD) and Aisle (A-ATD) ATD injury parameters for the RF 12g sled test

Injury Criterion	Threshold [9]	MADYMO (W-ATD)	Test (W-ATD)	MADYMO (A-ATD)	Test (A-ATD)
HIC15	700	72	17	79	70
Nij	1.0	0.25	0.14	0.27	0.22
Peak Neck Fz, lbf	+940/-900	+226/-45	+130/0	+242/-39	+230/-10
Chest Accel. *g*	60	14.4	11	13.7	15
Femur Load, lbf	2,250	240	n/a	580	50

11. Summary and Conclusion

Despite difficulties associated with test failures of the connection of the pedestal to the floor, the seating system design ultimately proved capable of withstanding quite severe loads and successfully protecting the occupants.

The final design of the three-person seating system represents a fairly straightforward modification to an existing two-seat design. The seat modules themselves did not require radical design changes. The headrest was extended upward to provide better compartmentalization and support during the impact of the face into the headrest cushion. The stiffness of the foam used in the headrest was increased so that it would absorb more energy and not be as likely to bottom out. Researchers originally thought that the seat frame's tubing would also need to be strengthened in order to increase its energy-absorbing capacity. However, tensile test results indicated that the measured yield and ultimate strengths of the A513 steel that the tubes were fabricated from – 71.2 ksi and 81.3 ksi, respectively – were actually much greater than the 50 ksi and 70 ksi specified minimum values for this type of steel. Moreover, the results of the quasi-static tests suggested that the effective strength of the seat back was about 10 percent higher than the measured values, likely as a result of the local hardening of the steel near the bends in the tubes that occurs during the frame forming process. The net effect of these two factors increased the energy absorption capacity of the seat back by about 60 percent relative to the estimated capacity based on specified minimum strength values.

Note that once a collision scenario is defined, the choice of seat tube material and size can be determined to yield a desired extent of seat back rotation. If less rotation is desired, the strength of the tubes can be increased accordingly. Such a change would likely be accompanied by an increase in injury levels. Using the modeling tools described in this report, the design of the seating system can be easily modified to accommodate different scenarios or different limits on seat rotation. The results of the tube and seat testing made it clear that such optimization must include both a thorough characterization of the component material properties and the dynamic system behavior, with particular attention paid to the strength of the connections.

Due to the extremely high forces that arose during the 12g crash pulse, it was necessary to make extensive modifications to the strength and stiffness of the seat support system. These changes ultimately included:

- Increasing the thickness of the channel
- Closing off the channel bottom
- Adding doubler plates at the pedestal and wall attachment points
- Adding an extra rivet nut at each seat-to-channel attachment bracket
- Increasing the thickness of the pedestal
- Adding bolted connections between the pedestal and the channel and between the pedestal and the floor
- Increasing the length of the weld at the base of the pedestal
- Increasing the size of the bolts at the connection to the floor and wall

It is worth noting that many of these changes were partly necessitated by two features of this system:

- The seats were required to accommodate three passengers instead of two.
- The RF collision load specification – a 12g, 250 ms triangular pulse – was quite severe.

For two-person seating systems, the design of the individual seat modules would not be affected, but the loads on the attachment points would be about one-third smaller, so that lower-gauge steel and smaller bolts might be suitable in the support channel and pedestal to save weight and cost. Similar weight and cost savings would be available for systems that would be subjected to less severe collision environments.

12. References

[1] American Public Transportation Association. (January 2003). APTA SS-C&S-016-99, Rev. 1. Standard for Row-to-Row Seating in Commuter Rail Cars. Washington, D.C.

[2] Tyrell, D., Jacobsen, K., Martinez, E. (November, 2006). A Train-to-Train Impact Test of Crash Energy Management Passenger Rail Equipment: Structural Results. American Society of Mechanical Engineers, Paper No. IMECE2006-13597.

[3] Severson, K., Parent, D. (November, 2006). Train-to-Train Impact Test of Crash Energy Management Passenger Rail Equipment: Occupant Experiments. American Society of Mechanical Engineers, Paper No. IMECE2006-14420.

[4] Tyrell, D.C., Severson, K.J., Marquis, B.J. (November, 1995). Train Crashworthiness Design for Occupant Survivability. American Society of Mechanical Engineers, AMD-Vol. 210, BED-Vol. 30, 59–74.

[5] Federal Railroad Administration. (July 2009). Occupant Protection Experiments in Support of a Full-Scale Train-to-Train Crash Energy Management Equipment Collision Test [DOT/FRA/ORD-09/14]. Washington, DC: U.S. Department of Transportation.

[6] Federal Railroad Administration. (January, 2002). Passenger Rail Two-Car Impact Test Volume II: Summary of Occupant Protection Program [DOT/FRA/ORD-01/22]. Washington, DC: U.S. Department of Transportation.

[7] Abaqus/Explicit, Version 6.8. Simula, Inc. Providence, RI.

[8] MADYMO, Version 7.0. TNO Automotive, Delft, The Netherlands.

[9] Code of Federal Regulations. (October, 2004). Title 49 Part 571, Standard 208; Occupant Crash Protection. Washington, D.C.

[10] Society of Automotive Engineers. (September, 1997). SAE AS8049, Performance Standard for Seats in Civil Rotorcraft, Transport Aircraft, and General Aviation Aircraft. Warrendale, PA.

Appendix A
Design Requirements for the Commuter Rail Passenger Seat Project

A.1. INTRODUCTION

A.1.1. PURPOSE

The purpose of this requirements document is to define the occupant protection portion of the design requirements for a commuter seat installed in Tier II passenger rail equipment, as described in 49 CFR Part 238, Section 401.

A.1.2. DEFINITIONS

a) ATD – anthropomorphic test device (also referred to as crash test dummy – see 49 CFR Part 572).

b) Compartmentalization – an occupant protection strategy that contains an occupant within a designated area during a collision, such as between an occupied row of seats and the adjacent row.

c) Crash energy management (CEM) – an occupant protection strategy that absorbs collision energy in a controlled manner, crushing unoccupied areas of the car first while better preserving the integrity of the occupied areas.

d) Commuter seat – a typical seat design used in commuter rail service.

e) Longitudinal – the direction in a horizontal plane parallel to the tracks and/or seat rails.

f) Lateral – the direction in a horizontal plane perpendicular to the tracks and/or seat rails.

g) Longitudinal crash pulse – the acceleration time history of a railcar during a collision, in a direction that is in-line with the tracks.

h) Occupant – a seated passenger occupying a seat placement in a normal manner.

i) Row-to-row seating – a seating configuration in which all rows of seats face the same direction, either fore or aft.

j) Seat pitch – the longitudinal distance between like points on adjacent rows of seats.

k) Secondary impact velocity – the speed at which an occupant impacts a fixed part of the car interior during a collision, generally a seat back or bulkhead.

l) Tertiary impact – passengers who have undergone a secondary impact and have glanced off of that object to impact another object in the car.

A.1.3. STANDARDS

A.1.3.1. Code of Federal Regulations, Title 49, Part 238, Section 401: Scope

A.1.3.2. Code of Federal Regulations, Title 49, Part 238, Section 435: Interior Fittings and Surfaces

A.1.3.3. Code of Federal Regulations, Title 49, Part 238, Section 503: Inspection, Testing, and Maintenance Requirements

A.1.3.4. Code of Federal Regulations, Title 49, Part 238, Appendix B: Test Methods and Performance Criteria for the Flammability and Smoke Emission Characterization of Materials Used in Passenger Cars and Locomotive Cabs

A.1.3.5. Code of Federal Regulations, Title 49, Part 571, Section 208: Occupant Crash Protection

A.1.3.6. Code of Federal Regulations, Title 49, Part 572: Anthropomorphic Test Devices

A.1.3.7. APTA SS-C&S-016-99, Rev 1, Standard for Row-to-Row Seating in Commuter Rail Cars

A.1.3.8. SEA AS8049: Performance Standards for Seats in Civil Rotorcraft and Transport Airplanes

A.2. GENERAL DESCRIPTION

In support of the Federal Railroad Administration, the Volpe Center conducts research in the area of rail equipment crashworthiness. Recent activity has focused on crash energy management (CEM) – the concept of building sacrificial crush zones at the ends of the cars – as a strategy for improving occupant survivability during a collision. The results of this research indicate that CEM technology can significantly reduce the loss of occupant volume during a collision. However, a consequence of preserving the occupant volume in the CEM design is potentially more severe occupant injuries due to secondary impacts, when compared with the conventional design. Improved interior crashworthiness via a new commuter seat design could help mitigate this consequence. Testing of the new seat design is required to demonstrate that the new seat does indeed provide improved crash protection.

The full-scale impact test of two coupled CEM cars impacting a rigid wall has shown that standard commuter seats may not be compatible with equipment that incorporates crash energy management. In a head-on collision involving CEM railcars, the leading car(s) may have a more severe longitudinal crash pulse than conventional cars in a similar collision. The CEM crash pulse results in a higher secondary impact velocity between the unrestrained occupant and the seat. As a result the seat must absorb more energy, which may cause significant deformation of the seat back, preventing occupant compartmentalization.

This document specifies the design requirements for an improved commuter rail passenger seat that provides occupant compartmentalization during an inline collision of CEM equipment while simultaneously limiting the occupant injury criteria.

The requirements listed here are derived from federal regulations and industry standards. The applicable regulations and standards are listed in Section A.1.3.

A.3. SPECIFIC REQUIREMENTS

The requirements are divided into six sections:

A.3.1 Seat Attachment Requirements

A.3.2 Physical Seat Requirements

A.3.3 Service Requirements

A.3.4 Seat Fabrication Requirements

A.3.5 Performance Requirements for Dynamic Sled Testing

A.3.6 Performance Requirements for Quasi-Static Testing

A.3.1. SEAT ATTACHMENT REQUIREMENTS

A.3.1.1. Attachment Points

The seat shall be attached to an existing passenger car by way of seat rails on the floor and/or wall of the carbody.

A.3.1.2. Mounting Hardware

The hardware used to attach the seat to the carbody shall not require modification of the seat rails. This mounting hardware shall conform to the Code of Federal Regulations, Title 49, Part 238, Section 233, Article (d): “To the extent possible, all interior fittings in a passenger car, except seats, shall be recessed or flush-mounted.”

A.3.2. PHYSICAL SEAT REQUIREMENTS

A.3.2.1. Geometry

The longitudinal distance measured from the forward most point of the seat to the rearward most point must not exceed the same measurement of the current M-style seat, which is approximately 26 inches. There are no limitations on the seat height, but maintaining a comfortable environment for the occupant may limit this dimension for visibility reasons. The width of a three occupant wide seat shall be maintained at approximately 59 inches.

A.3.2.2. Human Factors

The design of the seat geometry shall be with the comfort of the occupant as a secondary goal, with the first being safety.

A.3.2.3. Moment vs. Rotation Characteristic of Seat Back

As a guideline, the moment vs. rotation characteristic of the seat back may fall with the range highlighted in the plot in Figure A-1. Designs with moment vs. rotation performance that fall outside the highlighted range are acceptable as long as they meet the performance requirements set forth in this document.

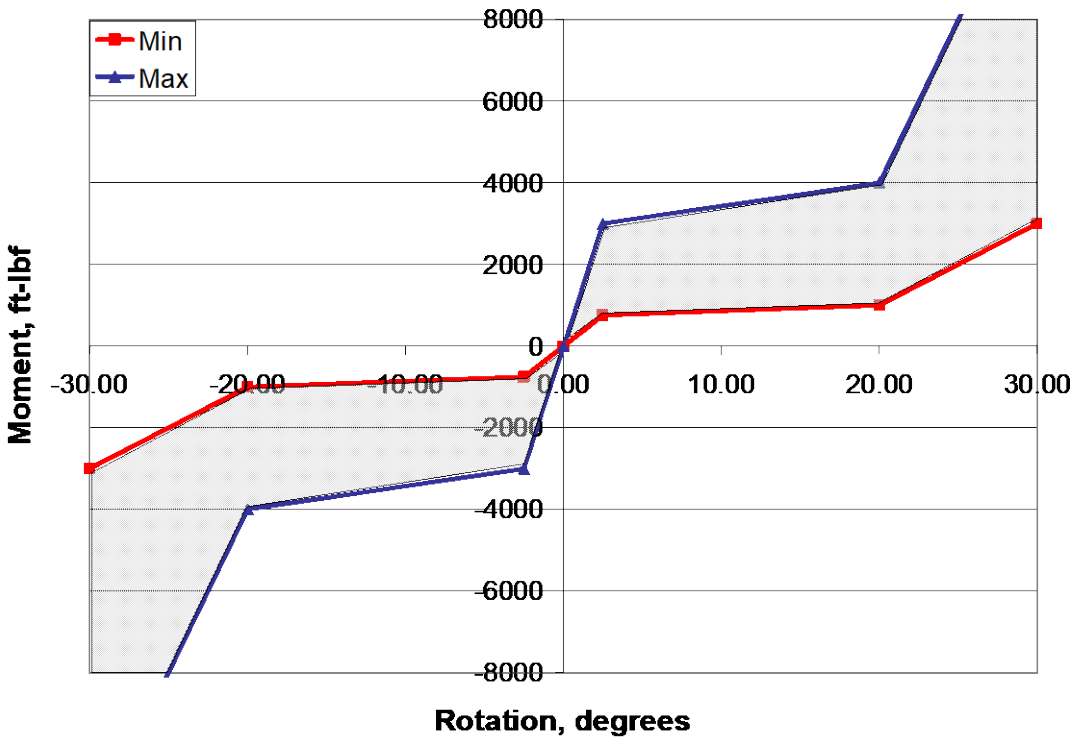

Figure A.1. Allowable range for moment vs. rotation characteristic of seat back

A.3.2.4. Cushions

Cushions should be contoured for occupant comfort and retention.

A.3.3. SERVICE REQUIREMENTS

A.3.3.1. Seat Attachment Strength

The seat attachments to the floor and/or wall shall not experience significant permanent deformation under a static horizontal load of 500 lbf (2,225 N) applied in a longitudinal direction at any point along the seat base/seat pan in the fore and aft direction. This could result in a larger than usual number of attachment points, or strengthening of the rails themselves.

A.3.3.2. Static Seat Strength

Seat frames and components shall be designed to meet the individually applied static load requirements given in APTA SS-C&S-016-99, Rev. 1, with no permanent yielding of structural materials, loss of function or change in appearance of the seat or component. Seats to be tested shall be mounted on a simulated car structure and all components comprising the attachment to the car shall be included. Where it is not feasible to use a simulated car structure, a rigid base may be used. These load requirements include:

- Backrest Strength – Apply a 300 lbf load per occupant perpendicular to the seat back at the upper back of the seat frame at the midpoint of each seat frame, and at a distance of 3 inches below the top of the seat back, as shown in Figure A.2. The load is to be distributed across the seat back. This load shall be applied separately in both directions.

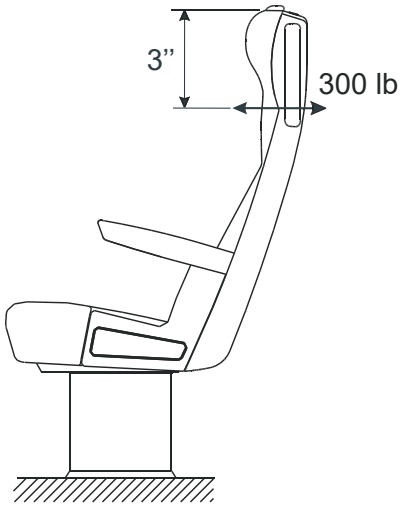

Figure A.2. Backrest strength test loading conditions

- Grab Handle Strength – Apply a 300 lbf load near the middle of the grab handle in the longitudinal direction, as shown in Figure A.3. This load shall be applied separately in both directions.

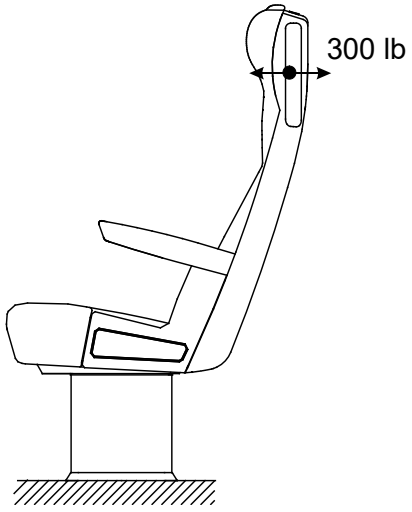

Figure A.3. Grab handle strength test loading conditions

- Vertical Seat Strength – Apply a 450 lbf load per occupant on the seat frame near the front edge of each occupant placement in a vertical downward direction at the midpoint of each occupant position, as shown in Figure A.4. The contact area of the applied load shall not exceed 4 square inches.

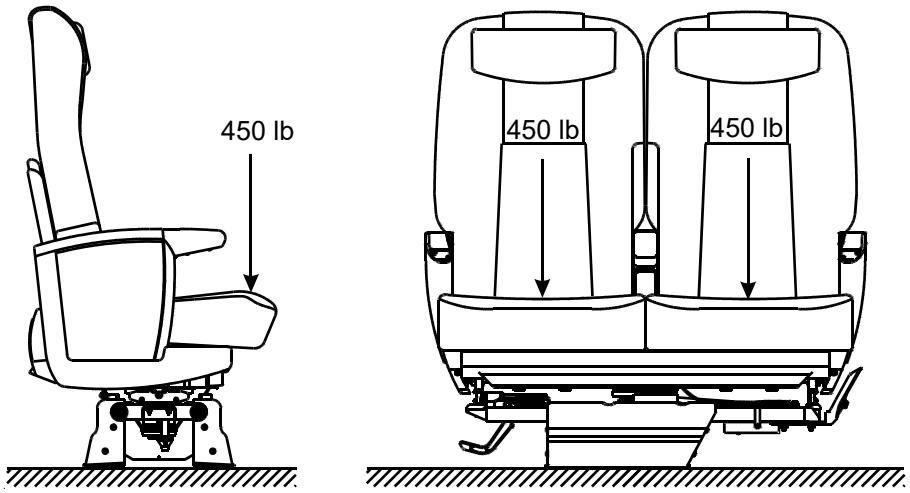

Figure A.4. Vertical seat strength test loading conditions

- Armrest Strength – A load of 250 lb. (113 kg) shall be applied to the horizontal member of the armrest structure at a point that produces maximum stress in the member, as shown in Figure A.5. The contact area of the applied load shall not exceed 4 square inches (26 square cm). This test shall be repeated for the two horizontal conditions (toward the aisle and toward the wall side of the seat) and then vertically downward.
- For seats with folding center armrests, the folding armrest shall be tested by applying a vertical 150 lbf (68 kg) load as near as practical to the end of the armrest, as illustrated in Figure A.5. Separately, a horizontal 150 lbf (68 kg) load shall be applied as near as practical to the end of the armrest. The horizontal load test shall be repeated for both directions. The contact area shall not exceed 4 square inches (26 square cm) in all cases.

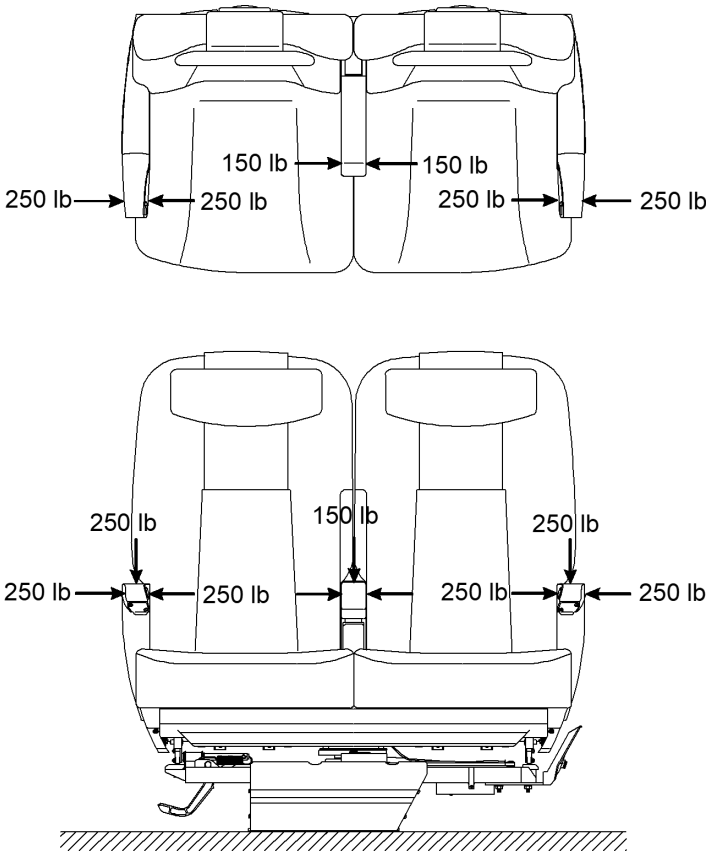

Figure A.5. Armrest strength test loading conditions

A.3.3.3. Maintainability Issues

The seats shall be designed for ease of cleaning and repair. The materials shall be resistant to staining, tearing, or other damage due to excessive wear or misuse. The seat shall be able to be cleaned by ordinary cleaning products. There shall be no pockets for dirt or debris to collect. No lubrication or adjustments should be necessary during the normal seat life. Repairs should require the use of only standard hand tools.

Ideally, the points of contact between the seat and the floor should be minimized in order to facilitate ease of cleaning or sweeping of the floor. This will also ensure occupant comfort with increased leg room.

The service life of the seats should reflect the length of time in service before a retrofit is needed, which is 8–12 years. For time less than 12 years, the seats shall not require regular checks, testing, or adjustments, if possible. Any mechanisms should be both simple and tamper-proof, or inaccessible to the passenger.

A.3.4. SEAT FABRICATION REQUIREMENTS

A.3.4.1. General

The design should utilize materials and fabrication methods suitable to the railroad environment.

A.3.4.2. Materials and Workmanship

The materials shall meet the flammability and smoke requirements given in 49 CFR Part 238, Appendix B. The seat design shall minimize the use of protrusions, sharp edges or corners that could cause injury, catch, or damage the clothing of passengers or crew members. The use of exposed fasteners should be minimized. The seat should be free of rattles or loose joints that could create noise or vibration during normal operation. All parts of the seat should be interchangeable with parts of like seats.

A.3.4.3. Drawings

To fabricate the seats, best manufacturing practices shall be used and documented. Drawings shall be released to describe the parts, assemblies, and processes required. The drawings shall, as a minimum, include the following:

- Overall dimensions and tolerances of the seat assembly
- Mounting requirements including hole sizes, recommended bolt sizes and torque requirements, and recommended grade of bolts to be used for mounting
- Description of materials

A.3.5. PERFORMANCE REQUIREMENTS FOR DYNAMIC SLED TESTING

A.3.5.1. Test Objective

The dynamic sled testing of the commuter seats shall be performed in accordance with the test requirements below.

The objective of these tests is to evaluate the crashworthiness performance of a newly designed commuter rail passenger seat under dynamic conditions. The dynamic tests will measure the forces and accelerations experienced by an occupant during collision conditions expected in the leading cars of a train-to-train collision of CEM equipment. The data collected will be used to evaluate the effectiveness of the seat design in meeting the objectives.

A.3.5.2. Approach

Two dynamic sled tests will be conducted. Each sled test will consist of two rows of three-passenger commuter seats mounted to a seat track, fastened to the test sled in the same manner that the seats will be fastened to a railcar. Instrumented ATDs will be placed in the seat row such that they face the next seat row. One test will be conducted with the seats and ATDs in a RF configuration. In the other test, they will be positioned in a FF configuration. The ATDs will be instrumented to measure forces and accelerations so that injury criteria can be calculated.

Each dynamic test will be conducted with a triangular crash pulse, or acceleration time history, of 0.25-second duration. The peak of the crash pulse used in the RF test will be 12g. This crash pulse will approximate the motion expected in a leading cab car in a train-to-train collision of CEM equipment. The intent of this test is to demonstrate that even in a severe collision environment, newly designed RF commuter seats can provide a sufficient level of occupant protection.

The peak of the crash pulse used in the FF test will be 8g. This crash pulse will approximate the motion expected in a coach car directly behind a leading cab car in a train-to-train collision of CEM equipment. The intent of this test is to demonstrate that an improved commuter seat can effectively compartmentalize occupants while simultaneously limiting the injury severity to survivable levels.

A.3.5.3. Test Conditions

Two dynamic sled tests shall be conducted. For each test, two commuter seats facing the same direction shall be fastened to a seat track, fastened to a sub-floor (and potentially a sub-wall) mounted to four tri-axial load cells. The seat pitch shall be 32 inches. Three Hybrid III 50th percentile male ATDs, in accordance with 49 CFR Part 572, Subparts B and E, shall be positioned in accordance with SAE AS8049, such that they face the seat back of the adjacent seat. The ATDs in the aisle and window seats shall be instrumented. The ATD in the middle seat may be un-instrumented. The seat mounting hardware shall be consistent with in-service hardware. See Figure A.6 for a schematic of the sled configuration.

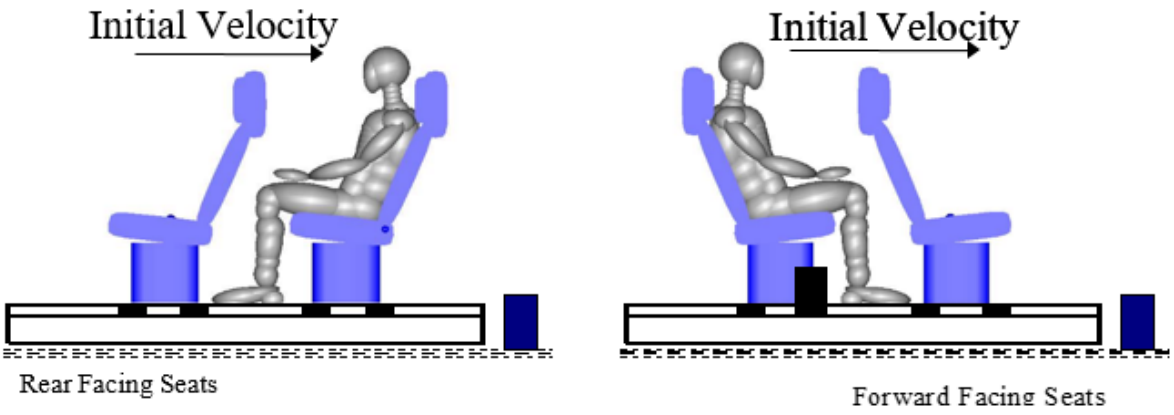

Figure A.6. Schematic of dynamic test configuration

The crash pulses for each test are shown in Figure A.7. The relative velocity vs. relative displacement curves associated with each crash pulse are shown in Figure A.8 to demonstrate that the triangular crash pulses specified result in a secondary impact velocity similar to those expected in a train-to-train collision of CEM cars.

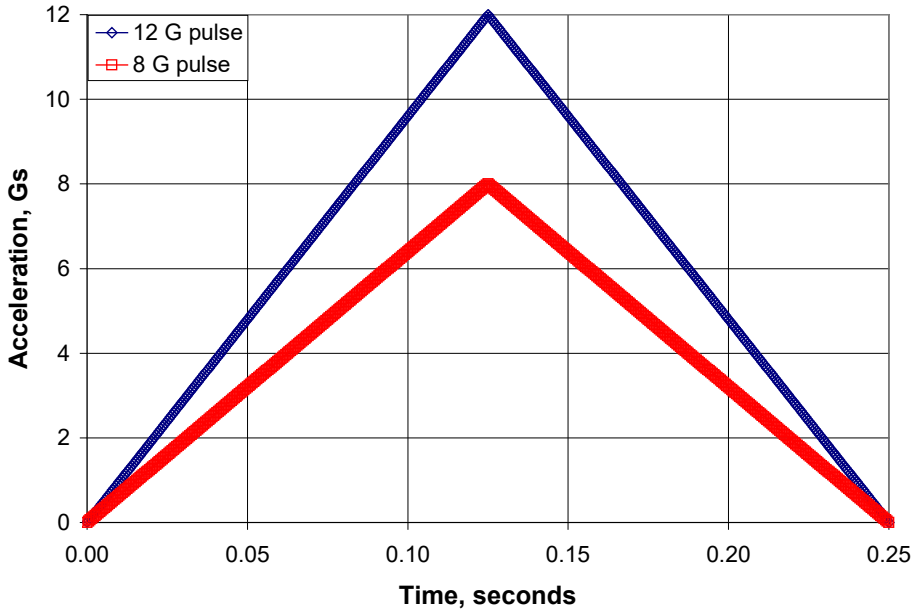

Figure A.7. Test crash pulses

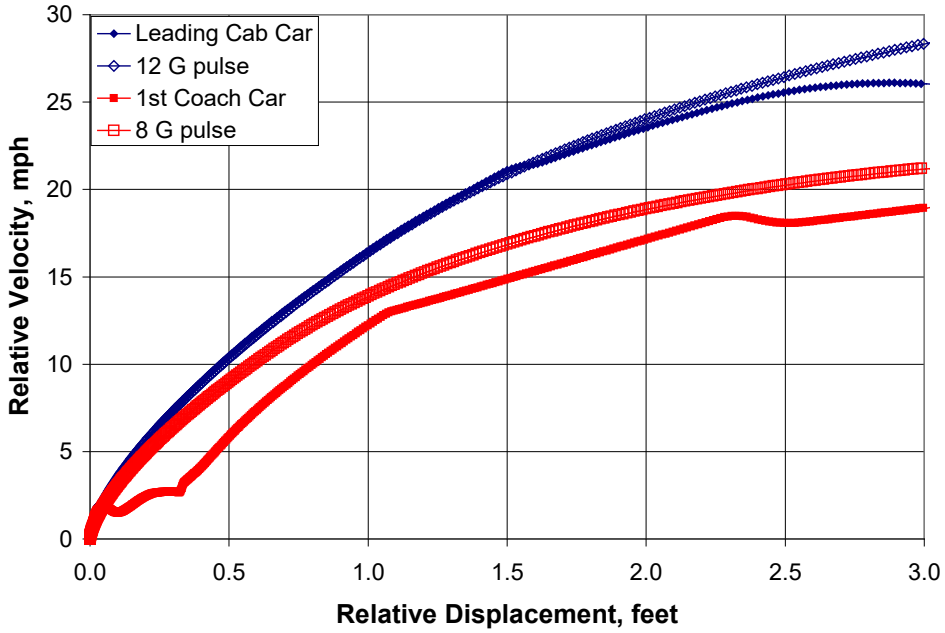

Figure A.8. Secondary impact velocities

A.3.5.4. Seat Performance

During dynamic testing, the seat must remain attached to the test sled at all attachment points. The deformation of the seat back shall not result in the formation of any sharp edges with which the occupant is at risk of coming into contact. The seat back must not rotate more than 30°in either direction.

A.3.5.5. Occupant Response

During the dynamic testing, all ATDs shall be compartmentalized. Successful compartmentalization requires that the resting position of the ATD after the impact be between the initial seating position and the adjacent seat. The injury indices derived for all ATDs must meet the following criteria, defined in CFR 49 Part 571, Standard No. 208: Occupant Crash Protection:

- HIC15 must not exceed 700.
- Nij must not exceed 1.0.
- Neck tension must not exceed 940 lbf (4,170 N).
- Neck compression must not exceed 900 lbf (4,000 N).
- Chest deceleration must not exceed 60*g* over a 3ms clip.
- Axial femur loads must not exceed 2,250 lbf (10,000 N).

A.3.6. PERFORMANCE REQUIREMENTS FOR QUASI-STATIC TESTING

The quasi-static testing of the commuter seats shall be performed in accordance with the test requirements below.

A.3.6.1. Test Objective

The objective of these tests is to evaluate the crashworthiness performance of a newly designed commuter rail passenger seat under quasi-static conditions.

A.3.6.2. Approach

The quasi-static test will be performed to measure the moment vs. rotation behavior of the seat back and to determine the force levels required to cause failure of the seat and its attachments.

A.3.6.3. Test Conditions

The moment vs. rotation behavior of the seat back shall be measured using a hydraulic loading ram. A single three-passenger commuter seat shall be fastened to the seat track, fastened to a sub-floor (and potentially a sub-wall) mounted on four tri-axial load cells (see Figure A.9). A linearly increasing load shall be applied to the back of the seat back in a horizontal direction. The load shall be applied at a point approximately 12 inches below the top of the seat back. The seat shall be tested to gross failure (significant, permanent deformation or component failure). Horizontal string potentiometers shall be used to measure the deflection at the top, center, and bottom of the seat back and the front of the seat pan. The load application bar shall span the width of all three seat positions.

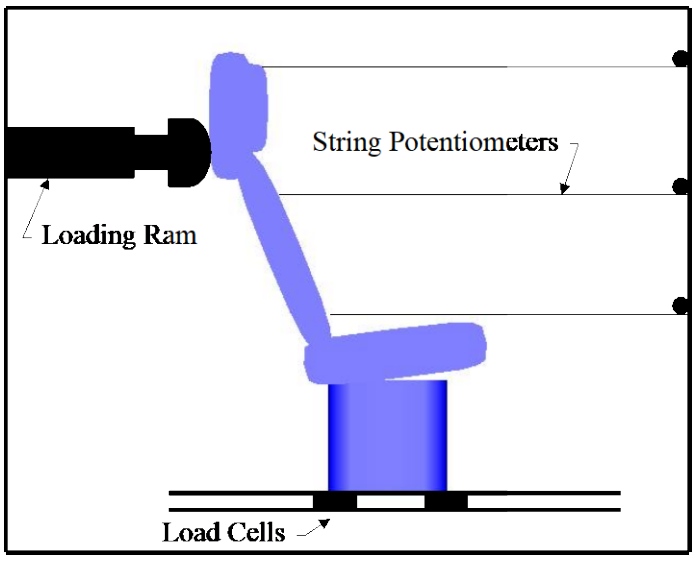

Figure A.9. Schematic of quasi-static test configuration

Abbreviations and Acronyms

ACRONYM	EXPLANATION
APTA	American Public Transportation Association
ATD	Anthropomorphic Test Device
CEM	Crash Energy Management
MADYMO	MAthematical DYnamic MOdel
FRA	Federal Railroad Administration
SAE	Society of Automotive Engineers